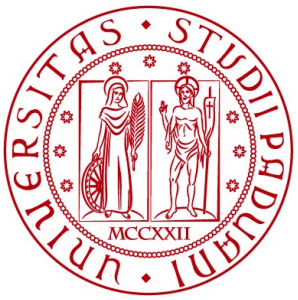

UNIVERSITÀ DEGLI STUDI DI PADOVA

**Università degli Studi di Padova**

DEPARTMENT OF CIVIL, ENVIRONMENTAL AND ARCHITECTURAL ENGINEERING
Ph.D. course in: Civil and Environmental Engineering Sciences

COORDINATOR: **Prof. Stefano Lanzoni**

# WIDTH VARIATIONS IN RIVER MEANDERING EVOLUTION AND CHUTE CUTOFF PROCESS

Thesis written with the financial contribution of the Erasmus Mundus program: AMIDILA

Ph.D. Student:
**Sergio Antonio López Dubón**

Advisor:
**Prof. Stefano Lanzoni**

Co-advisor:
**Dr. Daniele Pietro Viero**

**XXX Series**

# Abstract

Many models have been proposed to simulate and understand the long-term evolution of meandering rivers. Nevertheless, some modeling problem still needs to be solved, e.g., the stability of long-term simulations when width variations are accounted for. The present thesis proposes a physics-statistical based approach to simulate the river bank evolution, such that erosion and deposition processes act independently, with a specific shear stress threshold for each of them. In addition, the width evolution is linked with a river-specific parametric probability distribution. The analysis of a representative sample of meandering configurations, extracted from Lidar images, indicate that Generalized Extreme Values (GEV) probability density function nicely describe the along channel cross-section width distribution. For a given river, the parameters of the distribution keep almost constant in time, with significant variations observed only as after cutoff events that significantly sharpen the length of the river. The constraint of the river width based on the assumption of a GEV probability distribution ensures as the river moves throughout the floodplain adapting its width, the stability of long-term simulations. The application of the model to a reach of the Ucayali river appears to satisfactorily reproduce the planform evolution of the river and yields realistic values of the cross-section widths.

The second topic considered in the thesis is the formation of chute cutoffs, which produce substantial and non-local changes in the river planform, thereby affecting the morphological evolution. The occurrence of this type of cutoffs is one of the less predictable events in the evolution of rivers, as a multiplicity of control factors are involved in their formation and maintenance. Significant contributions have appeared in the literature in the recent years, which shed light on the complex mechanisms that first lead to the incision of chutes through the floodplain, and that eventually determines the fate of both the cutoff bend and the new channel. However, the subject is not yet settled, and a systematic physic-based framework is still missing. In this thesis, two different forcing factors leading to chute cutoffs are highlighted, the

channelized flow inertia and the topographic and sedimentary heterogeneity of the floodplain. Using two hydrodynamic models, the general features of the processes leading to chute cutoffs are investigated by assessing a few representative case studies.

# Acknowledgements

Already pass more than three years since I started my Ph.D., and many things happened since I left my home in Guatemala and arrived in Italy, which now I can call it my new home. And it is nice to remember how I went with so many feelings, and how actually when I finish, I find myself with so many mixed emotions again; but with the satisfaction of having completed this project. I had met a lot of people and lived a lot of things, some of them difficult, but the most, beautiful experiences that changed my self. For this, I want to thank:

To God that let me achieve another goal.

To Sergio and Vilma, my parents; Wendy, Marcia†, and Reina, my sisters; José and Benjamin, my nephews; and the rest of my family that always given me their love and support no matter the distance.

To my colleagues, which I have the fortune that most of them became my friends and my family in Italy. I do not have words to thank you for the support during my research, not just with your valuable suggestions and ideas, but also, for making me feel at home and for all the good memories that I will carry all my life. Alessandro, Arianna, Chiara, Davide, Enrico, Gianluca, Giulia, Irma, Lucia, Luigi, Manuel, Mara, Marta, Mattia, Pietro, Ricardo M. Ricardo T., Silvia, Tommaso, and Valentina.

To those students that visit us in Padova, people with I shared a lot of sweet moments, and in which I saw myself reflected while they discovered this beautiful city. Alfonso, Enrico, Fateme, Jhon, Lucia, Veronique.

To all my friends in Guatemala, always aware of me. And particularly to those persons that motivated me to leave and continue in Italy in particular to Karen, for the rest there is no need of name they know it pretty well.

To all my Latin-American friends, in particular to Aldo, Irene, Yenny and; the "Triangulo Norte" Ana, Carmen, and Carlos. "Y nos unió algo más: el descubrimiento de ser latinoamericanos al llegar a Europa, algo imposible desde Bogotá o Lima." Mario Vargas Llosa a Gabriel García Márquez.

To my supervisor Stefano Lanzoni, who gives me the opportunity to be a part of this project, guiding me through the research and forming as a researcher. But mainly, for going beyond your role of supervisor helping me to solve different problems; and also became my friend. It has been a pleasure working with you.

To my co-supervisor Daniele, that always hear my research problems, giving me his precious suggestions.

To all the people around the world that I meet at Padova and during the Ph.D. courses, they taught me that we are not so different.

To the Erasmus Mundus project AMIDILA that funded my research.

To my thesis reviewers, that took the time to read it, and for the kind comments and suggestions, I appreciate it.

To The University of Padova and all the people that were involved in my research.

While I wrote these words, a lot of memories came to my mind, and many feelings filled my heart. I realize that there are a lot of reasons and people which I have to be thankful and for sure I forget some of them. I apologize to them.

"Alea iacta est" Julius Caesar on January 10, 49 B.C.

# Contents

# List of Figures

# List of Tables

# Chapter 1

# Introduction

## 1.1 Research motivation

Meandering rivers are very common all around in the world Fig 1.1. They are fundamental morphological features of the landscape, can have an enormous impact on human activities (e.g., irrigation, transportation, flooding). Their environmental, biological and geological importance are also well known. The study of meandering rivers is relevant to many different fields.

Meanders are the results of the complex interplay between hydraulic and morphological processes, that drive erosion at the outer bank of bends and point bar accretion at the inner bank (Eke et al., 2014a,b; Iwasaki et al., 2016). Erosion and accretion processes are in fact strongly related to the secondary helical flow circulations induced by the curvature of the channel axis and the bed topography (Seminara, 2006). The spatial structure of the flow field controls the stresses transmitted to the channel banks and, consequently, the erosive processes that eventually determine the collapse of the outer bank (Rinaldi et al., 2008), and the sediment deposition responsible for the inner point bar accretion.

Several additional processes add complexity to the system. For example, vegetation, if present, affects the erodibility of the outer bank and contributes to stabilize the inner point bar (Bertoldi et al., 2014; van Oorschot et al., 2016; Zen et al., 2016). Floodplain heterogeneities, both planimetric and stratigraphic (Ielpi and Ghinassi, 2014), exert active control on channel bank erodibility and, consequently, on meandering dynamics (Bogoni et al., 2017).


Figure 1.1: Typical example of the river bends observed in the Usumacinta River.

The present study aims at improving the understanding of meandering river dynamics, with specifical attention to i) the effect of width variations on meander migration, and ii) the occurrence of chute cutoffs.

Traditionally, along channel variations, the cross-section width is not accounted when considering the long-term evolution of the river. Only recently, a few hydraulic models, with low computational cost, have been proposed to model the effects of width variations on the flow field (i.e., Frascati and Lanzoni (2013)) and on the long-term planform evolution of the river (e.g., Eke et al. (2014a,b)).

On the other hand, long-term models of river evolution usually account only for neck cutoffs, neglecting the possible occurrence of chute cutoffs. Indeed, while neck cutoffs can be treated from a geometrical point of view (by relating the beginning of a cutoff to the distance between two consecutive lobes), chute cutoffs have a much more complicated genesis, being related to the features of both the in-channel flow and the over-bank flow which, in turn, strongly depends on the floodplain topography. In any case, the abrupt channel shortening determined by a cutoff tends to limit channel sinuosity and to generate sediment pulse and well as heterogeneities in the floodplain

cut by the river.

## 1.2 Research objective

The primary objective of this research is to improve the mid and long-term simulations of meandering evolution, using physics-statistics based models with a reasonably low computational cost. A sub-model has bee developed explicitly for reproducing erosion and accretion process acting at the channel banks able to account for width variations through space and time. In addition, the mechanisms leading to chute cutoffs are identified, and their possible relationship with the in-channel flow and the topography of the adjacent floodplain are investigated through both theoretical and numerical models.

### 1.2.1 Research questions

The research questions tackled by the present thesis can be summarized as follows.

***How much do the cross-section width changes in space and time within meandering river?***

A statistical analysis has been performed on the river planform extracted from satellite images, in which the spatiotemporal width variations were evaluated, to quantify natural meandering widths oscillations and their statistical relevance.

***Is it possible to develop a simple but physics-based model that simulates erosion-accretion process at the channel banks, allowing the channel width to vary in space and time?***

A low-cost computational model has been developed to simulate erosion-accretion experienced by the river banks, based on physical relationships for erosion and deposition and the statistical characterization of observed river width data. The model appears to reproduce the cross-section width evolution correctly as the river migrates both in the mid and in the long term.

***Does the in-channel flow field has some incidence in the chute cutoff process? Moreover, which is the influence of the topography of the surrounding floodplain?***

A comprehensive review of the mechanisms that foster chute cutoff formation was performed. A series of case studies have been thoroughly investigated to establish the possible relationships among the inside channel flow, the floodplain topography and the inception of chute cutoff process.

## 1.3 Thesis structure

The thesis is divided into five different parts and three main Chapters. Each of these Chapters can be taken as a separate manuscript that has been already submitted, or it is going to be submitted for publication. Part I addresses the issues of width variations and meandering evolution and is divided into two Chapters. The first, Chapter 2, deals with the statistical characterization of channel width distribution in space and time, with the aim to have a better understanding of the natural oscillations of meandering widths values. The second, Chapter 3, develops a physics-statistics based model for simulating erosion and accretion process occurring at river banks, to be used for the mid to long-term simulations of channel evolution. Part II is composed by Chapter 4, dealing with the formative mechanisms and hydrodynamic forcing leading to the formation of chute cutoffs in meandering rivers. Next, in Part III a series of general conclusions and future work are mentioned. Part IV is composed by two appendixes (A and B), reporting the number of complimentary tables and figures referred to Chapter 2 and a comprehensive list of the erosion and deposition threshold relations available in the literature, mentioned in Chapter 3. Finally, Part V contains all the references mentioned in this thesis.

# Part I

# Width variations and meandering evolution

# Chapter 2

# Statistical characterization of channel width distribution in meandering rivers

## 2.1 Introduction

The use of statistics to understand a physical process is widely spread, especially when the physics behind a particular phenomenon is not entirely understood. The statistics allow us to process a significant amount of data, in order to give an interpretation of the process under analysis. In complex systems, such as meandering rivers, where several processes interact together, the selection of the correct set of variables to be analyzed and the elimination of possible noise effects is quite tricky. The introduction of random errors resulting from the measuring of the relevant quantities adds a further degree of uncertainty to the problem. In these situations, the use of probabilistic and statistical methods became fundamental for correct and reliable analysis and interpretation of the considered information (Troyan and Kiselev, 2010).

In the study of meandering river the use of statistics is a common practice, that goes from the computation of basic statistical parameters to more complex and recent theories like fractals and chaos theory (e.g., among others, Thakur and Scheidegger (1968); Surkan and Van Kan (1969); Chang and Toebes (1970); Ferguson (1976); Montgomery (1996); Perucca et al. (2005); Camporeale et al. (2005); Hooke (2007); Singh et al. (2009); Frascati and

Lanzoni (2010); Micheli and Larsen (2011); Bogoni et al. (2017)). Most of those studies used the statistics to objectively characterize the geometrical characteristics of meandering patterns (see Howard and Hemberger (1991)) and subsequently compare observed and numerically generated planforms (Frascati and Lanzoni, 2009; Bogoni et al., 2017). Another typical use of statistics in the study of meandering rivers is related to the search of possible correlations, linking the different variables that govern specific processes (e.g., channel widening/narrowing) and, consequently, individuate the relevant control variables.

The present thesis carries out a thorough statistical analysis an analysis of the spatial and temporal distributions of cross-channel width in meandering rivers, with the aims i) to better understand the natural response of the river to autogenic events such as cutoffs and ii) to model in the long term the channel width dynamics. The physical process controlling the erosion and accretion of channel banks in meandering rivers are in general quite complex and not yet completely understood, owing to the complicated interactions between the flowing current, the river bed, and the channel banks (Seminara, 2006). As a consequence, at present, the long-term simulation (at timescales of decades or centuries) of meandering river evolution accounting also for width variations suffers from many limitations, even if some significant efforts have been recently made (e.g., Parker et al. (2011); Motta et al. (2012, 2014); Asahi et al. (2013); Eke et al. (2014a,b)). In particular, it turns out very difficult to obtain physically reasonable values of the river width after long-term simulation periods.

In the present chapter of the thesis, taking advantage of the statistical characterization of the probability density distributions of channel width observed in the field, an interval of physically meaningful width values is identified to restrict the width oscillations that a meandering river can attain. This information will be subsequently used in chapter 3, to develop a simplified conceptual model whereby the cross-sectional width variations, experienced by a meandering river during its evolution as a result of bank erosion and accretion processes, are controlled on the basis of the probability density function distribution of widths typical of the considered river.

## 2.2 Materials and methods

Obtaining detailed topographic field data can, in general, be an expensive and time-consuming task, in particular when large spatial and temporal scales need to be considered. In the case of meandering rivers, however, the increasing availability of satellite images ensures the possibility to build up a large and reliable data set from which river planform configurations and channel width distributions can be extracted.

This thesis makes use of the Landsat images provided by the USGS portal (https://earthexplorer.usgs.gov/), which have the advantage of being free, georeferenced, and available since 1972 (U.S. Geological Survey, 2015). Each image corresponds to one single temporal instant and, differently from other free sources of satellite images, covers the entire extension of a given river. The only problem is the poor resolution in the case of small rivers.

Most of the images used in this study were taken from the Landsat 8 OLI (Operational Land Imager) and TIRS (Thermal Infrared Sensor). The data are available since February 2013, with a new image every 16 days. Each image has an approximate size of 170 km north-south by 183 km east-west (U.S. Geological Survey, 2015). Landsat 8 OLI and TIRS images consist of nine spectral bands with a spatial resolution of 30 meters for the bands 1 to 7 and 9. Of special interest is the ultra blue band 1, that is useful for coastal and aerosol studies (Barsi et al., 2014). More detailed technical information and common uses of these bands are reported in Table A.1 (see Appendix A and U.S. Geological Survey (2015)).

The identification of water bodies using satellite information had been used in many different applications and fields. Because of this, many approaches have been proposed (e.g., Gao (1996); Campos et al. (2012); McFeeters (2013); Li et al. (2013); Jiang et al. (2014); Ko et al. (2015)). For the present application, one of the more simple and common approaches has been selected. It makes use of a water index to identify water bodies, based on the wavelength satellite band measure and the reflectance of water. Two methods have been employed here to compute this index, namely the normalized difference water index (NDWI) of McFeeters (1996):

$$NDWI = \frac{Green - NIR}{Green + NIR}, \tag{2.1}$$

and the modified NDWI (MNDWI) of Xu (2006),

$$MNDWI_{Xu} = \frac{Green - SWIR1}{Green + SWIR1}. \tag{2.2}$$

These two indexes have been computed for a number of meandering rivers selected all around the world. These rivers have been chosen to represent different characteristics in terms of hydrological regime and geological composition of the floodplain (see Table A.2). The Landsat products used to extract the geometrical features of interest (channel banks and centerline) are: (a) multispectral image, (b) Landsat look image, (c) Green band, (d) NIR band and (e) SWIR1 band (see, e.g., Fig. A.1).

The images have been selected with the objective to capture bank full or nearly bank full conditions. The satellite images were thus searched during the autumn period (according to the river location). In the presence of high cloud cover levels, the images nearest to the autumn or raining season have been considered. In general, the more recent and the oldest available images were selected for each river. Some rivers, however, were analyzed considering the images collected in different, possibly consecutive, years (see Table A.2). In these cases, special attention has been paid to select representative Landsat images before and after important changes in the river planimetric configuration determined by cutoff events and or human interventions. Except for the Ucayali river, the general criteria used to select the images can be summarized as follows:

(a) more recent image (at time in which the data was collected);

(b) oldest image;

(c) images before and after important (known) changes in the river planimetric configuration,

(d) consecutive years;

(e) randomly.

The data concerning the Ucayaly River have been taken form Schwenk et al. (2017).

After selecting the images, the water index was computed according to equations 2.1 and 2.2. The river banks were then delimited on the basis of

the values attained by this index (Figure 2.1), using the software ArcMap. Finally, the central river axis was extracted in the middle of river banks, The coordinates of the points composing the bank and central axis lines are expressed in the projected system UTM/WGS 84, that allows one to work directly with real distance values.

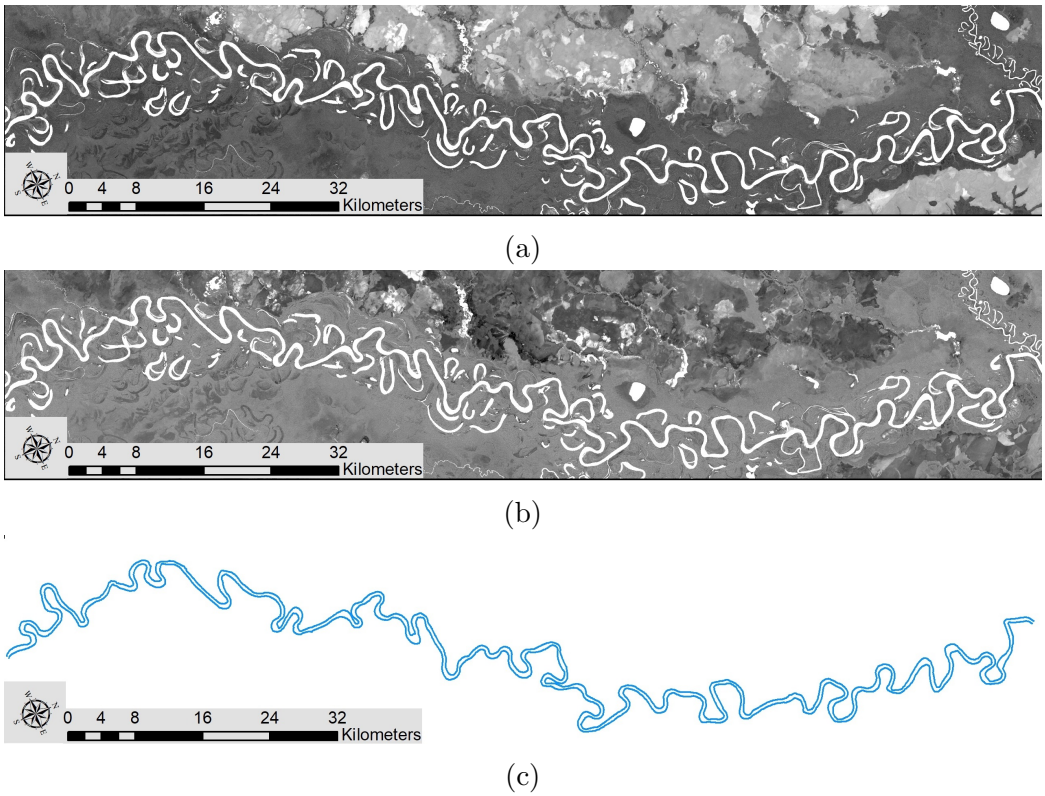


Figure 2.1: Image processing of Beni river Landsat data: (a) NDWI index; (b) MNDWI index; (c) final banks.

Eventually, the x and y coordinates of the bank lines were processed with a MATLAB code to obtain the along channel distribution of the cross-section width. Firstly, a Savitzky-Golay filter (Savitzky and Golay, 1964) was applied to smooth the channel axis and the river bank lines, in order to reduce the noisy irregularities that arise during the image extraction process. Next, the central channel axis was re-sampled according to a fixed interval (30 m, in accordance with the Landsat image resolution) determining the space interval between the $N_{line}$ cross sections for which the width is computed. Then, the code computes the normal lines across the center line, and searches for the intersection of $i-th$ $(i = 1 - N_{line})$ normal with the first segment

composing the left and right bank lines: if the normal line intersects these two segments, the width is computed as the distance between the two intersection points. Otherwise, the research of the intersection points continues with the next segment. Once all the width values were computed, the along channel distribution of the dimensionless half channel width is determined by using the reach averaged mean channel width as a normalizing factor.

Finally, the local curvature was computed as the inverse of the radius of curvature, through the equation (Schwenk et al., 2015):

$$\begin{aligned}\mathcal{C} = 2[(y_i - y_{i-1})(x_{i+1} - x_{i-1}) - (x_i - x_{i-1})(y_{i+1} - y_{i-1})] \\ \left[(x_i - x_{i-1})^2 + (y_i - y_{i-1})^2\right]^{-1/2} \\ \left[(x_{i+1} - x_{i-1})^2 + (y_{i+1} - y_{i-1})^2\right]^{-1/2} \\ \left[(x_{i+1} - x_i)^2 + (y_{i+1} - y_i)^2\right]^{-1/2}\end{aligned} \tag{2.3}$$

## 2.3 Statistical analysis

In this section, a frequency approach is used to analyze along the channel distribution of cross-section half-width. To this aim, the meandering rivers reported in Table A.2 are divided into two groups, depending on the number of years, one or more than one, for which the planform configurations have been extracted.

### 2.3.1 Spatial distribution of half channel widths

The first statistical analysis, was made using the software STATGRAPHICS, concerned the along channel distribution of the dimensional and dimensionless (i.e., scaled by the reach averaged mean) half-channel width observed at fixed times. The results of the analysis are summarized in Tables A.4 and A.5, reporting, for each river, the mean, the standard deviation, the coefficient of variation, the minimum and maximum values, the range of variations, the standardized skewness, and kurtosis. Note that these two latter coefficients, being standardized, do not vary when considering dimensional or dimensionless data. The coefficient of variation attains values around 20% for almost all the rivers. Higher values of the coefficient of variation are observed for the Bravo, Kyaukgy, Cauto and Gambia rivers, possibly as a consequence

of the proximity of the considered reaches to a delta region (see Table A.3, reporting the coordinates of the upstream and downstream points of each river reach considered in the analysis). Relatively high values of the coefficient of variation are observed also for the longer river reaches, namely those pertaining to Chapecó, Mamore and Irtysh Reka rivers.

| River | Count | Average (m) | Stnd. Dev. | Coeff. of Var. | Min. (m) | Max. (m) | Range (m) | Stnd. skewness | Stnd. kurtosis |
|---|---|---|---|---|---|---|---|---|---|
| Chincaga | 4921 | 39.86 | 7.33 | 18.40% | 22.65 | 65.86 | 43.21 | 11.62 | -2.78 |
| Nan | 4592 | 46.44 | 8.51 | 18.31% | 24.71 | 74.17 | 49.46 | 14.45 | 5.03 |
| Chet | 1677 | 21.66 | 2.75 | 12.71% | 13.05 | 29.86 | 16.81 | 4.72 | 1.08 |
| Tarauaca | 8496 | 75.47 | 18.11 | 23.99% | 24.63 | 132.40 | 107.77 | 11.86 | -1.03 |
| Murray | 5222 | 47.45 | 9.21 | 19.40% | 10.53 | 75.68 | 65.15 | 0.32 | 3.06 |
| Orthon | 18261 | 45.60 | 7.95 | 17.43% | 15.00 | 82.16 | 67.15 | 13.49 | 34.11 |
| Darling | 8699 | 15.55 | 3.14 | 20.21% | 5.50 | 29.26 | 23.76 | 20.03 | 11.92 |
| Bravo | 12688 | 20.19 | 8.98 | 44.46% | 1.89 | 73.83 | 71.94 | 104.57 | 162.76 |
| Kyaukgy | 3528 | 24.24 | 8.60 | 35.48% | 6.53 | 61.26 | 54.72 | 28.37 | 15.09 |
| Kwango | 3178 | 24.87 | 5.12 | 20.60% | 11.29 | 58.03 | 46.74 | 22.09 | 39.50 |
| Baver | 985 | 19.31 | 2.77 | 14.33% | 13.66 | 28.43 | 14.77 | 8.64 | 1.14 |
| Culym | 6953 | 107.24 | 19.62 | 18.29% | 42.92 | 188.52 | 145.60 | 10.09 | 17.81 |
| Ouachita | 4232 | 47.66 | 7.60 | 15.95% | 28.13 | 77.96 | 49.83 | 14.28 | 10.43 |
| Cauto | 5564 | 50.14 | 20.23 | 40.34% | 18.30 | 116.31 | 98.01 | 11.80 | -12.67 |
| Chapecò | 16547 | 256.04 | 82.66 | 32.28% | 97.15 | 560.59 | 463.43 | 30.22 | 1.42 |
| Brazos | 12058 | 64.26 | 11.18 | 17.39% | 31.04 | 126.17 | 95.13 | 37.32 | 30.30 |
| Gambia | 17948 | 59.47 | 16.42 | 27.61% | 27.40 | 197.15 | 169.75 | 134.19 | 327.14 |
| Mamore | 11742 | 168.78 | 48.33 | 28.63% | 72.97 | 496.88 | 423.90 | 72.76 | 85.77 |
| Irtysh Reka | 8585 | 164.93 | 44.36 | 26.90% | 79.16 | 397.79 | 318.63 | 43.64 | 46.60 |
| Beni | 4343 | 227.06 | 47.88 | 21.09% | 141.24 | 490.93 | 349.69 | 39.96 | 48.87 |
| White | 2230 | 88.19 | 14.36 | 16.29% | 48.64 | 153.03 | 104.40 | 19.39 | 19.32 |

Table 2.1: General statistic values of the dimensional half width for the river group 1.

### Analysis of outliers

This section has the purpose of identifying possible outliers among a normally distributed population. The considered data sample 21 rivers for a total of 162,449 sections is in fact large enough to consider the application of the central limit theorem, so is assume that the width data are distributed according to either a normal or a log-normal probability density function. An outlier can thus be defined as an observation which appears to be inconsistent with the overall behavior of the data (Iglewicz and Hoaglin, 1993). Focusing on the interesting outliers, that even if statistically are considering as outliers

they are accurate points (e.g., unusually wide bends) that could contribute to the knowledge of the phenomena (Aguinis et al., 2013).

The aim of an outlier analysis is to control the reliability of the larger values attained by considered quantity. The analysis was applied to both dimensional and dimensionless half channel width data, and the results are shown in Tables A.6 and A.7, respectively. The analysis yields: the location estimate (values that determines the shift of the distribution. Columns 2-5.); the scale estimate (values that determine statistical dispersion of the probability distribution. If are large, then the distribution will be more spread; if are small then it will be more concentrated. Columns 6-9.); and the confidence intervals (interval in which the true value of the population parameter could be find. Columns 10-13.).

(a) Location estimate. Columns 2 and 3 of Tables A.6 and A.7 report the mean and standard deviation computed considering all data; Column 4 shows the average computed after dismissing a given percentage (15%) of the smallest and biggest values; Column 5 reports winsorized mean values as the average obtained after replacing a given percentage (15%) of the smallest and biggest values. (So, the most extreme values are not contained, but the number of events remains the same).

(b) Scale estimate. Column 6 of Tables A.6 and A.7 shows the standard deviation determined considering all the data; Column 7 shows the median absolute deviation, as the absolute differences between each data value and the sample median; Column 8 reports the weighted sum of squares around the sample median, with the weights decreasing with distance from the median; Column 9 shows the squared deviations around the winsorized mean.

(c) Confidence intervals. Columns 10 and 11 of Tables A.6 and A.7 shows the upper and lower confidence intervals for the mean computed by considering the original set of data; Columns 12 and 13 are the upper and lower confidence intervals computed with reference to the winsorized statistics.

In the following, let us focus on the Chét river, exhibiting the lowest coefficient of variability, and the Bravo river, having the biggest coefficient of variability. In the case of the Chét the sample is composed of 1677 half-width data. The mean and the variance of this sample are equal to 21.66 m and 2.75 m, respectively, while the corresponding winsorized estimates, are

21.61 m and 2.88 m. When considering the dimensionless half-widths, the mean and variance of the original data sample are 1.0 and 0.127, while the corresponding winsorized values are 0.997 and 0.133. In the case of the Bravo river, the sample is composed of 12688 half-width data. The mean and the variance take the values 20.19 m and 8.98 m when considering the original dimensional sample, while the corresponding winsorized values are 18.86 m and 6.81 m. In the case of the dimensionless half-width, the original sample mean and variance are 1.0 and 0.445, whereas the corresponding winsorized estimates are 0.934 and 0.337. It is immediate to note the impact of the winsorized estimates on the confidence interval of the mean according to the coefficient of variability.

An overall comparison among the entire set of considered rivers is shown in Figure 2.2, reporting the notched box and whisker plots of the dimensionless half-channel widths. The boxes represent the interquartile ranges corresponding to the 50% of the data; the horizontal line within each box denotes the median value; the notches represent a confidence interval around the median; the whiskers extend up to 1.5 times the interquartile range. All the values outside the notches are considered as outliers.

From Figure 2.2, it appears that for almost all the rivers the line representing the median is not located in the center of the boxes and, hence, the mean and the median do not coincide. Also, even though the median values, in general, vary within a relatively limited range (0.904 to 1.013), the notches tend to differ significantly from river to river. Finally, the data falling outside of the whiskers concentrate mainly in the upper whisker. Only the Cauto river does not present any data outside of the whiskers but has a quite high extension of the upper whisker. The larger outlier values are found for the Kyaukgy river, while the Bravo river exhibits the smaller outlier values. Finally, the Chét river is characterized by the most compact box and has whiskers of almost equal length.

A series of statistical tests were applied for the detection of the outliers. The first was the maximum normed residual test proposed by Grubbs (1969), here applied with the assumption that the considered data can be described by either a normal or a log-normal distribution (Table A.8) The test evaluates the Z (studentized value) with a $\lambda 1$ (significance difference with the extreme values) for both tails and the Z value with a $\lambda 2$ (significance difference between extreme values) value between the tails.

For the normal distribution the biggest difference between the highest

width's Z and the $\lambda 1$ value is presented in the Kwango river, since this river presents the biggest dispersion outside the upper whisker, for the case of the smallest width's Z value and the $\lambda 1$ there are no outliers, the same case is presented with the Z value between the highest and smallest width and the $\lambda 2$. In the case of the log-normal assumption, there are no upper outliers, and just the Bravo river presents lower outliers, but in the case of the Z value between the highest and smallest width and the $\lambda 2$ there are 4 cases being the Bravo river the one which presents the biggest difference.

The second test is the Generalized Extreme Studentized Deviate (ESD), proposed by Rosner (1983). Also, in this case, a normal or a log-normal distribution are assumed to describe the data (Table A.9). Owing to the nature of this test, which considers just the variation with the extremes and not between them (not allowing an evaluation of the differences between the highest and smallest data values), only the tails of the distributions are considered. Under the assumption of a normal distribution, it is the Beni river that presents the largest number of outliers while, when considering a log-normal distribution the Orthon river has the larger number of outliers. In the case of the Kwango River, outliers are found for both the distributions.

Even if the presence of outliers is relatively few, the values of standard deviation and kurtosis (Table A.5) suggest, that the channel width data do not fit entirely to a normal or log-normal distribution. For this reason, other two outlier detection tests have been implemented (Table A.10), namely an adaptation of the ESD for the upper tail of the exponential distribution (Kimber, 1982), and a general nonparametric test with the hypothesis that the population has a common median value (Walsh, 1950). The results of these two additional tests, shown in Table A.10, indicate the absence of outliers when using the Kimber's test and the presence of just a few in the case of Walsh's test, applied to the Bravo river. This latter outcome can be explained by the high variability characterizing the tail of the corresponding distribution (Figure 2.2).

### Probability Distribution fitting

The statistical analysis reported in the previous section suggests that the along channel distributions of half channel width does not precisely correspond to a normal or log-normal probability distribution. For this reason, a series of different Probability Density Distributions (PDF) have been fitted to the considered data. They are those available in MATLAB pro-

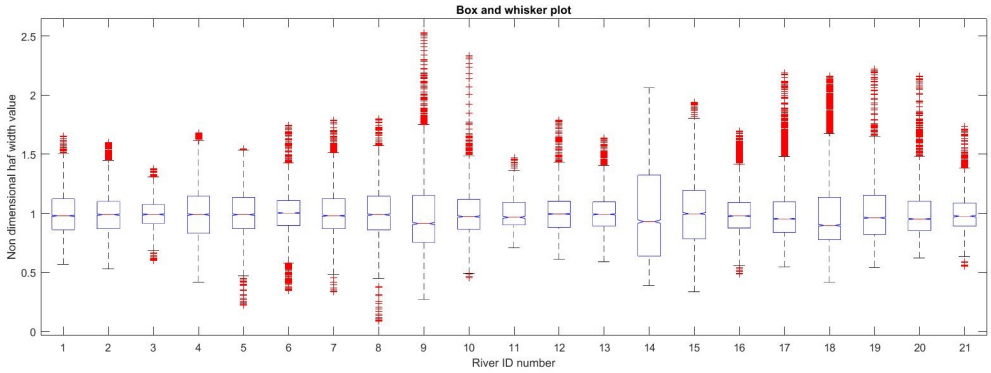


Figure 2.2: Notched box and whisker plot computed for the along channel distributions of the dimensionless half width. The river ID number reported on the horizontal axis is that specified in Table A.2).

gram, namely: Beta, Binomial, Birnbaum Saunders, Burr Type XII, Chi-square, Exponential, Extreme Value, F, Gamma, Generalized Extreme Value (GEV), Generalized Pareto, Geometric, Half-Normal, Hypergeometric, Inverse Gaussian, Logistic, Log-Logistic, Log-Normal, Nakagami, Negative Binomial, Noncentral F, Noncentral t, Noncentral Chi-square, Normal, Poisson, Rayleigh, Stable, T, Uniform, Discrete Uniform, and Weibull.

The choice of the PDF that best approximates each river dataset has been made by means of the Bayesian Information Criterion (BIC) proposed by Schwarz (1978), based on the likelihood function. The criterion has been applied to both dimensional and dimensionless half-width data. The results of this analysis, summarized in Table A.11, show that in most of the cases the Generalized Extreme Value (GEV) provides the best data fitting. Note that, when comparing the best fitting PDF with the GEV, the differences in BIC values are larger when considering the dimensionless data, since the normalization amplifies the sensitivity to any variation, affecting the fitting.

Some typical examples of the data histograms, the PDF's ensuring the first and second best fitting, and the GEV probability distribution function are depicted in Figures 2.3 and 2.4 report.

From the histograms, it is evident that there are some cases, like the Cauto river, that present a bi-modal distribution. Even in this case, the GEV is the PDF (among those investigated) that ensures the best data fitting. The occurrence of a bi-modal behavior is related to the presence of a drastic change in the geometry of the river (see, e.g., Figure 2.5a), possibly driven

| River | Best PDF | Dimensional case | | | Non Dimensional case | | |
|---|---|---|---|---|---|---|---|
| | | BIC | GEV BIC | Diff % | BIC | GEV BIC | Diff % |
| Chincaga | GEV | 3.34E+04 | 3.34E+04 | 0.00% | -2.87E+03 | -2.87E+03 | 0.0% |
| Nan | Log Normal | 3.25E+04 | 3.25E+04 | 0.02% | -2.75E+03 | -2.74E+03 | 0.2% |
| Chet | Gamma | 8.15E+03 | 8.16E+03 | 0.07% | -2.16E+03 | -2.16E+03 | 0.2% |
| Tarauaca | GEV | 4.24E+04 | 4.24E+04 | 0.00% | -4.52E+02 | -4.52E+02 | 0.0% |
| Murray | T-location scale | 3.56E+04 | 3.57E+04 | 0.11% | -2.27E+03 | -2.23E+03 | 1.7% |
| Orthon | Logistic | 3.39E+04 | 3.44E+04 | 1.42% | -3.18E+03 | -2.69E+03 | 15.4% |
| Darling | Burr | 2.56E+04 | 2.56E+04 | 0.07% | -1.89E+03 | -1.87E+03 | 1.0% |
| Bravo | T-location scale | 2.90E+04 | 2.91E+04 | 0.40% | -1.09E+03 | -9.77E+02 | 10.5% |
| Kyaukgy | GEV | 2.43E+04 | 2.43E+04 | 0.00% | 1.77E+03 | 1.77E+03 | 0.0% |
| Kwango | Log logistic | 1.91E+04 | 1.92E+04 | 0.54% | -1.32E+03 | -1.21E+03 | 7.9% |
| Baver | GEV | 4.73E+03 | 4.73E+03 | 0.00% | -1.10E+03 | -1.10E+03 | 0.0% |
| Culym | Log Normal | 4.19E+04 | 4.19E+04 | 0.09% | -3.98E+03 | -3.95E+03 | 0.9% |
| Ouachita | Log Normal | 2.90E+04 | 2.90E+04 | 0.10% | -3.69E+03 | -3.66E+03 | 0.7% |
| Cauto | GEV | 4.15E+04 | 4.15E+04 | 0.00% | 3.66E+03 | 3.66E+03 | 0.0% |
| Chapec | GEV | 5.71E+04 | 5.71E+04 | 0.00% | 1.37E+03 | 1.37E+03 | 0.0% |
| Brazos | Burr | 3.75E+04 | 3.76E+04 | 0.06% | -3.33E+03 | -3.30E+03 | 0.7% |
| Gambia | GEV | 3.70E+04 | 3.70E+04 | 0.00% | -1.60E+03 | -1.60E+03 | 0.0% |
| Mamore | GEV | 5.18E+04 | 5.18E+04 | 0.00% | 9.53E+02 | 9.53E+02 | 0.0% |
| Irtysh Reka | GEV | 4.97E+04 | 4.97E+04 | 0.00% | -6.52E+02 | -6.52E+02 | 0.0% |
| Beni | GEV | 4.47E+04 | 4.47E+04 | 0.00% | -2.44E+03 | -2.44E+03 | 0.0% |
| White | Burr | 1.88E+04 | 1.88E+04 | 0.17% | -2.12E+03 | -2.09E+03 | 1.5% |

Table 2.2: The best fitting PDF is compared with the GEV probability density function through a Bayesian Information Criterion (BIC). The considered rivers are those reported in Table Number. Both dimensional and dimensionless half channel width are considered.

by significant variations in flow discharge, bed slope, or backwater effects.

Another interesting case is the Beni river, the GEV adapts pretty well to the histogram, even if the river presents a lot of variations (Fig2.5c). Finally, it is worth to mention that the rivers that are better described by a well-defined PDF (mostly the GEV) are those with long enough reaches (i.e., with a large enough number of sampled cross sections) that, however, do not reach the river mouth or join to another river.

### 2.3.2 Spatio-temporal distributions of channel widths

The previous section suggests that different meandering rivers all around the world have similar PDF distributions of half channel widths. The modeling of meandering river evolution, however, poses the question whether or not the channel width undergoes some variations as the river migrates throughout

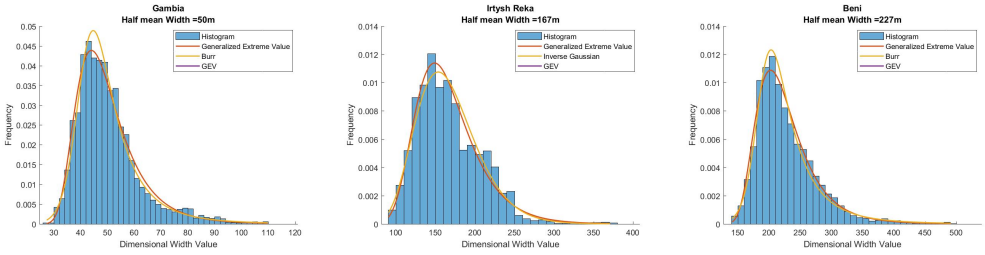


(a) Gambia river (b) Irtysh Reka river (c) Beni river

Figure 2.3: Typical examples of the histograms, the PDF's ensuring the first and second best fitting, and the GEV probability distribution function for the dimensional half width data.

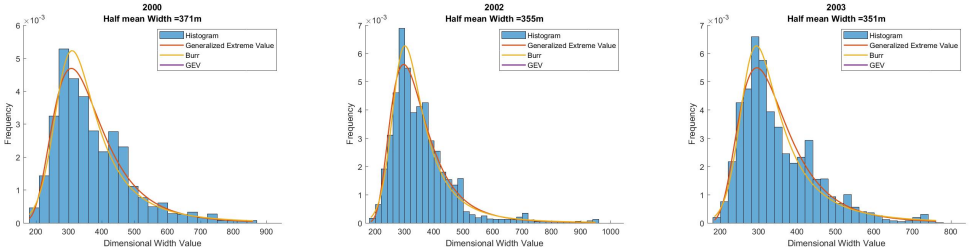


(a) Gambia river (b) Irtysh Reka river (c) Beni River

Figure 2.4: Typical examples of the histograms, the PDF's ensuring the first and second best fitting, and the GEV probability distribution function for the dimensionless half width data.

the floodplain. To accomplish this task, a number of river reaches have been analyzed at different times (Table A.12). In particular, the planforms corresponding to the Chixoy river have been selected on the basis of the criteria (a),(b),(c) (see section 2.2), i.e., taking an image before and after a chute cutoff. The planforms considered for the Sacramento river fulfill the criteria (a),(c), (d): a chute cutoff also occurred in this rivers, while the images corresponding to the more recent years since have a better spatial resolution. For the Bermejo and Segovia rivers, the criteria used to choose the planforms were the (a) and (e). Due to a large amount of data available for the Ucayali river, it is treated as a particular case study, that will be explicitly addressed in the Section 2.3.3.

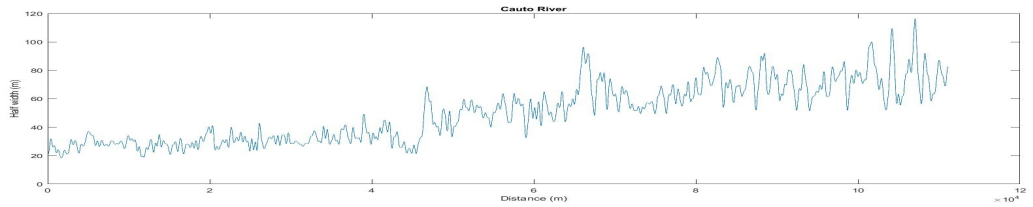


(a)

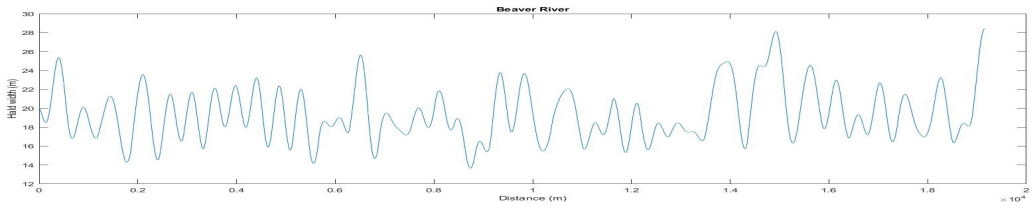


(b)

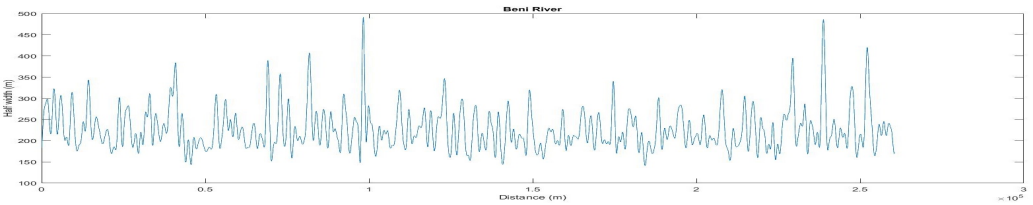


(c)

Figure 2.5: Along channel distributions of the half channel widths. The $x-$axis reports the distance from the upstream section of the considered river reach.

### Time distribution statistics

The general statistics reported in Tables 2.3 and A.13 indicate that the along channel distribution of river half-widths, in general, do not change significantly as the river moves across the floodplain. Figure 2.6 shows the remarkable similarities attained by the width distributions observed in the Segovia river after a time interval of 17 years, while larger width fluctuations characterize the Bermejo river (after 14 years), the Chixoy river (during three different time intervals, spanning in total 30 years), and the Sacramento River (during two different time intervals, spanning in total 20 years).

Different statistical tests have been implemented to determine if the differences in the values in Table 2.3 are statistically significant or not. The results of all these tests are summarized in the Tables collected in Appendix A. Here is list the tests that have been performed and present their results.

| River | Count | Average (m) | Stnd. Dev. | Coeff. of Var. | Min. (m) | Max. (m) | Range (m) | Stnd. skewness | Stnd. kurtosis |
|---|---|---|---|---|---|---|---|---|---|
| Chixoy 1986 | 1604 | 76.77 | 16.09 | 20.95% | 44.25 | 169.32 | 125.07 | 20.58 | 31.69 |
| Chixoy 2010 | 846 | 80.08 | 14.81 | 18.50% | 47.10 | 161.89 | 114.79 | 17.42 | 37.73 |
| Chixoy 2012 | 792 | 84.67 | 11.50 | 13.58% | 56.01 | 123.40 | 67.39 | 3.23 | 0.51 |
| Chixoy 2016 | 822 | 69.57 | 12.12 | 17.42% | 39.74 | 111.67 | 71.93 | 6.09 | 5.01 |
| Sacramento 1994 | 7753 | 75.12 | 13.58 | 18.08% | 41.38 | 144.64 | 103.26 | 27.20 | 24.21 |
| Sacramento 1996 | 5026 | 107.59 | 16.50 | 15.34% | 64.25 | 187.38 | 123.13 | 16.23 | 17.78 |
| Sacramento 2015 | 5112 | 83.41 | 14.06 | 16.85% | 49.06 | 135.15 | 86.09 | 8.72 | -1.76 |
| Sacramento 2016 | 7667 | 81.44 | 14.05 | 17.25% | 45.12 | 126.09 | 80.97 | 6.57 | -4.12 |
| Bermejo 2002 | 1749 | 141.84 | 43.02 | 30.33% | 66.19 | 319.10 | 252.91 | 20.50 | 14.42 |
| Bermejo 2016 | 1916 | 131.39 | 25.97 | 19.77% | 64.17 | 213.89 | 149.72 | 3.18 | 0.06 |
| Segovia 1999 | 6914 | 108.35 | 20.71 | 19.11% | 60.14 | 189.94 | 129.8 | 18.98 | 2.58 |
| Segovia 2016 | 10350 | 105.85 | 21.08 | 19.91% | 58.63 | 241.30 | 182.67 | 54.71 | 89.66 |

Table 2.3: General statistics of the along channel distributions of dimensional half channel width extracted at different times for the Chixoy, Sacramento, Bermejo and Segovia rivers.

The first was the Analysis of Variance (ANOVA), whose results are reported in Table A.14. The variance of the data is decomposed into two components: (a) a between-group component and (b) a within-group component. The F-ratio is then computed as the ratio of the between-group estimate to the within-group estimate. Since the P-value of the F-test is less than 0.05 for all the rivers, there is a statistically significant difference between the means at the 5% significance level.

The next step was to analyze the mean differences for each pair of data, using multiple range tests. The third column of Table A.15 shows the result from the Tukey's honest significant difference (HSD) test, which controls the experiment-wide error rate ($\alpha$), in the present case the possible error made during the definition of the rivers paths. If all the means are equal, the probability of declaring any of pairs of data to be significantly different equals $\alpha$. This test allows multiple comparisons among all pairs of means using Tukey's T studentized range distribution (Tukey, 1949). The fourth column of Table A.15 shows the Scheffe intervals. This test is designed to permit the estimation of all possible contrasts among the sample means, not just pairwise comparisons (Scheffe, 1999). The last column of Table A.15 reports the Bonferroni intervals obtained using the Bonferroni's inequality. This test is designed to estimate any pre-selected number of contrasts. The Bonferroni intervals are usually more extensive than Tukey's limits when all pairwise comparisons are being made (Dunn, 1961). Overall, the considered multiple range tests indicate that there is a significantly different between

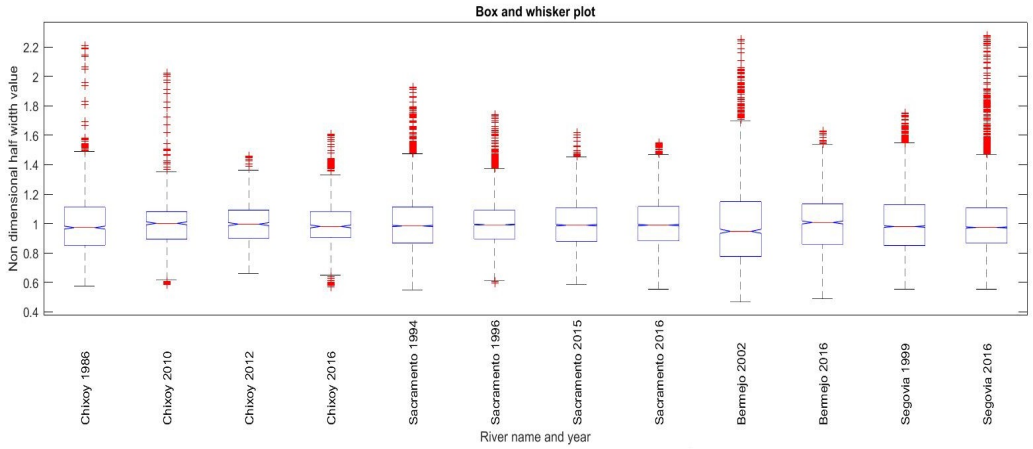


Figure 2.6: Notched box and whisker plot computed for the along channel distributions of the dimensionless half width, observed in different years for the Chixoy, Sacramento, Bermejo and Segovia rivers.

the means at a 95% confidence level.

Another important aspect to verify is if the variability of width values in a river change or not with time. Table A.16 shows the results of a variance check, made through Bartlett's test applied to each river. This test compares a weighted average of the within-sample variances to their geometric mean and could be applied to both equal and unequal group sizes (Bartlett, 1937). Table A.16 also shows the results of the Levene's test that performs a one-way analysis of variance on the absolute differences between each observation and its corresponding group mean (Levene, 1960), but is less sensitive than Bartlett's test. The variance tests indicate that just in 3 cases the variance did not change (values in column 9 of Table A.16 greater than 0.05). In summary, the statistical tests carried out on the possible temporal variability of width changes do not disclose any general behavior of the variance.

Finally, in order to analyze how the measure of central tendency could change in time, the behavior of median has been evaluated through the Kruskal-Wallis test (Kruskal and Wallis, 1952), a rank-based nonparametric test, and the nonparametric Mood's median test (Mood, 1954), a variant of the Pearson's chi-squared test. The results, reported in Table A.17, show that just in the case of the Bermejo river for the Mood's test the P value is higher than 0.05, while the rest of the rivers seem to not exhibit a significant difference between the medians.

### Analysis of outliers

It has already been seen (Section 2.3.1) that, for a planform configuration collected at a given time, the river width's values do not fit into a normal PDF distribution. For this reason, when considering, for a given river, the along channel width distributions observed at different times, just the non-normal outlier detection test described in Section 2.3.1 is here considered. According to the results shown in Table A.18, no relationship seems to exist between the different temporal instants in which an outlier was found and the other temporal instants under analysis. Also, it is worth to mention that the number of a detected outlier is not significant, been zero detentions in must of the cases and just three cases in which was found a single outlier.

### Probability Distribution fitting

The analysis described in Section 2.3.1 shows that the GEV probability distribution function ensures the best fit of width data for the most of the considered rivers. The question addressed in the following is whether or not the GEV distribution yields a good fitting even when the river evolves through the floodplain.

Figures A.5 and A.6 shows that, indeed, the GEV distribution fits reasonably well the width distributions observed for a given river in different years. The overall features of the fitting are quite similar to those already discussed in Section 2.3.1. For example in the case of the Chixoy river, the GEV distribution yields a reasonably good fit, despite the impact of few data, that as was mention before is one of the factors that could induce to poor fitting.

A comparative analysis has then carried out through the BIC criterion on the performance of the GEV fitting as compared to others PDFs. Table A.19 shows that actually the GEV ensures a general good fitting, with a maximum BIC difference around 1% for the Chixoy river. It is important to note that this maximum difference is attained after a chute cutoff has occurred. A similar, and even more evident behavior is observed in the Sacramento River, owing to the formation of a big chute cutoff. In the absence of events that change significantly the planform river configuration, the differences in the PDF's are relatively limited and the GEV distribution can be confidently used to fit the half channel width distributions.

| River | Best PDF | Dimensional case | | | Non Dimensional case | | |
|---|---|---|---|---|---|---|---|
| | | BIC | GEV BIC | Diff % | BIC | GEV BIC | Diff % |
| Chixoy 1986 | Inv Gauss | 8.60E+03 | 8.61E+03 | 0.05% | -5.56E+02 | -5.52E+02 | 0.82% |
| Chixoy 2010 | Stable | 6.82E+03 | 6.89E+03 | 0.98% | -7.57E+02 | -6.71E+02 | 11.37% |
| Chixoy 2012 | Bim-Saund | 6.06E+03 | 6.07E+03 | 0.13% | -9.07E+02 | -8.99E+02 | 0.89% |
| Chixoy 2016 | Log Logistic | 6.39E+03 | 6.41E+03 | 0.35% | -5.51E+02 | -5.29E+02 | 4.11% |
| Sacramento 1994 | GEV | 6.19E+04 | 6.19E+04 | 0.00% | -5.10E+03 | -5.10E+03 | 0.00% |
| Sacramento 1996 | Log Logistic | 4.23E+04 | 4.23E+04 | 0.17% | -4.77E+03 | -4.69E+03 | 1.53% |
| Sacramento 2015 | GEV | 4.15E+04 | 4.15E+04 | 0.00% | -3.78E+03 | -3.78E+03 | 0.00% |
| Sacramento 2016 | GEV | 6.22E+04 | 6.22E+04 | 0.00% | -5.24E+03 | -5.24E+03 | 0.00% |
| Bermejo 2002 | GEV | 1.77E+04 | 1.77E+04 | 0.00% | 3.83E+02 | 3.83E+02 | 0.00% |
| Bermejo 2016 | GEV | 1.79E+04 | 1.79E+04 | 0.00% | -7.69E+02 | -7.69E+02 | 0.00% |
| Segovia 1999 | GEV | 6.11E+04 | 6.11E+04 | 0.00% | -3.68E+03 | -3.68E+03 | 0.00% |
| Segovia 2016 | GEV | 9.07E+04 | 9.07E+04 | 0.00% | -5.78E+03 | -5.78E+03 | 0.00% |

Table 2.4: The best fitting PDF is compared with the GEV probability density function through a Bayesian Information Criterion (BIC). The considered rivers configurations are those reported in Table A.12 and, for a given rivers, have been extracted for different times. Both dimensional and dimensionales half channel width are considered.

For a given river, the GEV parameters generally vary in time (see Figure 2.7). However, in the absence of significant variations of the river planform (e.g., owing to cutoff processes or human interventions) the variations are relatively small. Some differences in the GEV parameters are also observed when considering either the dimensional or the dimensionless distributions. In the case of dimensionless widths, the GEV distributions look more similar to each other, even though evident departures from this similarity are observed just after cutoff events. Remarkably, after a cutoff event, the river tends to progressively recover a PDF distribution of channel width similar to the pre-event one. This finding reinforces the idea that the river width oscillates around an equilibrium width, whose probability density distribution is described by a GEV distribution with well-defined parameters, i.e., almost constant in time.

The visual inspection of Figure 2.7 suggests that changes in the fitted GEV distribution in more of the cases seem to be small changes. In order to quantify the amount of these differences, a statistical distance has been used to measure the statistical divergence between two distributions observed at different times. The Bhattacharyya coefficient (BC) and the Bhattacharyya distance coefficient (BDC), i.e., the negative logarithm of BC, allows one to objectively approach the similarity problem in a geometric sense, identifying the overlapping between two distributions (Bhattacharyya, 1943).

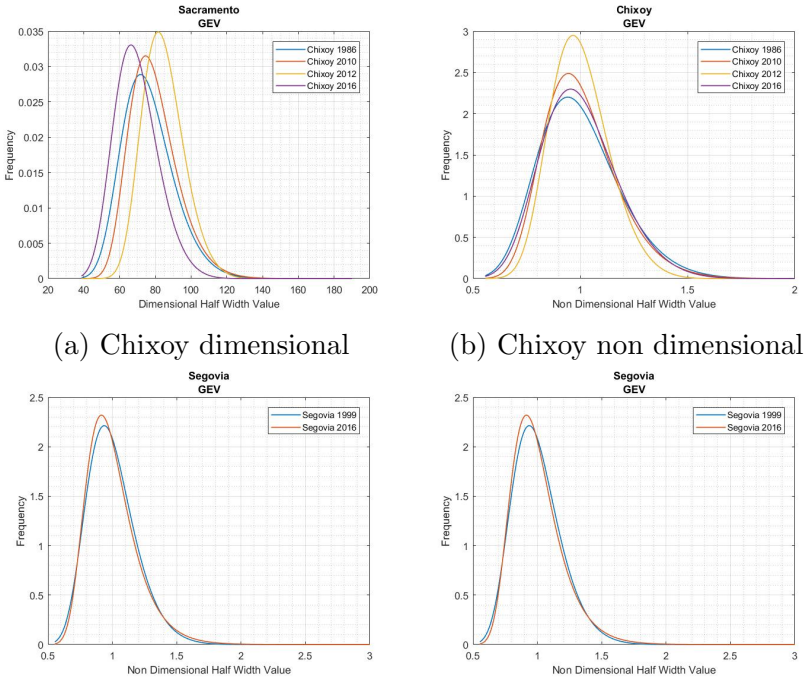


(a) Chixoy dimensional (b) Chixoy non dimensional

(c) Segovia dimensional (d) Segovia non dimensional

Figure 2.7: Typical examples of the temporal variations experienced by the GEV ptobability density distribution fitted to either dimensional or dimensionaless observed half channel widths.

The results of the analysis, applied to GEV distributions corresponding to different years, are reported in Table A.20. It appears that just in the case of the Sacramento river values below 0.97 are observed. Remarkably, the lower values of BC (and, consequently, the higher values of BDC) are attained between the configurations before and after chute cutoff events and in general with the configuration after the event, while for the rest of the years under analysis the BC and BDC coefficients suggest a relatively high degree of similarity. A much-closed degree of similarity is observed when analyzing the dimensionless width data. This trend, once again, is more evident in the case of the Sacramento River.

### 2.3.3 Case study Ucayali river

As mentioned in Section 2.3.2, the Ucayali river has been treated as a particular case study. This choice is due to two main factors. Firstly, the

Ucayali river is subject to a low level of human interventions: no significant hydraulic structures exist that can interfere with the natural evolution of the river (Ettmer and Alvarado-Ancieta, 2010), even if a chute cutoff has been artificially induced (Abizaid, 2005; Coomes et al., 2009). Secondly, detailed geometrical information about the river course is available in RivMAP (see Schwenk et al. (2017)). The Ucayali basin has an approximated area of $350,305\ Km^2$, is located in Perú, and drains part of the upper Amazon basin until joins with the Maranon river, forming the Amazon river. The Ucayali is characterized by a high rate of migration, up to 750 m/y (Wickert et al., 2013; Constantine et al., 2014; Schwenk et al., 2015). Finally, the available information on the Ucayali river accomplish the criteria (a),(b),(c),(d) listed in Section 2.2.

The general statistics of the channel width distributions are reported in Tables A.21 and A.22. The changes in the average width value range from a few meter to almost 50 m from one year to another, with a coefficient of variability of around 30% for almost all the considered years. The standard deviation and the kurtosis values are out of the ranges typical of a normal probability density distribution.

The fluctuations experienced by the river width (Figure 2.8) are better appreciated when considering the dimensionless half width distributions (Figure 2.8b). Of particular interest is the year 2007, when a lot of high values are observed. In this year the reach where subject to important elongation rates and, consequently, experienced high migration rates, presenting the most significant difference between the erosion and the accretion rates (Schwenk et al., 2017). This could be related with the neck cutoffs occurred in the years 2005 and 2006, that had a length of around 28 and 9.6 kilometers, respectively (Schwenk and Foufoula-Georgiou, 2016).

In order to establish if the width fluctuations experimented a long time have a statistical significance or not, an ANOVA analysis (Section 2.3.2) has been carried out. The results indicate that there is a statistically significant difference between the means of the 32 annual configurations of the Ucayali river at the 5% significance level. The results of multiple range tests are shown in Table 2.5. The Tukey HSD and Bonferroni tests are represented with the lighter color, the Sheffe tests with the darker color. Of the 496 possible couples through all the 32 years ($C_{32}^2$ combination without repetitions), only those that do not present a statistically significant difference are considered. The Tukey HSD and the Bonferroni test detected the same 57 couples, while the Sheffe test detected 107 couples. Nonetheless, in both cases, there

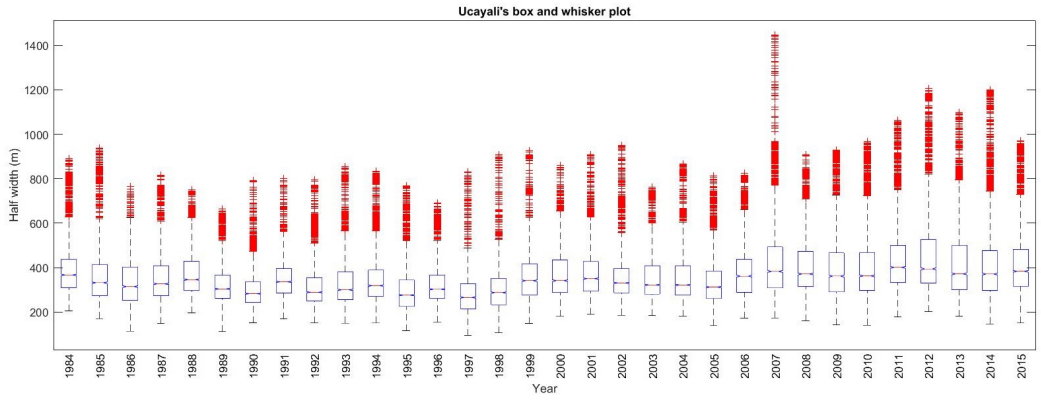


(a) Dimensional

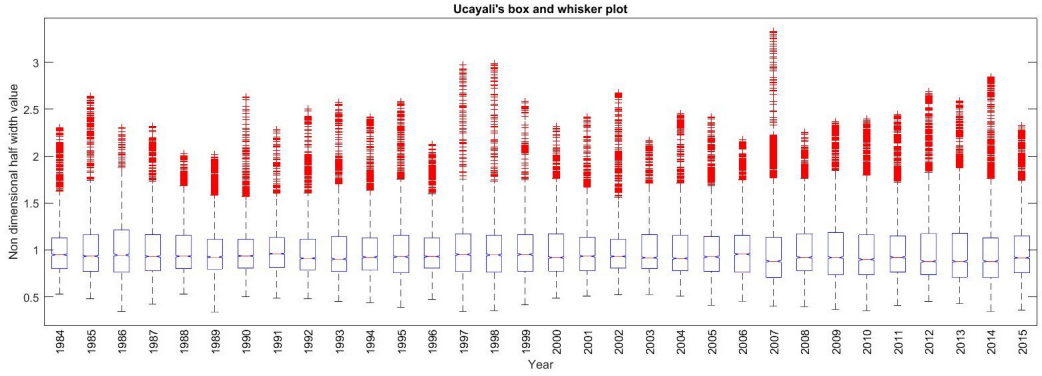


(b) Dimensionless

Figure 2.8: Notched box and whisker plot computed for the along channel distributions of the dimensionless half width data observed at different years in the Ucayali river.

is a clear difference in the data before and after 2006. Note that, on the basis of the Sheffe test, the year 2005 is the one with the bigger number of couples without a difference, followed by the years 1985 and 2004. The other two tests give similar results, with the greatest number couples in the years 1985, 1987, 2004.

The results of the statistical tests concerning the variance are shown in Table A.23, reporting the outcomes of the Bartlett and Levene tests with the same couples that do not have a statistically significant difference in terms of variance. In both tests the P value is less than 0.05, implying that there is a statistically significant difference between the river variances observed

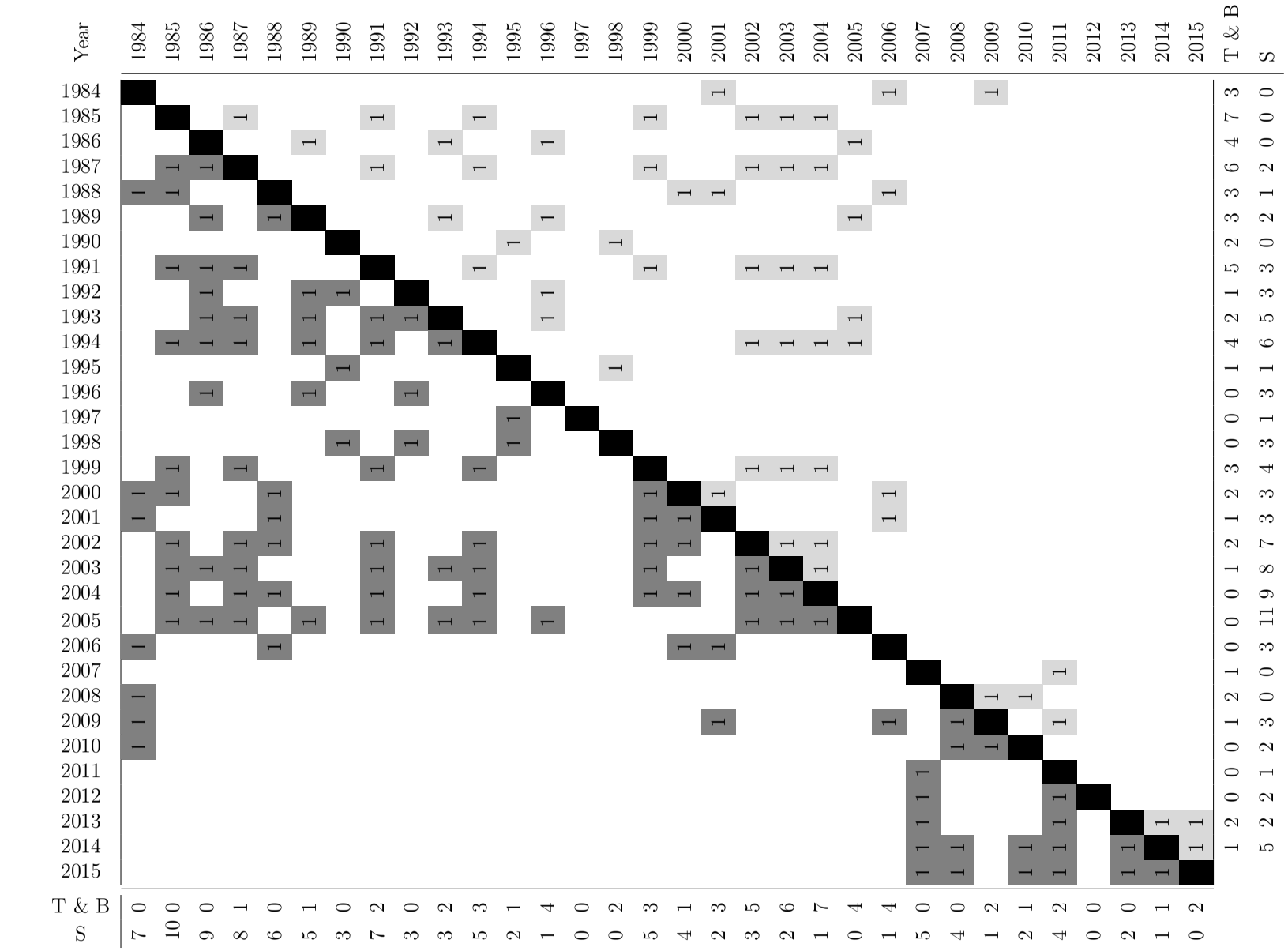

Table 2.5: Results of the multi range tests for evaluating the mean differences in the Ucayali river. Notations are as follows: T, Tukey HSD test; S, Scheffe test; B, Bonferroni test. The number indicates the amount of pairs that show no statistically significant differences).

in the various years. When considering the single couples, 65 do not exhibit a difference regarding both variance and mean. The analysis highlights the existence of two groups of data, before and after 2006. The year 1984 is that presents more couples without differences, followed by 2005.

The Mood's median test gives a P value lower than 0.05, implying the existence, in terms of groups of statistically significant differences among the various river configurations. The Kruskal Wallis test for the median difference (see Table A.24), indicate that there are 68 couples that do not present a statistically significant difference between the medians. In terms of medians, it is much more difficult to single out two different groups of data before and after 2006. The year 1997 does not show any single match with the other years, while the years that yields the more significant number of matching couples are 1986, 1988, 2004.

Table A.25 and Figures A.8 and A.9 show that, once again, the GEV is the probability density function which ensures the best fitting (for 30 of the 32 planform configurations observed in the various years). Even in the two years for which the GEV does not yield the best fitting, the differences with the optimal PDF are quite small. For example, in 1997 the GEV gives the second best fit, but the differences are less than 0.05% when considering dimensional half-width data. Note also that, in this case, the dimensional data present a better fit than the dimensionless data, unlike what has been observed for the other river configurations.

Once verified that the GEV could be used as general PDF for the Ucayali river, an analysis has been performed on the changes among the 496 possible couples of years through all the 32 years. A visual inspection of Figure A.10 suggests that the dimensionless data show a more compact group of PDF shapes. Anyway, apparent differences can be detected among the various years. The BC and BCD indexes, reported in Table A.26 for both dimensional and dimensionless quantities, indicate that the lower similarity is attained for the years 1997 and 2012 for the dimensional data and in years 1988 and 2014 for the dimensionless data. Conversely, it is difficult to single out the years for which the PDF's shows a higher similarity. Anyway, Figure A.11 suggest the presence of two different groups of configurations, before and after 2006, for the group of higher valuer of BC (best case) in the dimensional form there are two groups one before and one after 2006, a behavior similar to one of the measures of central tendency. Nevertheless, this behavior does not befall in the dimensionless form; this can be related to the location and scale parameters of the GEV.

As far as the years that present the lower similarities are concerned, the lower $BC$ value (=0.752) is observed between 1997 and 2012 for dimensional data and between 1988 and 2014 for dimensionless data ($BC = 0.936$). Some critical morphological changes occurred in the river during these years. The biggest was in 1997 and consisted of a human-induced chute cutoff that cuts a 72 km bend, just a few kilometers downstream the investigated river reach. Also during 2012, there was a chute cutoff, in this case of natural origin, which involved relatively short river segment ( 11 Km). Consequently, the changes experienced by the river width are less substantial than those attained after the 1997 cutoff but still significant. Indeed, according to the general statistics in 2012, the second biggest width value was registered. Note that this extreme value and the one resulting in 2007 should be analyzed carefully since the corresponding Landsat images are not so apparent with reference to the river path. At one bend the river appears to re-enter into an old channel and is not possible to define the correct river width in this part. Consequently, some outliers could have been introduced in the dataset.

## 2.4 Discussion

The comparison among along channel distribution of dimensionless half-width values from all the rivers suggests similar behavior in their general statistical values, with a relatively low number of data that tend to depart from the general tendency. This behavior is depicted in different box and whisker plots. The outlier analysis confirms this trend, in particular when was consider a not normal probability density distribution (e.g., the GEV distribution).

One of the more remarkable aspects of these findings is that they apply to an extensive set of rivers all around the world, selected from tropical to high latitudes and, therefore, is characterized not only by different river configurations but also by different hydrological regimes, different land uses, a different type of soils. Consequently, the present study is deemed to entail a wide range of applicability.

In particular, the present results suggest that the GEV is the PDF that more frequently better describe the half-width data (Figure 2.9). Indeed, only for two out of the 26 rivers and 65 configurations investigated, the GEV distribution does not ensure the best fitting. These two rivers do not present any particular different feature with respect to the other rivers, except the

fact that they are located almost at the same latitude. Nevertheless, some other rivers, for which the GEV yields the best fitting, are present at similar latitudes.

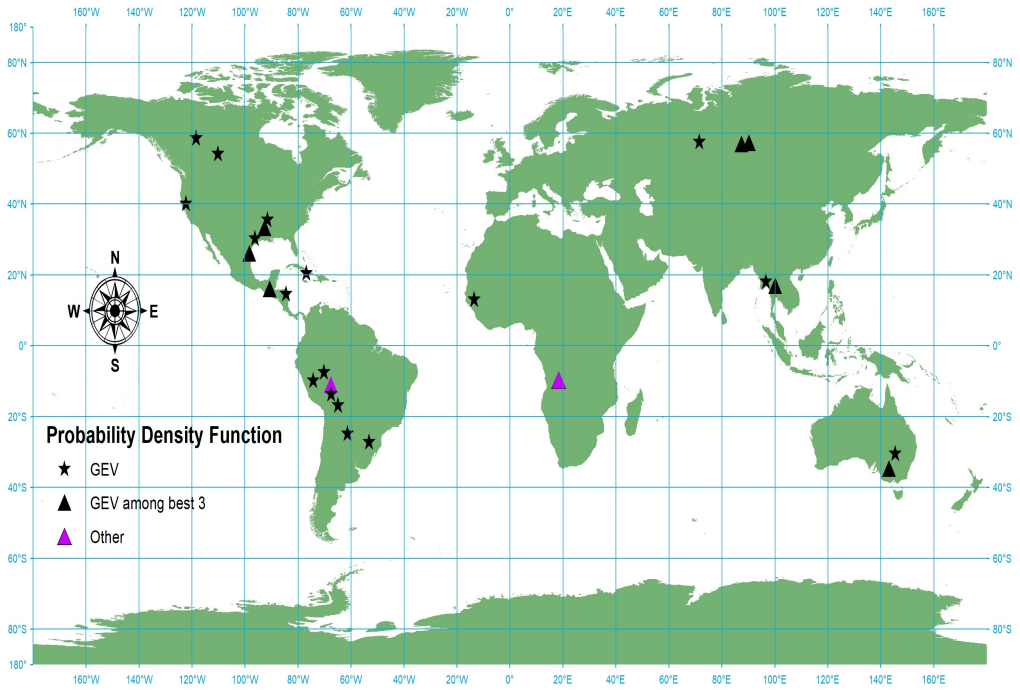


Figure 2.9: Location on the world map of the investigated rivers. The stars indicate rivers in which the GEV provides the best or second best fitting PDF; back triangles denote rivers in which the GEV is among the best three fitting PDF.)

It is also remarkable what the statistics reveal about the evolution of river width through time, especially in the case of the Ucayali river for which a significant amount of information is available. In general, the mean channel width does not remain constant in time. The fluctuations with respect to the mean value appear to be significant from the statistical point of view. Reinforcing in this way, the use of a model with variable width. Anyway, the statistics change through time, and it appears that a given river tends to modify its state continuously in time around some specific interval, such that the differences between two different configurations are not of statistical significance in terms of river widths (see Tables 2.5, A.23, A.24).

These findings suggest the use of a variable width when modeling the long-

term evolution of meandering rivers. The cross-section width of given river tends to vary in a relatively limited range of values, oscillating through them. During these oscillations, the couples of years with no statistical significance are not consecutive (in most of the cases). This behavior could be associated with the morphological changes in river platform.

The GEV distribution turns out to provide the best fit of width data even if the width distribution tends to evolve in time. Even though the three parameters controlling the GEV shape change from year to year, the statistical distances between each distribution keep relatively limited, thus implying an almost complete similarity of the distributions. Significant variations in the GEV parameters are however observed during periods in which significative morphological changes happen inside or nearby the studied river reach. However, a few years after each significative planform modification, the GEV parameters tend to recover the pre-change values. The most prominent similarities between different years do not follow a specific trend; in the case of the worst similarity values, two specific years exist in which those values repeat.

A particular limitation of the study is related to the choice of the effective river width. Even if all the Landsat images were taken in the absence of clouds and during the rainy season, to capture the bank-full width, in some bends it was particularly complicated to estimate reliably the channel width. This is because, on the one hand, during floods, the point bars at the inner bend are submerged by the flow cover. On the other hand, even having an image during small discharge is not possible to define the effective width, due to the lack of depth information. A clear example of these difficulties is represented by the case of the Ucayali river, for which the extraction procedure was made almost automatic by means of the computational code by Schwenk et al. (2017). Figure 2.10 gives an idea of the effect of floods when estimating the superficial cross section river width.

Finally, it can be stated that the more reliable width data are obtained when along with the investigated reach:

1. no important changes in the river slope occur;
2. the discharge remains almost constant;
3. there are not important tributaries;
4. the number of the section that can be surveyed is large enough.

All these factors, are needed to represent efficiently and reliably the along channel width distribution in terms of a suitable PDF, like the GEV.

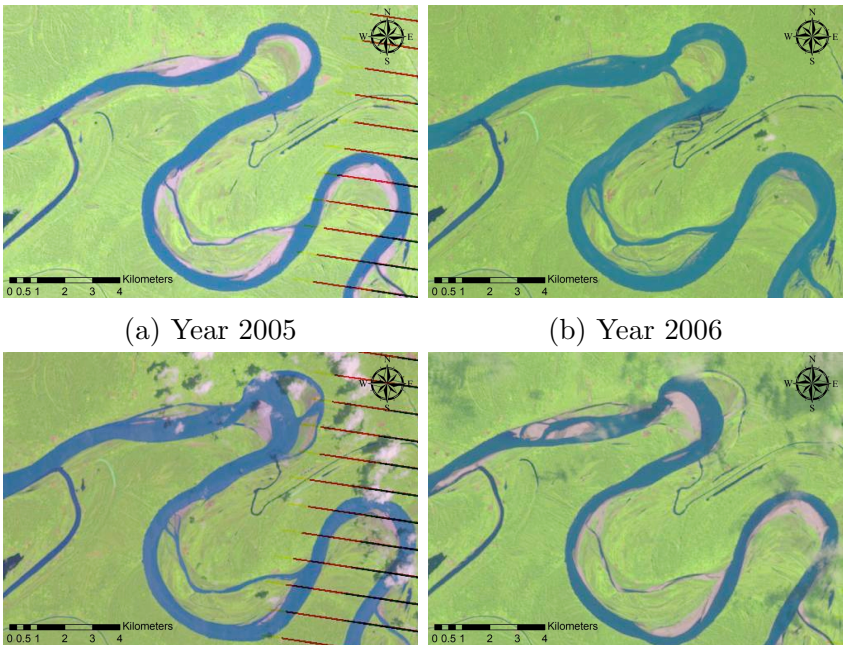


(a) Year 2005 (b) Year 2006

(c) Year 2007 (d) Year 2008

Figure 2.10: Typical examples of Landsat images of superficial width changes due to floods.

## 2.5 Conclusions

This chapter focused on the statistical behavior of the along river distribution of cross section width, considered for different rivers and, for a given river, considering different years. A number of statistical measures have been computed and tested to clarify if the observed changes in width river are statistically significative and can be explained by a simple statistical model.

The statistical analyses carried out in the present chapter, which was mainly concentrated on the widths values. Highlighted: the widths variance cross space for a specific river configuration is great enough to discard the mean width value as representative width values. This is confirmed by the box plot graphics and the variance coefficients.

Similar behavior was observed during the meander evolution, where mean width value experiment statistical significance changes across time. However, the average width value eventually returns to previously observed values. Suggesting in this way, that these fluctuations could be part of a hysteresis cycle.

There is a sort of "signature" in the along river distribution of cross-section width specific for each river. This distribution, in general, does not vary appreciably in time, except when the river undergoes significant morphological changes such as those due to the occurrence of cutoffs. The along channel distribution can then be represented by a probability density function (PDF). According to the Bayesian Information Criterion, it is the General Extreme Value (GEV) distribution that better fits the observed data distributions.

After the modification suffered due to a significant morphological change, the GEV slightly tends to progressively recover a configuration similar to one that had before the event.

All these conclusions can be applied in meandering rivers that do not present important changes in discharge or slope (among other factors), as usually assumed in available meandering evolution models (e.g., Ikeda et al. (1981), Frascati and Lanzoni (2010), Motta et al. (2014)).

# Chapter 3

# Meandering evolution and width variation: a physics-statistical based modeling approach

## 3.1 Introduction

A meander consists of a series of alternate bends connected at the points of inflection by short, almost straight crossings. Meandering rivers are in general single channels with a sinuous platform (Hooke, 2013) that form as the result of stream bed instability, in particular when instability affects the river banks (Dey, 2014). They are one of the most common rivers in the world, that can be found in many different environments and even in the bottom of the ocean. Meandering rivers provide the habitat for many different species and are an essential water resource for humans. As a consequence, the time changes (of natural origin, or due to humans interventions) experienced by this kind of rivers have great importance and make the study of meandering rivers a crucial field (Luchi et al., 2010).

During the last decades, the study of meanders has fascinating the scientific community, not just for their importance, but also because of their complexity, allowing a better understanding of meandering rivers (Güneralp et al., 2012). Many theories have been proposed to understand the devel-

opment meanders. One of the most popular is the instability concept (Dey, 2014) that describe meanders as products of bend instability (Ikeda et al., 1981). Based on this approach, we considered meanders as a dynamic system that migrates and evolve along a floodplain as a consequence of complex interactions involving the channel forms, flow, and sediment transport (Seminara, 2006).

With the aim of understanding meander rivers, different models have been developed for the simulation and explanation of the meander evolution. These models analyze the hydraulics of the in-channel flow and the river bank movement (driven by erosion/accretion processes) in different ways (Camporeale et al., 2007). In particular, the hydraulic of meandering channels is a complex process that entails three-dimensional helicoidally flow structures whose study, in principle, requires the use of 3D models. Nevertheless, especially with reference to long-term river evolution, the flow field has been analyzed with simplified models (quasi-2D) ensuring reasonable computational costs.

Most of the simplified models for the in-channel hydraulic of meandering rivers are derived through linearization and dimensional analysis. These models have good accuracy and a low computational coast making them ideal for long-term simulations. Among these models, one of the most accepted and diffuse model is the Hasegawa, Ikeda, Parker, and Sawai (HIPS) model (Parker et al., 2011), which makes use of a relation between the variations of velocity due to the streamwise curvature and the central channel migration (Ikeda et al., 1981). More refine models have been also developed (e.g., Johannesson and Parker (1989); Odgaard (1990); Sun et al. (1996); Seminara et al. (2001); Frascati and Lanzoni (2009)); a review and a comparison among some of them can be find in Camporeale et al. (2007). However, all these models have the limitation of assuming a constant width and a simplified river bank movement.

Considering the advantages and limitations embodied by simplified models, this chapter implements a simplified model that solves the in-channel hydraulics considering possible width variations and a physics-based model for the river bank movements. The chapter is dived in four sections: the first explains the basis of the hydraulic model; the second section describes the river bank model and discusses the process of erosion and accretion that affect the meander evolution; the third part proposes a statistical-based approached to link the river bank movements; the fourth presents the application of the model to a case study and, finally, discusses the results and presents the most

relevant conclusions.

## 3.2 Hydraulic Model

The considered in-channel hydraulic model is that developed by Frascati and Lanzoni (2013). It consists of a steady flow model, that is linearized for the momentum and mass conservation equations and parameterized for the centrifugally induced secondary flow. The linearized equations are solved perturbatively, taking advantage of the small curvature ratio, and the small width variations with respect to the mean often observed in meandering rivers. The relatively low computational cost required by the solution of the resulting set of equations makes the model suitable for long-term meandering simulations (Camporeale et al., 2007; Frascati and Lanzoni, 2009).

In order to simplify the analysis, an orthogonal intrinsic reference system $(s^*, n^*, z^*)$ is considered (see Fig A.3), defining the longitudinal (streamwise) coordinate, coinciding with the channel axis, the lateral coordinate, orthogonal to the channel axis, and the vertical coordinate, pointing upward. Hereafter a $^*$ indicates dimensional quantities. In the application of

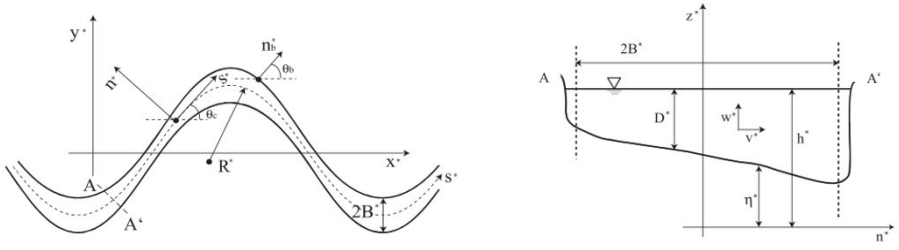


(a) Planimetric configuration.

(b) Cross section.

Figure 3.1: Coordinate system based on the river path and width.

the perturbation method techniques, it is, however, convenient to work with

dimensionless quantities, namely (Frascati and Lanzoni, 2013):

$$
\begin{aligned}
(B^*, s^*) &= B^*_{avg}\,(B, s) && (3.1)\\
(n^*) &= B^* n && (3.2)\\
(u^*, v^*, w^*) &= U^*_u\,(u, v, {}^{w}\!/_{\beta_u}) && (3.3)\\
(D^*, h^*, z^*) &= D^*_u\left(D, F_u^2 h, z\right) && (3.4)\\
(\nu^*_T) &= \nu_T\sqrt{C_{fu}}\,(U^* D^*) && (3.5)\\
(q^*_s, q^*_n) &= \sqrt{g d^*_s\,(\rho_s - \rho)\,/\rho}\, d^*\,(q_{s,n}) && (3.6)
\end{aligned}
$$

where $B^*$ is the half width, $B^*_{avg}$ is the reach averaged half width, $C$ is the axis curvature, the left hand side (LHS) of equation (3.3) is the velocity vector (averaged over turbulence), $D^*$ is the local flow depth, $h^*$ is the free surface elevation, $\nu^*_T$ is the turbulent eddy viscosity, the LHS of equation (3.4) represent the sediment flux per unit width, $g$ is the acceleration due to gravity, $\rho$ and $\rho_s$ are water and sediment density, respectively, $d^*$ is sediment grain size, $C_{fu}$ is the friction coefficient, $\beta_u = \left(B^*_{avg}/D^*_u\right)$ is the aspect ratio of the channel and $F_u$ is the Froude number. The subscript $u$ refers to properties of uniform flow in a straight channel having constant width $2B^*_{avg}$.

Substituting the dimensionless variables into the steady Reynolds equations for longitudinal and transversal momentum yields:

$$
\begin{aligned}
NuL_b u + B^{-1} v u_{,n} + w u_{,z} + N\nu C u v &= -N\,(L_b h - \beta C_{fu}) \\
&\quad + \beta_u\sqrt{C_{fu}}\,(\nu_T u_{,z})\,_{,z} && (3.7)\\
NuL_b v + B^{-1} v v_{,n} + w u_{,z} + N\nu C u^2 &= \beta^{-1} h_{,n} + \beta_u\sqrt{C_{fu}}\,(\nu_T v_{,z})\,_{,z} && (3.8)\\
NL_b u + \left(N\nu C + B^{-1}\frac{\partial}{\partial n}\right) v + w_{,z} &= 0 && (3.9)\\
NL_b q_s + \left(N\nu C + B^{-1}\frac{\partial}{\partial n}\right) q_n &= 0 && (3.10)
\end{aligned}
$$

where a comma indicates partial derivative. In these equations, $C$ is the dimensionless channel axis curvature and $\nu$ is the curvature ratio:

$$
\begin{aligned}
\nu &= \frac{B^*_{avg}}{R^*_0} && (3.11)\\
C\,(s) &= \frac{R^*_0}{R^*\,(s^*)} && (3.12)
\end{aligned}
$$

with $R^*_0$ is some characteristic value of the radius of curvature $R^*$ of the channel axis (normally taken as the minimum value for meandering rivers).

Moreover,

$$\frac{\partial \theta_c}{\partial s} = -\nu C(s) \tag{3.13}$$

$$N = \frac{1}{1+\nu n B C} \tag{3.14}$$

$$L_b = \frac{\partial}{\partial s} - \frac{n}{B} B_{,s} \frac{\partial}{\partial n} \tag{3.15}$$

where $\theta_c$ is the angle that the local tangent to the channel axis forms with a given reference axis $x$, $N$ is a longitudinal metric coefficient, and $L_b$ is a differential operator.

At the leading order of approximation, the depth-averaged shallow-water equations governing the morphodynamics of meandering channels with variable width results:

$$(UU_{,s} + VU_{,n}) + H_{,s} + \beta_u \frac{tau_s}{D} = \delta f_{01} + \nu f_{10} \tag{3.16}$$

$$(UV_{,s} + VV_n) + H_{,n} + \beta_u \frac{\tau_n}{D} = \delta g_{01} + \nu g_{10} \tag{3.17}$$

$$(DU)_{,s} + (DV)_{,n} = \delta m_{01} + \nu m_{10} \tag{3.18}$$

$$q_{s,s} + q_{n,n} = \delta n_{01} + \nu n_{10} \tag{3.19}$$

where $\tau_s$ and $\tau_n$ are the longitudinal and transverse components of the bed shear stress, $f_{ij}, g_{ij}, m_{ij}$ and $n_{ij}$ are constant coefficients and $\delta$ is the intensity of width variability along the stream wise direction, define as:

$$\delta = \frac{B_0^* - B_{avg}^*}{B_{avg}^*}, \tag{3.20}$$

with $B_0^*$ some characteristic value of the half width $B^*$ of the channel (normally taken as the maximum value in the meandering reach).

The set of equations ((3.16)) - ((3.18)) is subject to the physical requirements that channel walls are impermeable to flow and to sediment flux. These constrains can be expressed as:

$$-UB_{,s} + V = 0 \qquad -q_s B_{,s} + q_n = 0 \qquad (n = \pm 1) \tag{3.21}$$

Finally, using equations ((3.11)), ((3.20)), equations ((3.16))- ((3.18)), the constraints ((3.21)), and expanding the solution in powers of the small perturbation parameters $\nu$ and $\delta$, yields:

$$\begin{aligned}(U, V, D, H) = {} & (1, 0, 1, H_0) + \delta(u_b, v_b, d_b, h_b) \\ & + \nu(u_b, v_b, d_b, h_b) + ...\end{aligned} \tag{3.22}$$

where $H_0 = 1 - \beta C_{fu} s$ while $(u_b, v_b, d_b, h_b)$ and $(u_b, v_b, d_b, h_b)$ are the perturbations associated with channel axis curvature and channel width variations, respectively. The perturbation expansion is applied also to the friction coefficient $C_f$, the dimensionless bed shear stress (i.e., the Shields parameter) $\tau_*$, and the intensity of the sediment transport $\Phi$, namely:

$$C_f = C_{fu}\left(1 + \nu C_{f1} + \delta C_{f2}\right) \tag{3.23}$$

$$\tau^* = \tau_u^*\left(1 + \nu \tau_1^* + \delta \tau_2^*\right) \tag{3.24}$$

$$\Phi = \Phi_u\left(1 + \nu \Phi_1 + \delta \Phi_2\right) \tag{3.25}$$

where the subfix $u$ denotes to the uniform flow values of the considered variables.

A set of perturbed equations is eventually obtained at each order of approximation by substituting expansions ((3.22))-(3.25) into the governing 2-D dimensionless equations ((3.16))-((3.18)). Note that the perturbed equations include local values of the channel width and the channel axis curvature and, therefore, describes both the laterally antisymmetric flow field due to the channel curvature and the laterally symmetrical pattern due to width variations.

The model, owing to its linearized character, has obviously some limitations. Its correct applicability requires are (Bolla Pittaluga and Seminara, 2011; Frascati and Lanzoni, 2013): (a) the free vortex effect due to river bending is small and, consequently, the longitudinal metric coefficient $N^{-1}$ does not differ significantly from one; this requires that the dimensionless parameters $\nu$ and $\delta$ should be small; (b) the secondary flow due to the bar-pool topographic pattern is small; this is achieves in long enough bends ensuring a small value of the intrinsic meander wave number ($\lambda_c$) which means long bends; (c) the centrifugally driven secondary flow is also small, a requirement that implies small values of $\nu/\left(\beta_u\sqrt{C_{fu}}\right)$; (d) the bed perturbations with respect to the the uniform flow depth should be small for linearization be valid, a small, a condition fulfilled when the maximum values of $\nu\sqrt{\tau_u^*/C_{fu}}$ and $\lambda\beta_u\sqrt{\tau_u^*}$ are small.

As far as the input data are concerned, the model requires: (a) the planimetry of the river banks and of the channel axis, to obtain for each cross section the curvature and width variation along the $s$ axis (the distance between consecutive cross sections should not be bigger than the average width); (b) the water discharge; (c) the average longitudinal bed slope of the river under analysis; (d) the characteristic sediment grain size $d^*$. Based on these data the following dimensionless parameter are computed:

(a) the aspect ratio of the channel; (b) the dimensionless sediment grain size $d_s = d^*/D_u^*$; (c) the Shields parameter for the reference uniform flow; item the particle Reynolds number. For further details of the model see Frascati and Lanzoni (2013).

## 3.3 River Bank model

Traditionally, the model proposed by Ikeda et al. (1981) for the displacement of the river centerline (equation (3.26)), has been widely used in modeling meander migration. This equation reads:

$$\xi = E\Delta U \tag{3.26}$$

where $\xi$ denotes the rate of meander migration for a particular cross section, $E$ is a bank erosion coefficient, and $\Delta U$ is the differences between the depth-averaged near-bank velocity and the cross section averaged velocity.

It appears that this model proposes a linear relation between the in-channel velocity and the coefficient of bank erosion. This dimensionless coefficient requires a field calibration and generally depends on different soil and morphometric parameters (Constantine et al., 2009). Even if this formulation seems to mimic reasonably the behavior of natural meanders, it is very simplified. Indeed, the erosion of the outer bank and accretion of the inner bank are simply lumped in the coefficient $E$ and, consequently, the channel width keeps constant as the river migrates. In recent years, many researchers (i.e. Nagata et al. (2000); Darby et al. (2002); Darby and Delbono (2002); Chen and Duan (2006); Motta et al. (2012); Eke et al. (2014b,a)) were thus motivated to improve this simplified approach, introducing more physics-based treatments of the problem.

In the following, a relatively simple physics-based approach is developed to describe the river bank evolution, assuming that the erosion and accretion processes are activated independently, depending on two different shear stress thresholds. An overlapping region is also prescribed, in which neither erosion nor deposition dominates, but a transportation regime takes place, as depicted in the scheme of Figure 3.2.

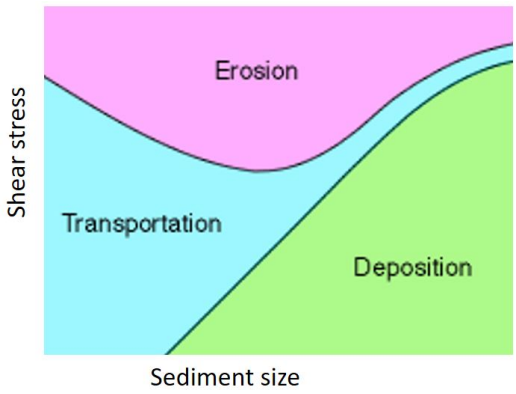


Figure 3.2: Bank erosion and deposition processes as a function of the bed shear stress and the sediment grain size.

### 3.3.1 Erosion

The erosion rate at the outer bank is estimated through an excess threshold linear formula of form (Darby et al., 2002; Motta et al., 2012):

$$\xi_E^* = M_E^* \left( \frac{\tau^* - \tau_c^*}{\tau_c^*} \right) \tag{3.27}$$

where $\xi_E^*$ is the erosion rate, $M_E^*$ is the dimensional erosion rate coefficient, $\tau^*$ is the near bank shear stress, and $\tau_c^*$ is the critical shear stress threshold over which erosion occurs.

Many different approaches exist to estimate when sediment particles begin to be entrained by a flowing current. The threshold of incipient sediment movement can be in general expressed by considering either the flow velocity (Yalin, 1963; Beheshti and Ataie-Ashtiani, 2008; Simoes, 2014) or the bed shear stress. In this latter case, the proposed relations are of empirical (Kramer, 1935) or semi-empirical (Shields, 1936; Brownlie, 1981; Van Rijn, 1984; Soulsby and Whitehouse, 1997; Parker et al., 2003, 2011) origin. Probabilistic and turbulence-based approaches (Dey, 1999; Ali and Dey, 2016) have been developed as well (see., e.g., the review by Dey and Papanicolaou (2008)). A list of the main relationships predicting the critical shear steers for erosion is reported in the Appendix B. Among these relationships, that used in the present research is that of (Dey, 1999), which relates the critical shear stress for erosion $\tau_c^*$ to the characteristic grain size $d$ (e.g., the mean

diameter) through the relation:

$$\widetilde{d} = Re_p \left( \frac{\hat{d}}{\tau_c^*} \right)^{0.5} \tag{3.28}$$

where $\widetilde{d}$ is a particle parameter expressed as:

$$\widetilde{d} = d \left( gd \left( \rho_s - \rho \right) / \rho \right)^{0.5} / \nu, \tag{3.29}$$

$Re_p$ is the particle Reynolds number:

$$Re_p = \frac{\sqrt{\left[ \left( \rho_s - \rho \right) / \rho \right] gd} d}{\nu} \tag{3.30}$$

and $\hat{d}$ is a particle parameter expressed as:

$$\hat{d} = \frac{2 \tan \phi \left[ 6 \tan \phi + \left( 48 \tan^2 \phi + 27 \right)^{0.5} \right]}{4 \tan^2 \phi + 9} \tag{3.31}$$

Moreover, here $g$ is the acceleration due to gravity, $\rho_s$ is the density of the sediment, $\rho$ and $\nu$ are the density and kinematic viscosity of water, and $\phi$ is the angle of repose of the sediment.

These equations are applicable for non-cohesive material, that is the most common bed material in meandering river banks. However, the banks of many rivers have an upper much cohesive layer generated by floodplain evolution through the deposition of fine silts and clays. This layer is often encroached by vegetation that tends to counteract grain by grain erosion (Lagasse et al., 2004).

### Slump block failure

The failure of the upper, highly cohesive soil layers forming the river banks occurs mainly for planar and cantilever mechanisms (Motta et al., 2012) and leads to the formation of slump blocks, which protect from erosion the bank toe (Parker et al., 2011; Motta et al., 2012, 2014; Eke et al., 2014b,a). Slump blocks, in fact, the shift of the local high streamwise velocity away from the bank (Kean and Smith, 2006a,b) thus leading to a reduction of the shear stress acting on the bank toe. Even if the behavior of submerged slump blocks is complex, due to their size and orientation that can even increase erosion

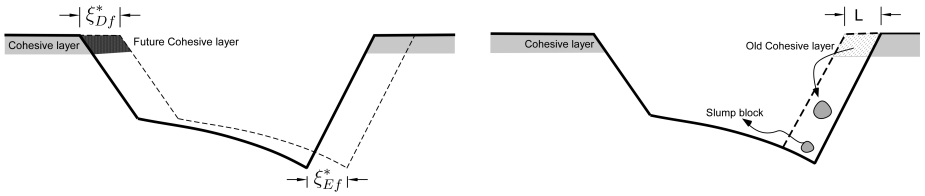


(a) River bank displacments. (b) Slump block generation.

Figure 3.3: Displacement of river banks and the slump block generation.

during a certain part of their life (Hackney et al., 2015), in the following only the armoring effect is considered (see Fig. 3.3).

Many different methods have been proposed to determine the stability and possible failures of bank slopes. The most common methodology, adopted here, is the general limit equilibrium approach (Fredlund et al., 2012). It makes use of a safety factor, defined as the ratio of the resisting forces and momentum acting on the block subject to failure to the corresponding destabilizing forces and momentum. If this factor is less than the unit, the bock remains stable (Darby and Thorne, 1996).

The idealized (trapezoidal) cross section used here to approximate the real channel shape does not allow to simulate planar failures, but only cantilever failures, e.g., through the relation proposed by Langendoen et al. (2009).

$$FS = \frac{\sum_{j=1}^{J} \left( L_j c'_j - P_{w_j} \tan \phi^b_j \right)}{\sum_{j=1}^{J} W_j} \tag{3.32}$$

where $j$ refers to a specific slide of the block to analyze, $J$ is the total number of slides that compose the block, $L$ is the block length, $c'$ is the effective cohesion of the soil, $P_w$ is the pore water force, $\phi^b$ is the angle indicating the increase in shear strength for an increase in matrix suction, and $W$ is the weight of the soil.

The above-defined safety factor is in general sensible to changes in bank geometry and soil proprieties (i.e., heterogeneity of the soil and variation of the soil humidity (Simon et al., 2000)). Here are consider constant.

The armoring effect consequent to slump blocks produced by continuous cantilever failures is accounted for through the approach proposed by Eke

(2013); Motta et al. (2014):

$$\xi_E^* = K_a \xi_{E_{unarmored}}^* \tag{3.33}$$

$$K_a = \exp -c_a A_{Blocktotal}^* \tag{3.34}$$

where $K_a$ is a reduction factor, $A_{Blocktotal}^*$ is the total area of the slump block, $c_a$ is a coefficient that amplifies or reduce the effect of the slump block. This final coefficient should be estimated according to the conditions of each river.

Slump blocks are also subject to erosion effects and, as time passes, their armoring effect on the bank toe decays until a new cantilever failure is produced. The slump block degradation is estimated by applying the relation proposed by Parker et al. (2011):

$$A_{Blocktotal}^* = A_{Block}^* + A_{Blockinitial}^* \exp\left(-\frac{T_{flow}^*}{T_{block}^*}\right) \tag{3.35}$$

where $A_{Blockinitial}^*$ is the area of the slump block a the previous time step, $A_{Block}^*$ is the area of slump block produce by a cantilever failure at the actual time step, $T_{flow}^*$ is the length of the time step which means the duration of the flow, $T_{block}^*$ is the characteristic lifetime of a slump block. Due to the complex of the $T_{block}^*$ is still determine from observed data (Motta et al., 2014). Here a simple approach to determine this value was implemented. Considering $T_{block}^*$ equal to the block length ($L$) divided by half the erosion rate.

### 3.3.2 Deposition - accretion

The accretion of the inner bend is assumed to depend on deposition, described in the relation proposed by Krone (1962) and Mehta and Partheniades (1975):

$$\xi_D^* = w_s C_b \left(\frac{\tau_b^* - \tau^*}{\tau_b^*}\right) \tag{3.36}$$

where $\xi_D^*$ is the deposition rate, $w_s$ is the settling velocity of the sediment, $C_b$ is the sediment concentration near the bed, and $\tau_b^*$ is the critical shear stress for deposition. For the sake of simplicity, $w_s C_b$ is taken as constant. The erosion equation then takes the form:

$$\xi_D^* = M_D^* \left(\frac{\tau_b^* - \tau^*}{\tau_b^*}\right) \tag{3.37}$$

where $M_D^*$ is the dimensional deposition rate coefficient.

The critical threshold for deposition can be assumed as the shear stress for which all the sediment is transported in suspension. Different studies have been made to determine the relation between the shear velocity and the settling velocity of sediment (Bagnold, 1966) and to incorporate this relation into the Rouse equation (Xie, 1981). The particle parameter relations (Van Rijn, 1984), following this line, the works based on the shields Reynolds number (Sumer, 1986; Celik and Rodi, 1991), the probabilistic approach that consider the last approaches (Cheng and Chiew, 1999). A list of the various relationships proposed in the literature to estimate the deposition rate is reported in the appendix B.

In the present context, the probabilistic approach proposed by (Bose and Dey, 2013) has adopted, according to which the dimensionless critical shear stress reads:

$$\tau_b = \frac{Re^2}{\dot{d}^3} \tag{3.38}$$

where $Re$ is the shear Reynolds number given by:

$$Re = \frac{\upsilon_* d}{\nu} \tag{3.39}$$

with $\upsilon_*$ the shear velocity and $\dot{d}$ a particle parameter that could be calculated as either $\tilde{d}$ or (Cheng, 1997):

$$\dot{d} = \sqrt{\frac{1}{1.2}\left(\frac{Rew_s}{\upsilon_*}\right)^{2/3}\left[\left(\frac{Rew_s}{\upsilon_*}\right)^{2/3} + 10\right]} \tag{3.40}$$

The total probability function for threshold of suspension $P_s$ is given by:

$$P_s = \frac{1}{16}\left[16 - \left(\frac{u_*}{\sigma_2}\right)\frac{w_s}{u_*} - \left(\frac{u_*^2}{\sigma_2^2}\right)\frac{w_s^2}{u_*^2}\right]\exp\left[-\left(\frac{u_*}{\sigma_2}\right)\frac{w_s}{u_*}\right] \tag{3.41}$$

where $\sigma_2$ is the root-mean square of fluctuations of the instantaneous flow velocity in vertical direction. According to the empirical formulation of Grass (1971) for hydraulically smooth flow regime:

$$\frac{\sigma_2}{u_*} = 1 - \exp\left(-0.093 Re^{1.3}\right) \tag{3.42}$$

and, consequently, $\sigma_2 \approx u_*$ for large enough values of $Re$.

This probabilistic approach first defines the probability threshold for suspension, set as $P_s = 0.1$ in the present case. Then, the value of $w_s/s_*$ is obtained through equations (3.41) and (3.42). This value is then used to solve equation (3.40), obtaining $\dot{d}$ and, finally, $\tau_b$ by means of equation (3.39).

It should be mentioned that the ratio $u_*/w_s$ defines the mobility number $\Lambda$ (Liu, 1957), a a parameter that can use alternative to the Shields criterion (Shields, 1936) for establishing the particle initiation of motion.

## 3.4 Statistical Method

The simple physics-based approach described in Section 3.3 present some weakness. It tends to become unstable for long-term simulations; produces local problems of widening or narrowing yielding unrealistic width values; has problems to handle cutoff events; does not connect at all bank erosion and bank accretion (Eke, 2013; Eke et al., 2014a,b).

To eliminate these limitations, it is useful to better understand the statistical behavior of width variability. In particular, it is essential to establish how accurate is the assumption of a spatially constant mean river width and if this value changes or not in time. The results of the statistical analyses reported in the Chapter 2, based on observed data, indicate that the average half width can experience significant changes in space and time. The statistical results also suggest that the inner and outer bank movements are somehow related.

The idea is used to model the width values that can be attained by the river with a river-specific probabilistic density function that implicitly accounts for the link between the inner bank accretion and outer bank erosion. Figure 3.4 shows 32 years of observed data from the Ucayali River (see Section 3.6 of this Chapter). The time cycles of erosion and accretion (Figure 3.4a) and the strict relation between them (Figure 3.4b) are evident. A weakening of this interrelation, however, seems to start around the year 1998, likely owing to a massive artificial chute cutoff induced downstream of the considered river reach. Finally, Figure 3.4c indicates that erosion/accretion time cycles are strictly connected (as was expected) to channel width oscillations.

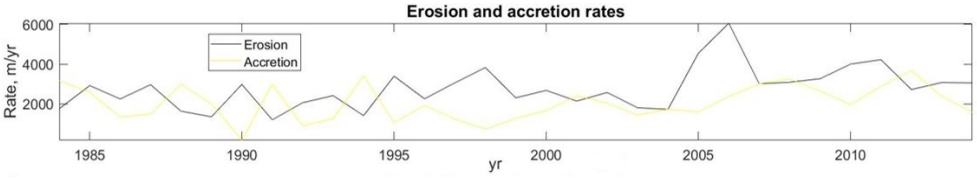


(a) Time distribution of erosion and accretion rates.

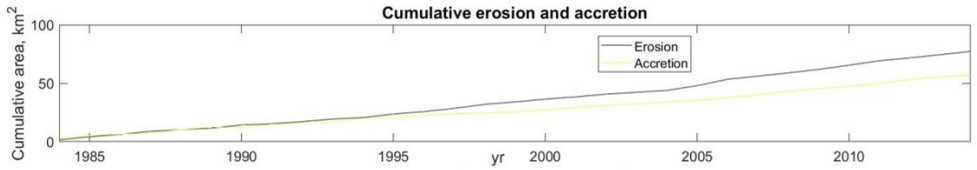


(b) Cumulative erosion and accretion rates in time.

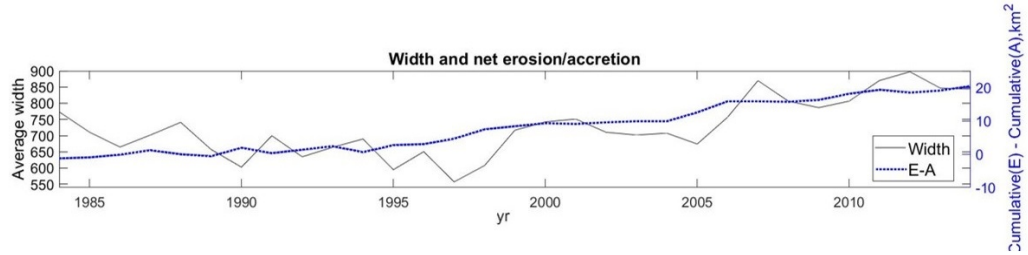


(c) Time distribution of river width and net erosion/accretion.

Figure 3.4: Time distribution of erosion and accretion rates observed in the Ucayali river(graphics from RivMAP see Schwenk et al. (2017)).

### 3.4.1 Statistical corrections

Based on the observational evidence presented so far that outer bank erosion and inner bank accretion are somehow related, a simple statistically-based model is here proposed to control channel width variations as the river migrates through the floodplain.

The cumulative density function (CDF) of the generalized extreme value (GEV) distribution is assumed to describe the spatial and temporal distribution of channel width. The rate of erosion at the outer bank $\xi^*_{Ef}$ and deposition at inner bank $\xi^*_{Df}$ are thus computed as:

$$\xi^*_{Ef} = \xi^*_E * R_{Ecf} \tag{3.43}$$
$$\xi^*_{Df} = \xi^*_D * R_{Dcf} \tag{3.44}$$

where the coefficients $R_{Ecf}$ and $R_{Dcf}$ are computed as:

$$\begin{aligned} &\textit{If } cdf_v \leq 0.5 \\ &\qquad R_{Ecf} = 1 \qquad (3.45) \\ &\textit{If } cdf_v > 0.5 \\ &\qquad R_{Ecf} = 2\,(1 - cdf_v) \qquad (3.46) \\ &\textit{If } cdf_v \geq 0.5 \\ &\qquad R_{Dcf} = 1 \qquad (3.47) \\ &\textit{If } cdf_v < 0.5 \\ &\qquad R_{Dcf} = 2\,(cdf_v) \qquad (3.48) \end{aligned}$$

This statistical approach has to main aims. The first is to connect the two banks, by favoring or restricting the bank movement as a function of the CDF and the mean channel width. The second is to set lower and upper limits to the channel width, thus avoiding extreme, nonphysical width values during the rivers evolution. Equations (3.46) and (3.48) thus frozen the bank retreat/accretion when the width attains values corresponding to one of the two PDF extremes. In this way, the bank movement governed by the physical rules embodied by equations (3.27) and (3.37) is corrected in a statistical sense through equations (3.43) and (3.44).

Figure 3.5 reports an example of application of the present physics-statistical based framework to the Ucayali river. In particular, Figure 3.5a shows the cumulative density function for the dimensionless width, while Figure 3.5b shows how the correction factors $R_{Dcf}$ and $R_{Ecf}$ change on the basis of the GEV probability distribution function. Note the different behavior of these latter two factors resulting from the statistical analysis of channel width data.

## 3.5 Banks displacements

The river axis movements are computed using the relations described in section 3.3.1, and adopting the correction factors introduced in section 3.4.1. The channel centerline is computed as the mean distance between the two banks:

$$\begin{aligned} x_c &= 0.5(x_l + x_r) \qquad (3.49) \\ y_c &= 0.5(y_l + y_r) \qquad (3.50) \end{aligned}$$

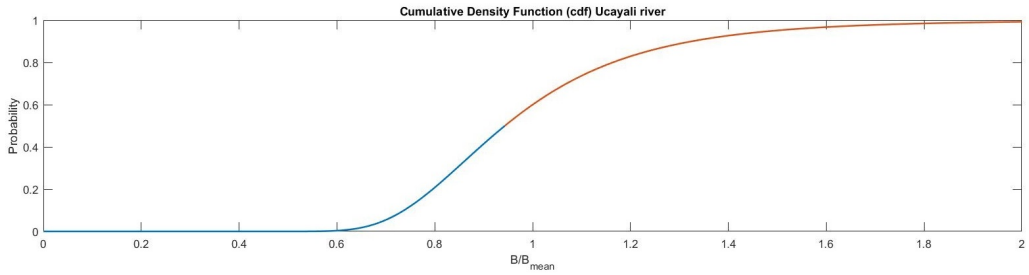


(a) Non dimensional width cumulative density function of the Ucayali river.

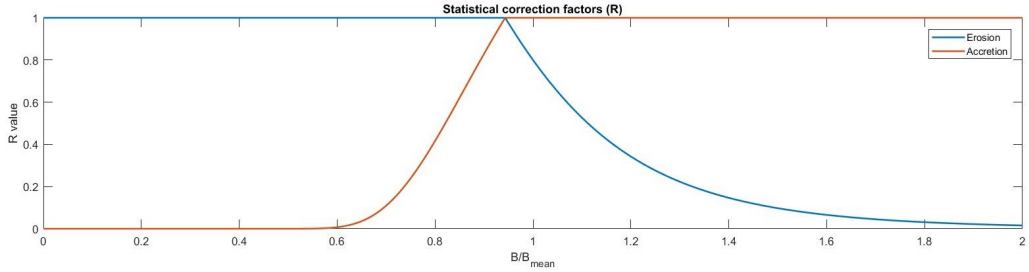


(b) Statistical correction factor.

Figure 3.5: Statistical correction factor based on the width cumulative density function.

At each time step, the bank displacements are determined first computing the erosion and accretion rates ($\xi^*_{Ef}$ and $\xi^*_{Df}$) for each bank. According to the model described in sections 3.3 and, depending on the near bank shear stress, there could be both accretion and erosion. For each bank, the final migration rate ($\xi^*_f$) is given by:

$$\xi^*_{f_{l,r}} = \xi^*_{Ef_{l,r}} - \xi^*_{Df_{l,r}} \tag{3.51}$$

where the sub index $l$ and $r$ refer to the left and right bank, respectively. And the total displacement rate of the central axis turns out to be:

$$\xi^*_f = \xi^*_{f_l} - \xi^*_{f_r} \tag{3.52}$$

Once the total rate of displacement of the channel axis has been computed, a suitable time steep has to be chosen for obtaining the final displacement of each central axis point. Two different cases can occur. The first is related to slump block failures (see Section 3.3.1). In this case, a fixed and small-time steep (one month) is assumed to capture the armoring effects of the slump block. In the absence of slump blocks, a variable time steep is chosen, lower than the threshold that ensures the stability of the computations,

namely:

$$\Delta t \leq \frac{100}{B^*_{avg} \max\left(\xi^*_f\right)} \tag{3.53}$$

$$\Delta t^* = \frac{\Delta t B^*_{avg} \max\left(\xi^*_f\right)}{\max\left(M^*_E, M^*_D\right)} \tag{3.54}$$

Eventually, the displacements of the central axis points are given by:

$$x^j_i = x^j_{i-1} - \sin\left(\theta^j\right) \Delta t_i \, \xi^{*^j}_{f_i} \tag{3.55}$$

$$y^j_i = y^j_{i-1} + \cos\left(\theta^j\right) \Delta t_i \, \xi^{*^j}_{f_i} \tag{3.56}$$

where the sub index $i$ refers to the time steep while the apex $j$ defines the $j-th$ cross section under analysis. Since only the central axis is displaced, the width changes for each cross section are computed as:

$$B^{*^j}_i = B^{*^j}_{i-1} + \frac{1}{2}\left(\xi^*_{f_l} + \xi^*_{f_r}\right) \Delta t_i \tag{3.57}$$

After the new meandering configuration is computed, all the input data to the hydraulic model are updated. By assuming an equivalent uniform flow along a channel of width $B^*_{avg}$, intrinsic length $L^*$, constant discharge $Q^*$, grain size $d^*$, and considering as fixed the elevation at the beginning and end of the channel channel reach (constant $\Delta z^*$) the new average values of the channel slope, the flow depth, and the flow velocity are:

$$S_i = \frac{\Delta z^*}{s^*_i} \tag{3.58}$$

$$D^*_{avg_i} = \left(\frac{C_f {Q^*}^2}{4 B^*_{avg_i} g^* \, S_i}\right)^{\frac{1}{3}} \tag{3.59}$$

$$U^*_i = \left(\frac{g^* Q^* S_i}{C_f \, 2 B^*_{avg}}\right)^{\frac{1}{3}} \tag{3.60}$$

This procedure is repeated at each time steep. When the intrinsic channel length suffer a change bigger than the 10% of its original value (.i.e. abrupt shortening because of a neck cutoff or an elongation due to the channel migration) the position of all the section is recomputed according to a specific distance between cross sections.

## 3.6 Case Study

The model has been tested concerning a specific reach of the Ucayali river. This choice is motivated by two main factors. Firstly, the Ucayali river is subject to a low level of human interventions: no significant hydraulic structures exist that can interfere with the natural evolution of the river (Ettmer and Alvarado-Ancieta, 2010), even if a chute cutoff has been artificially induced (Abizaid, 2005; Coomes et al., 2009). Secondly, detailed geometrical information about the river planform are available in RivMAP (see Schwenk et al. (2017)).

The Ucayali basin is located in Perú and has an approximated area of $350,305\ Km^2$. It forms part of the upper Amazon basin until, after joining with the Maranon river, forms the Amazon river (see Figure 3.6). The Ucayali river is characterized by high migration rates, up to 750 m/y (Wickert et al., 2013; Constantine et al., 2014; Schwenk et al., 2015).


Figure 3.6: Overall map and location of the Ucayali river.

The mean annual discharge is about 6905 $m^3/s$ at the Lagarto gauging station, where the area of the drainage basin is $191,180\ Km^2$. The discharge

increases up to 8675 $m^3/s$ at Pucallpa gauging station, draining an area of 261,070 $Km^2$ (Santini et al., 2014; SENAMHI, 2016). The mean slope of the overall reach is 0.000049 $m/m$, while the slope between Pucallpa and Tiruntan reduces to 0.000033 $m/m$. The mean sediment size $D_{50}$ varies from 0.25 to 0.4 mm (H&O - ECSA, 2005) and, hence, is transported mainly in suspension, with concentration ranging from of 1,260 $mg/L$ at Lagarto to 950 $mg/L$ at Pucallpa (Santini et al., 2014).

As mentioned in Chapter 2, RivMAP provides 32 years of planimetric data (Schwenk et al., 2015). The generalized extreme value (GEV) probability distribution was fitted to the spatial width distributions observed during each of these years. The parameters of the distribution vary from year to year, but can also vary with the along river sampling distance of the cross-section. A sensibility analysis was thus carried out for each temporal configuration, by progressively increasing the cross section interaxis of 10 $m$, starting from 10 $m$ up to 700 $m$, this upper limit being dictated by the mean channel width along the reach.

In total, 2240 configurations (70 per year for the 32 years) have been considered. The different probability distributions have been compared together by computing the Bhattacharyya distance coefficient (BDC) (see Section 2.3.2). The values attained by the BDC index were quite high (generally larger than 0.99), hence supporting the use of a GEV probability distribution to describe the along channel width distribution, independently of the considered year. The BDC values are also quite high when changing the cross-section distance: in the worst case (i.e., for a cross-section distance of 700 m) it takes the value 0.994. In the following, a cross-section sampling distance of 60 m (i.e., double of the Landsat image resolution) is then considered, and the GEV distribution is used to describe any of the observed width distributions.

The temporal interval chose to test the model is that from 1997 to 2007, during which a neck cut of was observed inside the study reach. The mean half channel width is 313 $m$, yielding a width to depth ratio of 30 (Ettmer and Alvarado-Ancieta, 2010). The considered slope, 0.000033 $m/m$, is that between Pucallpa and Tiruntan (H&O - ECSA, 2005), that is the one closer to our study area (see Table A.3). The values of the erosion and deposition coefficients $M_E^*$ and $M_D^*$ are those determined for the observed data, i.e., the mean of the values shown in Figure 3.4a. The resulting mean annual erosion and accretion rates are equal to 215 $m/y$ and 189 $m/y$, respectively. These input parameters were then used to compute $\tau_c^*$, $\tau_b^*$, *cdf* and, eventually, the

$\xi^*_{Ef}$ and $\xi^*_{Df}$ values for each time steep.

Figure 3.7 show the results of the 10-year long simulation, namely the initial (black) and final (blue) observed configurations and the final simulated configuration (grey). Despite the model limitations (i.e., constant discharge, homogeneous sediment and constant floodplain erodibility), the models appear to reproduce with an acceptable degree of approximation the observed river evolution. The biggest discrepancy between observed and computed planforms is obviously attained for the sharper bends, for which the relevant parameters attain values out the interval of applicability of the model (see Section 3.2).

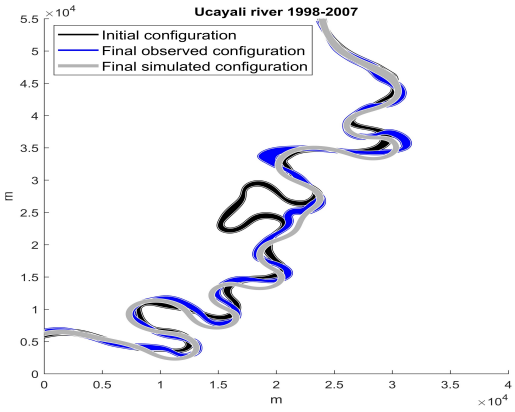


Figure 3.7: Results of a short term simulation of the Ucayali river temporal evolution.

The results of a much longer simulation (7,000 years) are shown in Figure 3.8. The simulation keeps stable, always yielding physically reasonable values of the channel width. The river moves inside the entire meander belt from left to right, leaving behind a large number of oxbow lakes.

A fascinating behavior is that exhibited by the mean half width as a function of the mean slope, depicted in Figure 3.9. These two quantities appear to be strongly correlated: at any change in slope, it corresponds a change in channel width, in some cases with a small time lag (Figure 3.9a). When plotted channel width versus the slope (Figure 3.9b), the channel width follows a concave down trajectory, increasing progressively, attaining a maximum and then decreasing.

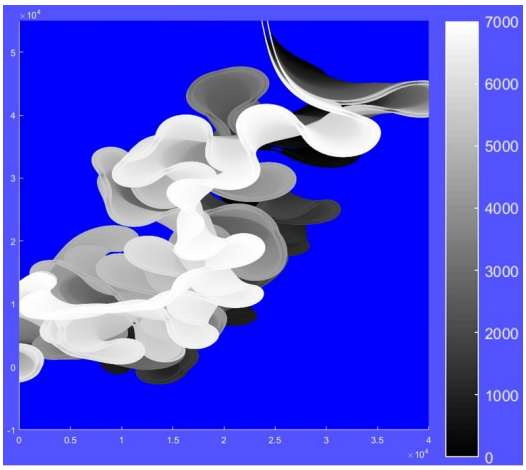


Figure 3.8: Long term simulation (7000 years) of the Ucayali river evolution. The color bar indicates the year of simulation.

## 3.7 Discussion

The results described in the previous section demonstrate that the use of a simple statistical correction, linking the erosion and accretion according to the probability of obtaining a particular width, allows one to obtain stable long-term simulations. This approach, apparently, is unable to reproduce the width values corresponding to both the tails of the GEV distribution. Nevertheless, the model yields realistic values of the mean river width.

Also, the evolution of the channel width as a function of the channel slope, depicted in Figure 3.8, is physically sounding. The channel within computed by considering two different critical shear stresses for erosion and deposition. These shear stresses depend on the velocity which, in turn, depends on the slope. The lower the slope, the lower is the velocity, thus favoring deposition and, consequently, river accretion. This dynamic process is strongly influenced by the occurrence of cutoffs (in the present model just neck cutoff). The shortening of the channel after each cutoff produces a sudden increase in channel slope that, in turn, triggers a readjustment of the channel width to a new, larger mean value. This behavior is well described in Figure 3.10, reporting the $B - S$ trajectories resulting from the simulation (Figure 3.10a) and those determined from the observed data (Figure 3.10b).

Figure 3.10 confirms that, when plotted against the channel slope, the channel width first attains a maximum, then starts to decrease until the oc-

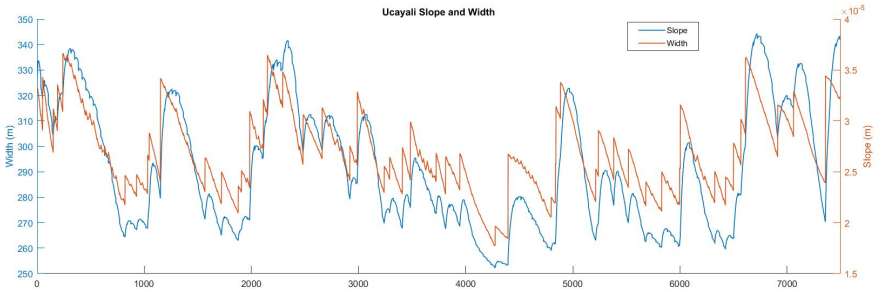


(a) Slope and Width vs Time

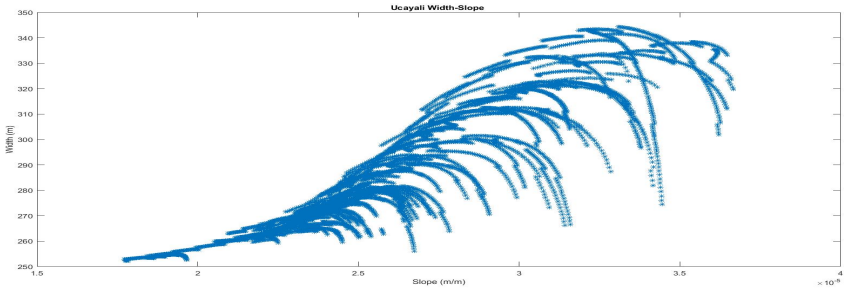


(b) Slope vs Width

Figure 3.9: Slope and width trajectories resulting from a long term simulations

currence of a cutoff event. The abrupt channel shortening induced by the cutoff leads to a change in the average slope. The corresponding change in the average channel width is slightly delayed in time and is initially relatively small. However, the slope increment determined an increase of the in-channel flow velocity, favoring the erosion process and, hence, determining a progressive widening of the channel, until a new maximum value is reached and the channel starts again to narrow.

The simulation also reveals that in a few occasions (especially for low channel slopes) the river tends to attain a quasi-stable configuration, with very slow bank displacements and shear stress values close to the critical thresholds for erosion and deposition. Just a sudden morphological change as this induced by a cutoff event can break this pseudo-equilibrium, by changing the slope and forcing the river width to attain a new stable value.

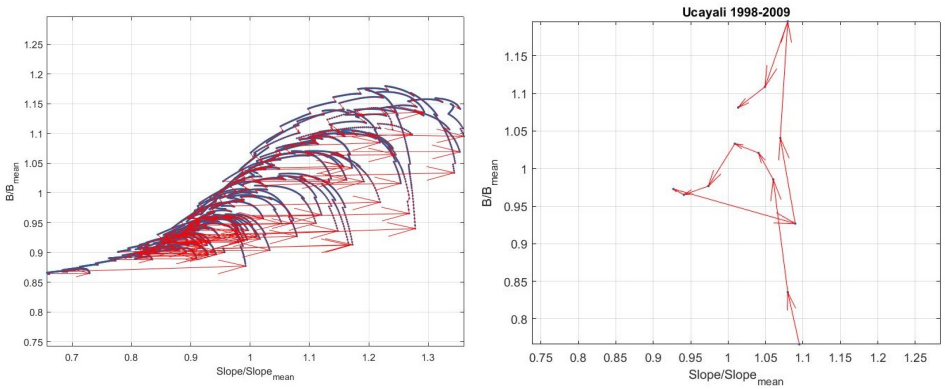


(a) Simulated data. (b) Observed data.

Figure 3.10: Width-slope trajectories induced by a cutoff event. The arrows indicate the direction of evolution process.

## 3.8 Conclusions

This chapter develops a new migration model for describing the bank erosion-accretion process, based on a statistical characterization of the mean channel width. This model is coupled with an existing model for determining the in-channel flow and bed topography. The final aim is to simulate the long-term evolution of a meandering river, accounting for also channel width variations.

The migration method mutually constrains bank erosion and accretion, restricting width variations within a meaningful range of values, based the statistical probability distribution of observed river width. The short and long-term simulations carried out concerning a given reach of the Ucayali river, confirm that the proposed approach allows stable long-term simulations with realistic width values.

Both field observations and simulated results suggest the existence of a strict relationship between the mean channel slope and the average channel width. The width-slope trajectories are characterized by hysteresis cycles, whereby the width first increases up to a maximum and then decreases as the slopes decreases owing to the progressive channel elongation, until a cutoff shorten the channel, leading to an abrupt decrease of the slope.

Long-term simulations also reveal that this hysteretic cycle could yield a quasi-steady static planform configuration, in general with high sinuosity and high energy dissipation.

# Part II

# Chute cutoff in meandering rivers

# Chapter 4

# Chute cutoffs in meandering rivers: formative mechanisms and hydrodynamic forcing

## 4.1 Introduction

Migration and stream bed evolution of meandering rivers are fundamental processes that determine both the morphology and the sedimentary record of floodplains (Toonen et al., 2012; Slowik, 2016; van de Lageweg et al., 2016a). This inherent correlation between the history of river and the floodplain where it flows entails that, on one hand, detailed stratigraphic studies are crucial in order to know the past evolution of a river and, on the other hand, that modeling the morphodynamic processes can guide the research of sedimentologists as well, e.g., (Erskine et al., 1992; Ghinassi, 2011). Accordingly, and due as well to the charm inherent in the complex interactions between free-surface flows and the surrounding land, migration of meandering rivers attracted the interest of many researchers worldwide, who faced the problem from different points of view (Hooke, 2013).

Among the others, geomorphologists are trying to shed light on the processes that underpin the migration of meandering rivers and their interactions with the surrounding environment (Seminara, 2006) by following a quantitative approach, i.e., by developing mathematical and numerical models meant to mimic the primary actual processes of riverine dynamics. Different

hydro-morphological models have been developed in the last decades after the seminal work by Ikeda et al. (1981), who first showed that the planimetric evolution of large meandering rivers could be roughly predicted by accounting for the excess velocity at the outer bank due to the secondary (, i.e., helical ) flow driven by stream bed curvature. Their relatively simple model had the great merit of identifying one of the leading processes that determine the evolution of meandering rivers.

Significant improvements have been made so far (Bolla Pittaluga and Seminara, 2011; Asahi et al., 2013; Iwasaki et al., 2016; Ferreira da Silva and Ebrahimi, 2017). Nonetheless, it has to be admitted that predicting the migration of meandering rivers is a challenging task when large temporal (and spatial) scales are involved (Guneralp and Marston, 2012). One of the main reason is apparently shown in Fig. 4.1, where the Digital Elevation Model (DEM) of the Allier River, upstream of Moulins (France), is reported using a colored, shaded relief (in the figure, the mean slope of the valley is subtracted to highlight the floodplain landforms). In real-world meandering rivers, floodplains are all but "white canvas", and rivers are indefatigable painters that indefinitely draw sinuous curves one above the other. Therefore, floodplains are the byproduct of a long-lasting, antecedent river migration, a process in which the effects of each morphological change can substantially affect the subsequent evolution of both the river and the floodplain (Bogoni et al., 2017).

Beside topographical heterogeneity, which is manifest in Fig. 4.1, further complexity can be ascribed to, e.g., *i*) variability of hydrological regime (Nicholas et al., 2016), ii) remarkably different spatial and temporal scales involved in the process (Guneralp and Marston, 2012), iii) planimetric and stratigraphic heterogeneity of soils (Ielpi and Ghinassi, 2014), ii) heterogeneity of vegetation cover, characterized by elaborate feedbacks between flow, sediment dynamics, plant growth and removal (Bertoldi et al., 2014; van Oorschot et al., 2016; Zen et al., 2016). Also, hydrological regime, sediment transport, and vegetation dynamics can be significantly altered by natural and anthropogenic modification of the environment such as climate change or the construction of reservoirs (Dury et al., 1972; Kiss and Blanka, 2012; Constantine et al., 2014; El Gammal, 2016).

Obtaining realistic and precise long-term forecasts of river migration using analytically or numerical models is, in fact, prohibitive. Rather, numerical models may be more efficient, and the obtained predictions more reliable, if they are applied back-in-time, i.e., to reproduce the river migration in the

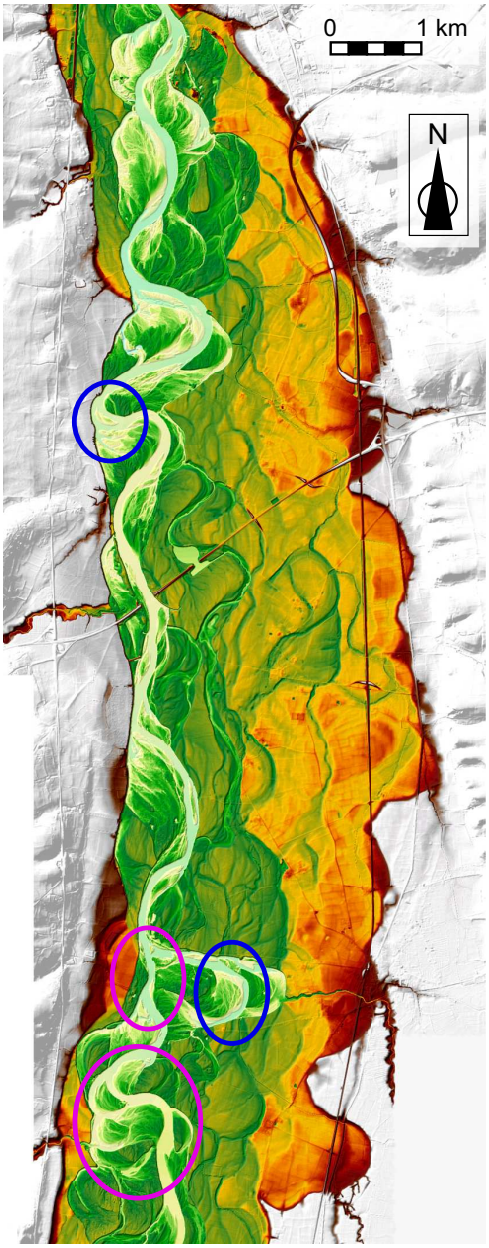


Figure 4.1: Allier River upstream of the city of Moulins, France (river n. 112 in the data set in Kleinhans and van den Berg (2011); see also (Van Dijk et al., 2014) for a detailed study). Water flows from South to North. The original Digital Elevation Model is here de-trended to highlight the topographical variability. The blue and magenta circles highlight chute cutoffs related to different formative mechanisms, as described later in the text (data courtesy of IGN-France and Ministère de l'Ecologie et du Développement Durable).

past. In this case, their predictive power can be improved by assimilating data referring to both the present and the past river configurations. Far from being a useless theoretical exercise, such model applications can provide crucial insights to infer the sedimentary architecture of floodplains, which is of interest for example to study pollution in groundwater reservoirs, for subsoil water management, availability, and withdrawals, hydrocarbon exploration (van de Lageweg et al., 2013, 2016b).

To be effective, predictive models need to correctly simulate all the different critical processes that affect the morphodynamics of rivers, i.e., meander migration, bank erosion, the formation of bars, and occurrence of cutoffs (Iwasaki et al., 2016). The focus of the present works is on cutoffs and, specifically, in the formation of chute cutoffs (Constantine et al., 2010), which is one of the most fascinating and less predictable of the mechanisms above mentioned.

Commonly, chute cutoffs form in meandering channels when floodwaters can no longer be contained within the main channel, thus incising a channel, or chute, in the floodplain, which can finally evolve into the dominant conveyor of river discharge. In this way, streamflow can find a pathway that is considerably shorter, and steeper, than the main meander loop. Chute channels may develop over an extended period (Hooke, 1995; Gay et al., 1998), with only floodwater flow at first, or during a single flood event (Iwasaki et al., 2016). The cutoff meander may either be filled with sediment to create a channel fill deposit, or, less frequently, remain active along with the chute channel (as, e.g., in the Strickland River, Fig. 4.2, and Grenfell et al. (2012)).

From a morphological standpoint, chute cutoffs control the river sinuosity by counteracting the bend lengthening that is inherent in meanders migration (Howard and Knutson, 1984; Stølum, 1998; Camporeale et al., 2005; Tal and Paola, 2010; Ghinassi, 2011; Van Dijk et al., 2012; Schuurman et al., 2016). Hence, chute cutoffs are autogenic mechanisms of meandering rivers (Hooke, 2003, 2007; Slowik, 2016) and, as well, they can be seen as a mechanism of transition from meandering channel to braided channel (Kleinhans and van den Berg, 2011; Zolezzi et al., 2012; Iwasaki et al., 2016). Their occurrence is related to floods as, unlike neck cutoff, high water levels and high rates of bedload transport are required (Lewis and Lewin, 1983; Howard, 1996; Zinger et al., 2011; Van Dijk et al., 2014) . The incision of chute channels causes the removal of relatively large amounts of floodplains materials, thus delivering intense sediment pulses downstream (Zinger et al., 2011) that

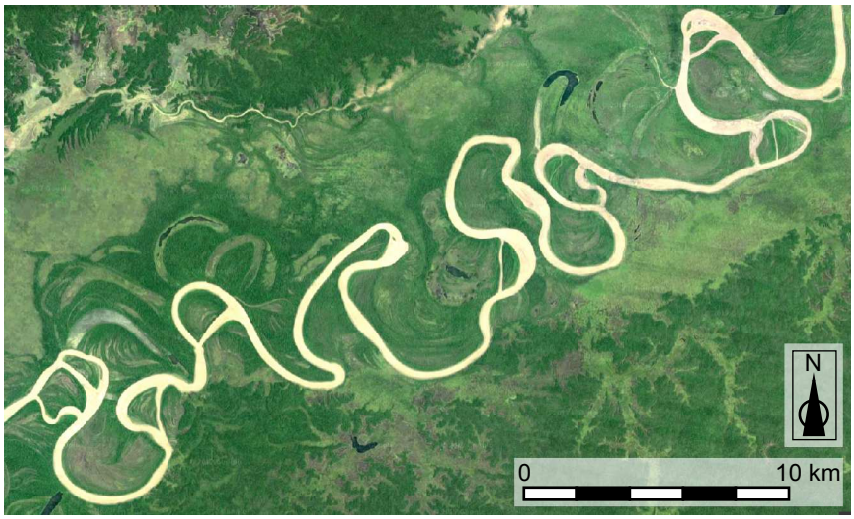


Figure 4.2: Strickland River in Papua New Guinea (see also Grenfell et al. (2012, 2014)), about 50 km North-East of the confluence with the Fly River (aerial photo from Google Earth, 2017). The flow is from right to left.

stimulate downstream bar formation (Fuller et al., 2003; Dieras et al., 2013; Zinger et al., 2013). More generally, individual cutoffs were shown to accelerate the river migration and to drive channel widening both upstream and downstream of the cutoff locations (Schwenk and Foufoula-Georgiou, 2016).

The issue of chute cutoffs has attracted increasing attention in the last years. Different mechanisms leading to the formation of chutes have been identified (Constantine et al., 2010; Van Dijk et al., 2014; Eekhout and Hoitink, 2015). However, due in part to the lack of extensive field observations (Micheli and Larsen, 2011), and especially to the multiplicity of mechanisms and heterogeneous controls involved in the process, the predictability of chutes cutoffs occurrence remains an open, stimulating question.

The present work principally focuses on the hydrodynamic drivers that lead to the initiation of chute cutoffs, whose analysis allows the identification of two different categories of mechanisms: one, mainly related to the inertia of the in-channel flow upstream the chute channel; the other, which mainly depends on the flow field forming over the floodplain to be incised.

The chapter is outlined as follows. After a thorough literature review of processes and factors involved in the formation of chute cutoffs, two case studies are presented that are representative of different mechanisms of chute initiation. Supported by numerical results obtained using two-dimensional

(2D) and linearized three-dimensional (3D) models, distinct features in the hydrodynamic flow field are shown to crucially affect the initiation of chute cutoff. The matter is then objected of an in-depth discussion, also in the view of other findings presented in the literature. A criterion is proposed to classify chute cutoff based on the principal hydrodynamic drivers responsible for chute incision.

## 4.2 Processes and factors controlling chute cutoff dynamics

### 4.2.1 Mechanisms of chute cutoff formation

Chute cutoffs occur when water flows from river channels to adjacent floodplains so that the flow interacts with the floodplain topography and vegetation leading to a chute that cuts across a meander neck, the inner side of the point bar, or exposed alluvial bars (McGowen and Garner, 1970; Erskine et al., 1992; Gay et al., 1998; Bridge, 2003; Ghinassi, 2011). Chutes, which typically forms within the active channel belt (Hooke, 1995), are segments with length on the order of one meander wavelength (David et al., 2016) linking together reaches of the same river.

Different mechanisms have been showed to lead to the incision of a chute channel. Concerning the schematics of Fig. 4.3 is possible to distinguish between (at least) three major types of mechanisms:

1. downstream extension of an erosional embayment, which forms because of localized bank erosion at the outer bank along the downstream part of a bend located upstream of the meander undergoing cutoff (Constantine et al., 2010). Subsequent floods extend the embayment downstream until it intersects the riverbank downstream, thereby forming a chute. During intermediate stages of the process, a chute bar can form at the downstream end of the chute incision (Kleinhans and van den Berg, 2011) , and it is destined to be completely eroded if the cutoff finally occurs;

2. headward erosion of a channel (or gully) through the floodplain, in which a headcut migrates from the downstream end of the forming

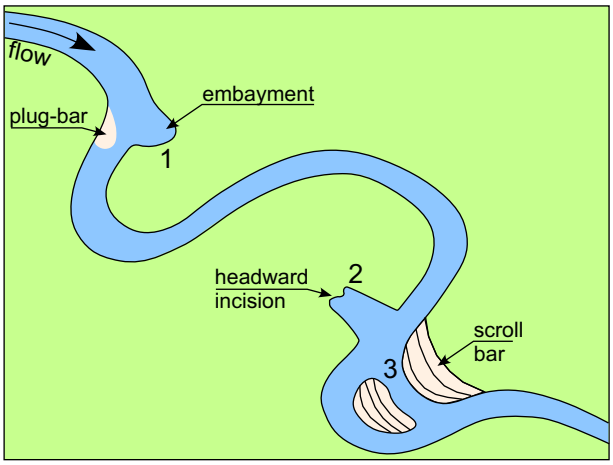


Figure 4.3: Different mechanisms of chute cutoff formation in meandering rivers. 1) Embayment formation, 2) headward incision, and 3) swale enlargement aligned to main scroll bar direction (adapted from David et al. (2016)).

chute towards its leading section, progressively capturing an increasing fraction of the over-bank flow and finally causing the cutoff of the original bend (Gay et al., 1998; Thompson, 2003; Ghinassi, 2011; Zinger et al., 2011, 2013; Eekhout and Hoitink, 2015);

3. gradual erosion of existing swales (or sloughs) within the inside of the bend, which provides a predominant flood routing path, until most of the discharge is conveyed by the new channel, thus leading to a chute cutoff. This type is the first and more widely recognized mechanism (Fisk, 1947; McGowen and Garner, 1970; Bridge et al., 1986) and it is frequently found along meandering rivers that produce marked ridge and swale topography, i.e., scroll-bars (Hickin and Nanson, 1975; Grenfell et al., 2012).

A chute may form by following one of these mechanisms, but also a combination of different processes (Kleinhans and van den Berg, 2011).

Each different mechanism requires specific conditions to occur. The formation of chutes according to Type 1, besides a sufficient stage difference across the floodplain (as recognized by Constantine et al. (2010)), requires that the flow within the bend upstream of the embayment possess a quite significant amount of inertia (this aspect will be discussed later). In Type 2, if over-bank flow occurs, the formation of chutes is quite insensitive to

the upstream flow field. Instead, the water level in the main channel at the downstream end of the forming chute must be sufficiently low, for the free-surface to drop at the head cut, thus enduring head ward erosion (Zinger et al., 2011, 2013). The Type 3 mechanism implies the existence of a swale that links an upstream and a downstream section of the river; the erosion power along the forming chute mainly depends on the stage difference and the so-called gradient advantage associated with the shorter path through the point-bar (Grenfell et al., 2012). Van Dijk et al. (2014) observed that sloughs, and hence chute channels, from where inner-bank attachment of scroll bars is interrupted, this behavior is observed in rapid meandering migration, in which the scroll bars attachment is not entirely possible due to the differences between the erosion and aggradation rates (Braudrick et al., 2009; Zolezzi et al., 2012; Grenfell et al., 2014).

The fate of the newly formed chute is another interesting issue that depends on many factors. Among the many, it is worth mentioning the intensity of helical flow due to the upstream channel curvature, that influences the bifurcation asymmetry which, in turn, plays a significant role on the division of bed-load sediment between the two branches (Kleinhans et al., 2006, 2008; Bolla Pittaluga et al., 2015). Due to the division of water discharge, the sediment transport capacity in the previous main branch reduces. If the resulting transport capacity is still higher than the supply, the main channel can remain active along with the chute (Grenfell et al., 2012). Alternatively, a sandy plug bar causes the closure of the main branch (Constantine et al., 2010; Van Dijk et al., 2012, 2014) and leads, later, to a slower filling by fine material supplied by over-bank flow (Toonen et al., 2012; Dieras et al., 2013). The role of bars in determining the fate of bifurcations has been suggested by experiments conducted in straight channel (Bertoldi et al., 2009) and by analytical findings (Redolfi et al., 2016). Zinger et al. (2013) assessed the fate of an already formed chute, performing measurements of flow velocity and morphology, and developed a conceptual model of chute-cutoff dynamics in which the upstream and downstream ends of a cutoff channel are treated as a bifurcation and confluence, respectively.

### 4.2.2 Controlling factors

Besides the various mechanisms that can lead to the formation of a chute cutoff, different controlling factors have been identified in previous studies and reported in the literature. Such controlling factors concern specific fea-

tures of both the river and the floodplain and are plus or less important in determining the actual occurrence of the chute incision.

### Features determining/affecting overbank flow

About all types of mechanisms, the incision of chutes needs overbank flow to occur (Howard and Knutson, 1984; Bartholdy and Billi, 2002). This means that chute formation needs relatively high water levels (sufficient, at least, for overbank flow to occur), and a significant stage difference between the upstream and the downstream ends of the forming chute, so that the chute channel is characterized by a significant gradient advantage with respect to the original bend (Grenfell et al., 2012).

Water levels usually raise during floods, and stage difference can be further increased due to the presence of obstructions along the meander undergoing cutoff. Obstruction can be ascribed to piling up of woody debris or ice (Keller and Swanson, 1979; Gay et al., 1998) or, as recently identified, to the formation of central- or plug-bars (Peakall et al., 2007; Grenfell et al., 2014; Iwasaki et al., 2016). Seminara (2006) observed that the formation of a central bar at the bend apex promotes a tendency of the stream to bifurcate into an outer and an inner branch, the latter being a potential precursor of chute cutoff (see also Jager (2003)). Recently, (Eekhout and Hoitink, 2015) described the formation of a chute cutoff triggered by the formation of a plug bar within the main channel, owing to a backwater effect; after the plug bar was deposited, an embayment (Type 1) formed in the floodplain at a location where a former channel was located, in which the sediment was likely less consolidated, and hence, prone to erosion. The formation of plug bars as a driver of chute channel incision is an interesting feature, as it can lead to chute incision also in steady flow conditions and with water discharges that are unable to produce overbank flow until the formation of a plug bars leads to a marked increase in water levels. However, the occurrence of chute cutoffs under a constant water discharge is so far related to the laboratory or controlled experiments (Peakall et al., 2007; Braudrick et al., 2009; Van Dijk et al., 2012; Visconti et al., 2012).

Backwater effects are one of the factors promoting the formation of point-, central-, and plug-bars (Kasvi et al., 2013), and they were also proved to control meander avulsion (Chatanantavet et al., 2012). More generally, such in-channel bars form due to a reduction of bed shear stress in the downstream direction, of which backwater effects are only one of the possible causes.

Indeed, bed shear stress can reduce because of, e.g., channel widening (Miori et al., 2006), lengthening (Van Dijk et al., 2014), curvature driven helical flows (Kleinhans et al., 2008), presence of bars (Kleinhans and van den Berg, 2011), and inlet steps (Bertoldi et al., 2009). Also, changes in the frequency of flood events were shown to be related to the frequency and the occurrence of chute cutoffs (Ghinassi, 2011; Micheli and Larsen, 2011; El Gammal, 2016) , thus confirming the role of discharge variability on the formation of chute cutoff (Schuurman et al., 2016).

### Floodplain characteristics

As observed by Constantine et al. (2010), environmental conditions on the floodplain, such as local differences in topography, sediment composition, and vegetation, can alter the floodwater surface in such a way as to promote or inhibit erosion, and so it is reasonable to expect that not only the characteristics of chute incision but also its actual occurrence and complete development, may vary considerably between settings.

It is widely recognized that small channels crossing the point bar play a key role in the formation of chutes (Brierley, 1991), as they provide preferential pathways where overbank flow concentrates thus increasing the shear stress and, in turn, the chance of removing sediments. Obviously, the presence of paleo-meanders and abandoned channels, not filled, can promote the formation of chute cutoffs (Constantine et al., 2010). An example is the chute channel that formed in 2011 along the Chixoy River, Guatemala (Fig. 4.4). It is worth noting that the presence of paleo-meanders within the river belt is a widespread and common feature of a meandering river, of which both Fig. 4.1 and Fig. 4.2 are clear examples. David et al. (2016) performed a detailed reach-scale mapping of floodplains and found that up to seventy-five percent of channel reaches within floodplain channels are likely paleo-meander cutoffs. The topographical heterogeneity of the floodplains, which crucially affects the formation and the development of chute cutoffs, must be properly accounted for to assess the occurrence of chute cutoffs.

Besides topography, the floodplain erodibility is another crucial factor in determining the success or failure of a chute cutoff. It is well known that erodibility mainly depends on the floodplain sediment composition and the vegetation cover (Lewis and Lewin, 1983; Braudrick et al., 2009; Constantine et al., 2010; Tal and Paola, 2010; Micheli and Larsen, 2011; Dunne and Aalto, 2013; Grenfell et al., 2014; Harrison et al., 2015; Schuurman et al., 2016;

Slowik, 2016; El Gammal, 2016; Iwasaki et al., 2016).

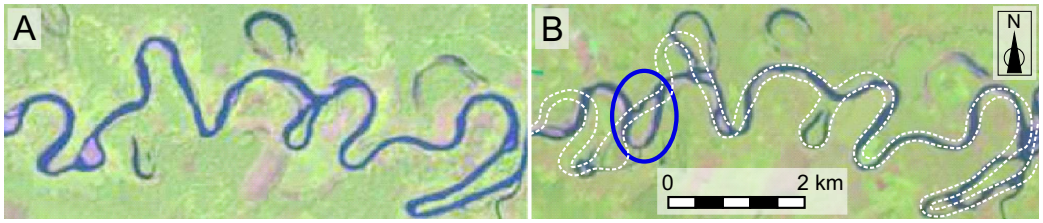


Figure 4.4: Chute cutoff occurred in 2011 along the Chixoy River (Guatemala). The chute channel (blue circle in panel b) is clearly a paleo-meander, still active in 1988 (panel a), and re-activated by over bank flow during a severe flood. The white dashed line in panel b represents the river configuration in 1988 (panel a).

### River morphometry

Observed data suggest that chute cutoff occurrence is linked to specific morphometric configurations of the river, first of all to relatively high gradient reaches (Lewis and Lewin, 1983; El Gammal, 2016), which is related to the flow velocity both within the channel and over the floodplain.

The field data collected by Lewis and Lewin (1983) suggest that chute cutoff is a more probable event when the radius of curvature to width is in the range between one and two. Micheli and Larsen (2011) carried out an in-depth morphometric analysis focusing on the occurrence of chutes along the Sacramento River (CA, USA). They concluded that the radius of curvature of the bend is one of the controlling factors for chute incision, as the larger radius of curvature implies more extended chute channel to form, which in turn requires a higher erosive power. Chute cutoffs were found to occur most frequently in wide channels where bend curvature is strong (Howard and Knutson, 1984). Micheli and Larsen (2011) identified a specific range of sinuosity and angle of entrance for which chute cutoffs were found occurred, but they also showed that chutes did not form in all the bends matching those characteristics. Then, the conditions for chute occurrence inferred by Micheli and Larsen (2011) were necessary but not sufficient for the incision of a chute.

The correlated oscillations of channel width and curvature can have possible implications for the occurrence of chute cutoffs since river widening is known to promote the formation of central bars and, in turn, the tendency to

originate channel bifurcation (Seminara, 2006; Camporeale et al., 2008; Luchi et al., 2010; Parker et al., 2011; Zolezzi et al., 2012; Frascati and Lanzoni, 2013; Grenfell et al., 2014; Church, 2015; Eekhout and Hoitink, 2015).

Aiming at identifying the factors that could predict chute cutoffs, Grenfell et al. (2012) analyzed three different rivers using binary logistic regression and found that the only statistically significant predictor of chute initiation at a bend was the average rate of bend extension, with an increased probability of chute initiation for a larger rate of bend extension. The bend widening in meandering rivers is in fact associated with large migration rates (Brice, 1975; Grenfell et al., 2014; Slowik, 2016). Mathematical simulations confirmed that a faster migration is related to the occurrence of chute cutoffs, which were not found to occur in case of lower migration rates (Schuurman et al., 2016).

### Sediments

Chutes are eroded in the floodplain provided that the energy of floods is sufficient to transport sediment delivered from the river to the floodplain, to remove sediments from the floodplain floor, and to transport this whole sediment load downstream, back into the river (Constantine et al., 2010). On the one hand, the importance of sediment dynamics is evident; on the other hand, the spatial and temporal patterns of erosion and deposition in topographically heterogeneous floodplains are extremely complex (Piegay et al., 2008).

Interestingly, chute cutoffs are more frequently found in the presence of poorly cohesive banks (Howard and Knutson, 1984; Howard, 2009) and where infill rates are lower (Hooke, 1995; Dunne and Aalto, 2013). It is worth recalling that the suspension of bed material is a crucial control on sediment transport direction and hence river morphology (Nicholas, 2013), as it limits the gravitational deflection of sediment in the direction of the local bed slope. Hence, in the long term, suspended sediment load leads to a more uniform filling of areas adjacent to the main course of the river, with repercussions on the aggradation and the resistance to erosion of the floodplains. Indeed, high rates of suspended sediment aid the connection of bars to floodplain (Braudrick et al., 2009) and, by leveling out the point bar, they limit the presence of sloughs and swales that play a significant role in chute formation by acting as preferential pathways to overflow.

**Anthropological factors**

For the sake of completeness, anthropogenic factors are also known to play a significant role in the evolution of rivers and, of course, in the formation of chute cutoffs. A chute cutoff can be the effect (done on purpose or not) of human interventions (Parker and Andres, 1976; Simon and Robbins, 1987). An interesting example recently described and analyzed in the literature, is the artificial cutoff produced in the Ucayali River, a tributary of the Amazon River that is extraordinarily active from a morphological standpoint. In 1997, a 72 km long, triple-lobed, meander bend was cutoff, and the chute formed where a small shortcut channel was decades early carved by local people to reduce the canoe travel time along the river (Abizaid, 2005; Coomes et al., 2009; Schwenk and Foufoula-Georgiou, 2016). Contrarily, anthropological modifications such as flood control structures and large impoundments, by diminishing frequency and magnitude of floods, and thus river-floodplain connectivity, reduce the chance of chute cutoffs (Edwards et al., 2016).

## 4.3 Materials and methods

A detailed examination of the hydraulic controls on chute incision is the first step towards a better understanding of how a chute cutoff occurs (Constantine et al., 2010). In the following, an analysis is presented, aimed at highlighting the critical hydraulic and topographic factors triggering the formation of chute channels, based on satellite and aerial photographs, digital terrain models, and on the use of mathematical and numerical models.

Linearized morphodynamic models, used to predict long-term migration of meandering river (e.g., Frascati and Lanzoni (2013); Bogoni et al. (2017)), are characterized by low computational costs. However, they typically model the water flow and the bed topography in the main channel, the outer channel bank erosion and neck cutoffs (Schuurman et al., 2016). The effects of chute cutoffs have been accounted for only adopting a heuristic statistical framework, e.g., by considering a quasi-random occurrence of chute cutoffs (Howard, 1996). On the other hand, more refined hydrodynamic models provide detailed information about the water flow both in the main channel and over the adjacent floodplain and, therefore, can be used to disclose the complex interactions associated with the transfer of momentum between the in-channel stream flow and the floodplain overflow (Shiono and Muto,

1998; Shiono et al., 1999; Patra and Kar, 2000; Patra et al., 2004; Wormleaton et al., 2004; Shiono et al., 2008; Shiono and Shukla, 2008; Shiono et al., 2009a,b; Khatua and Patra, 2009; Liu et al., 2013, 2014; Shan et al., 2015). Although full three-dimensional (3D) models offer a more detailed description of the flow field, two-dimensional (2D) depth-averaged models have been found to reproduce accurately many important hydrodynamic features, with a sensible reduction of computational costs (Rameshwaran and Shiono, 2003; Shiono and Shukla, 2008; Riesterer et al., 2016) that allow a sensible reduction in computational terms.

In the present contribution, is use a fully-coupled, although linearized, hydro-morphodynamic model (Frascati and Lanzoni, 2013) to compute the curvature-driven flow field and the bed topography within the main channel, in river reaches where bathymetric data, referring to the river configuration just antecedent to the chute formation, are not available. The model describes the steady, spatially varying flow and the sediment transport in channels with arbitrarily varying channel axis curvature and channel width. It is based on the two-dimensional shallow water equations for the flow field and the Exner sediment balance equation governing the bed dynamics. These equations are suitably linearized and solved using a two-parameter perturbation expansion technique, taking advantage of the facts that alluvial rivers often exhibit mild and long meander bends, as well as evident but relatively small width variations. The model, which accounts for the dynamic effects of secondary flows induced by both curvature and width variations, allows us to compute the flow field (, i.e., water elevation, flow velocity and depth) and the equilibrium bed elevations corresponding to a given flow discharge.

The hydrodynamic interactions between the in-channel stream flow and the floodplain overflow are investigated using a two-dimensional finite-element model that solves the full 2D shallow water equations on irregular grids (Defina, 2000). The model uses a statistical, physically based subgrid approach to account for wetting and drying processes over highly irregular topographies (D'Alpaos and Defina, 2007; Viero et al., 2013). The shallow water equations are solved using a semi-implicit staggered finite-elements method, based on mixed Eulerian-Lagrangian approach. The depth-integrated horizontal turbulent and dispersion stresses are evaluated using the Boussinesq approximation (Stansby, 2003), and the eddy viscosity according to Uittenbogaard and van Vossen (2004). The considered hydrodynamic model can be easily coupled with an Exner-based model to describe channel bed dynamics (Defina, 2003), Nevertheless, the numerical modeling of chute cutoffs, from chute inception, to meander bypass and, possibly, abandoned channel

infilling, requires a more sophisticated numerical approach, to include fundamental processes such as bank erosion (see, e.g., Iwasaki et al. (2016)). In the following then attention is restricted to the hydrodynamic forcing that likely controls the initiation of chute incisions.

In all study cases, the obtainment of data for the meandering modeling follows the next sequence: first model input data is extracted from available maps and remote sensing data, including Digital Elevation Maps (DEM) and NASA-USGS Landsat images in which the cloudiness was low enough to make the main channel clearly visible. Denoting by IAC the first image in which the chute cutoff is visible, and by IBC an image just before its occurrence is digitized the rivers banks and the main channel from the IBC and noted down the chute location from the IAC. Then is analyzed the available discharge time series, in the period between images IAC and IBC were taken, to estimate the potential discharge that could lead to chute formation. The sediment size was assumed based on qualitative or quantitative granulometric information. Next, the geometric input data is pre-processed and cast in dimensionless form to apply the mathematical model. Finally, in a post-processing step, the variables are recast to their dimensional form.

## 4.4 Case studies

In this Section, the modeling framework described above will be used to identify the hydraulic controls on chute cutoffs with reference to two case studies: the Sacramento River and the Cecina Rivers. The 2D hydrodynamic model of Viero et al. (2013) will be used to compute the flow field within the channelized paths and over the floodplain while, given the absence of specific topographic data, the model of Frascati and Lanzoni (2013) will be used to estimate the bed topography to be considered within the main channel. The topography of the floodplain, on the other hand, is derived from available DEM information. For the rest of the case studies was applied just the model of Frascati and Lanzoni (2013) due to the absences of an accoutered DEM information to model in a reasonable way the floodplain.

### 4.4.1 Sacramento River

The Sacramento River is the largest river in California (USA). It collects precipitation and snowmelt runoff from the western slopes of the Sierra Nevada, the eastern slopes of the Coast Range and the southern Trinity and Klamath ranges, and finally, discharges into the Pacific Ocean via the San Francisco Bay (Micheli and Larsen, 2011). The river channel is about 480 km long, flowing from north to south. The Sacramento River Valley is mainly comprised of sedimentary rocks and recent alluvium, with a meander belt dominated by Pliocene–Pleistocene alluvium and fluvial deposits. In the area of interest, the reach of the Sacramento River is predominantly an unconstrained, single-thread, sinuous channel, with slope ranging from 0.0002 to 0.0007. The riverbed material is primarily sand and gravel with a median grain size ranging from 5 to 35 mm. The average height of the top of the bank varies from 2 to 8 m concerning the channel bed. The average channel width is about 250 m at full bank conditions. The construction of the dam at Shasta Lake in the early 1940s, and of some flood control structures diverting excess flow into overflow catchment basins during peak floods, caused a sensible increase of return period associated with both and major peak flows (Singer, 2008; Micheli and Larsen, 2011). At downstream of bend under analysis is the USGS (https://waterdata.usgs.gov) gauge station no. 11389500 with a register from 1921 to 2017 a mean annual discharge of $322 m^3/s$ and maximum peak discharge of 1467 $m^3/s$, at the upstream is the USGS gauge station no. 11377100 with a register from 1879 to 2017 a mean annual discharge of 353 $m^3/s$ and a maximum peak discharges of 8240 $m^3/s$.

The reach considered in this study is characterized by the presence of two consecutive bends (Fig. 4.5), and it is located about 15 km South of Red Bluff, between the river miles 233 and 236 (according to the U.S. Army Corps of Engineers river miles, from the 1991 Army Corps of Engineers Sacramento River Atlas). The second of these bends experienced two distinct chute cutoffs, approximately in 1976 (Fig. 4.6A) and in 1995 (Fig. 4.6B). The Digital Elevation Models (DEMs) shown in Fig. 4.6 are characterized by different resolution. The first (Fig. 4.6A) has a resolution of 10 m (1/3 arc-second) and has been selected after comparing together the planform paths attained by the main channel in the last 100 years, available in the form of shapefiles at the Sacramento River forum website (www.sacramentoriver.org). This DEM, which was then extracted from the U.S. Geological Survey (USGS) National Elevation Dataset (NED), refers approximately to the year 1976, just before the occurrence of the chute cutoff.

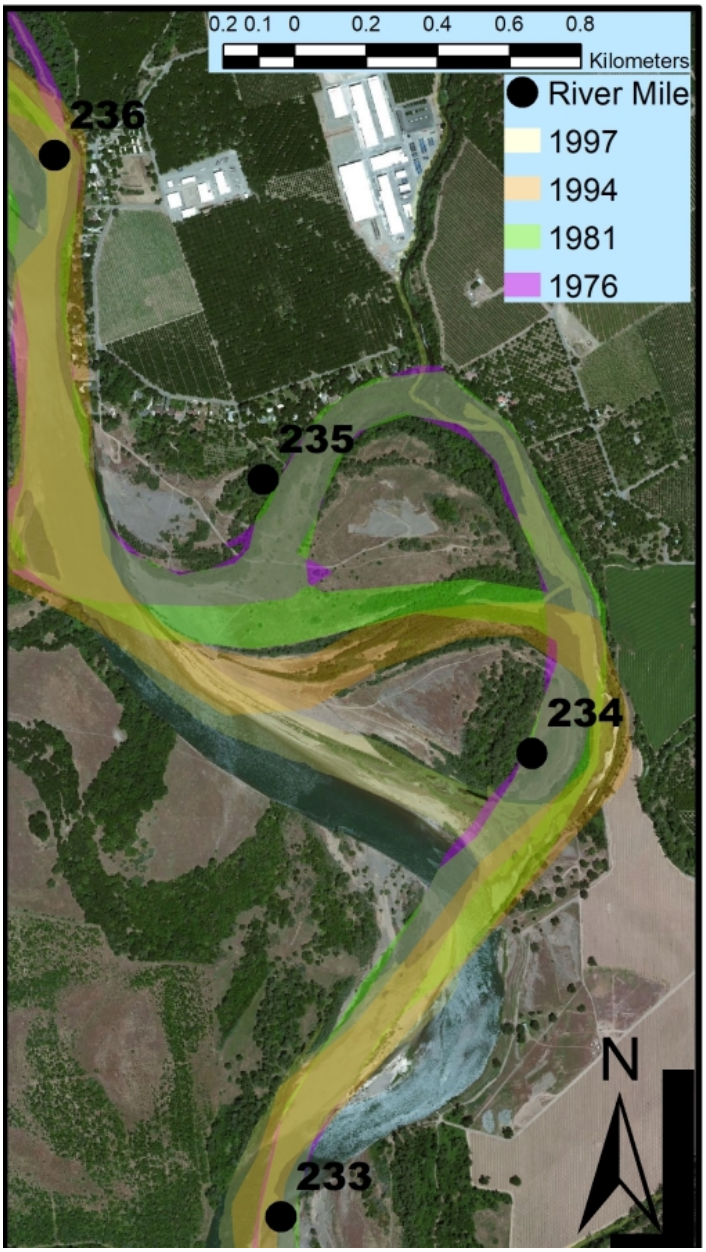


Figure 4.5: Historical channels of Sacramento river (California, USA). Water flows from up to down. Satellite images from Bing, historical channel paths from Sacramento River forum.

The high-resolution DEM depicted in Fig. 4.6B, provided by the California Department of Water Resources, was acquired from the CVFED LiDAR survey. Although being useless for our modeling purposes (it refers to a post-cutoff configuration), it provides a fascinating picture of the topographic heterogeneity that characterizes the Sacramento floodplain, with the presence of many scroll bars, floodplain channels and paleo-meanders cutoffs (David et al., 2016), The gross features of the floodplain are very similar to those emerging from the lower resolution DEM of 1976 (Fig. 4.6A). This suggests that small-scale morphological features affect the flow field locally, at a spatial scale that has likely little influence on the formation of chute cutoffs.

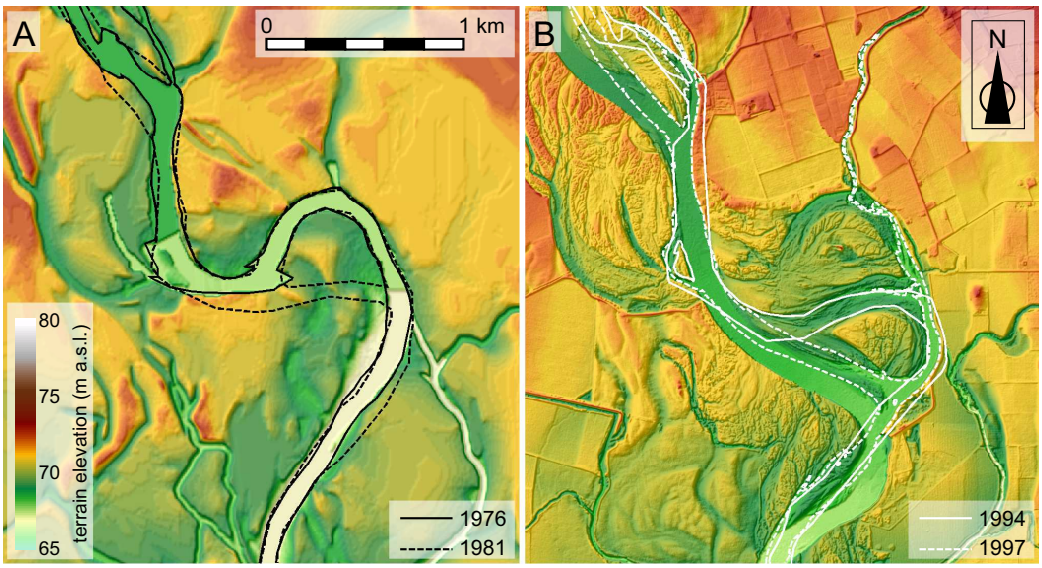


Figure 4.6: Sacramento River (California, USA) about 15 km downstream of Red Bluff (CA). The flow is from North to South. A) Digital elevation model (DEM) from USGS National Elevation Dataset (NED), referring to 1976 (resolution 10 m); B) DEM from the CVFED LiDAR survey, provided by the California Department of Water Resources, referring to 2010 (resolution 3 m).

Fig. 4.6A indicates that both the considered bends are strongly confined by relatively high banks on the outer side, with flattened elevations at the apex of the upstream bend and just after the apex of the downstream bend. One of the most exciting aspects of the 1976 channel configuration is the presence of an encroachment locates just upstream of the inflection point between the two bends, which shows similarities with that investigated by Constantine et al. (2010). Nevertheless, differently from Constantine et al.

(2010), who linked the presence of embayments to nearly uniform floodplains, in the present case the floodplain is markedly irregular, and the embayment developed in correspondence of the remainder of an abandoned (and partially filled) paleo-meander channel with a sinuous shape.

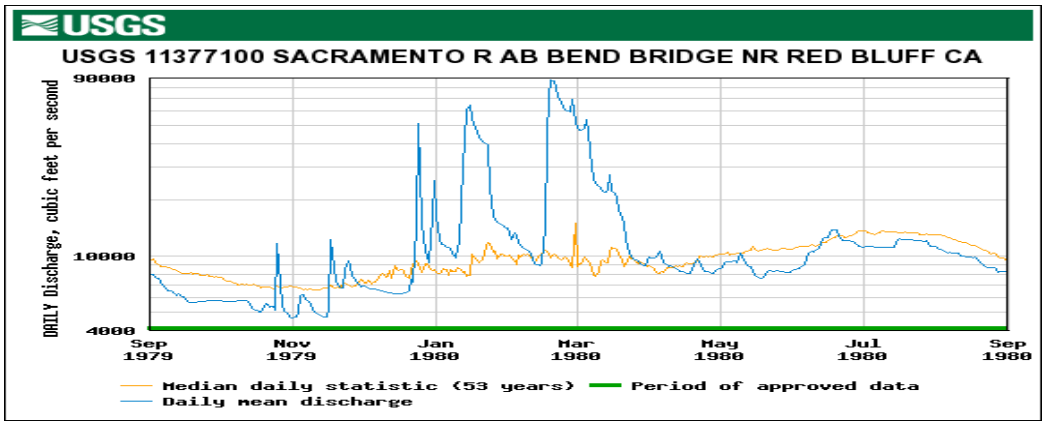


Figure 4.7: Hydro-graph from gauge station USGS no.11377100 in the period that correspond to a chute cutoff.

For the simplified model, as planimetric input data is using the configuration from 1976, and for the slope, sediment and depth-width relationship, mentioned previously. The model parameters were chosen to obtain full bank condition. The cross sections were discretized every 10 meters, and each cross section is dived in 200 points, equally spaced among them. For the flow discharged is based on the maximum hydrograph found between the configurations in which the chute occurred.

Since there are not available satellite images for this period, the discharge was chosen according to the record of the USGS gauge station No. 11377100, selecting the main flood during the period between the available channel configurations (see Fig. 4.5) as the discharge that produced the chute channel. This discharge was presented in 1980 as can be appreciated in the Fig. 4.7, it is also possible to see that a series of 3 main floods occurred during this period, one in December, another one in January and a final and most significant flood in February. Due to the lack of topographic data (including satellite images), it is not possible to indicate the flood that produces the chute channel.

Fig. 4.8 show the bead mean shear stress and velocity flow field computed with the model of Frascati and Lanzoni (2013), in this results there is an apparent concentration of shear stress, but especially of velocity around the

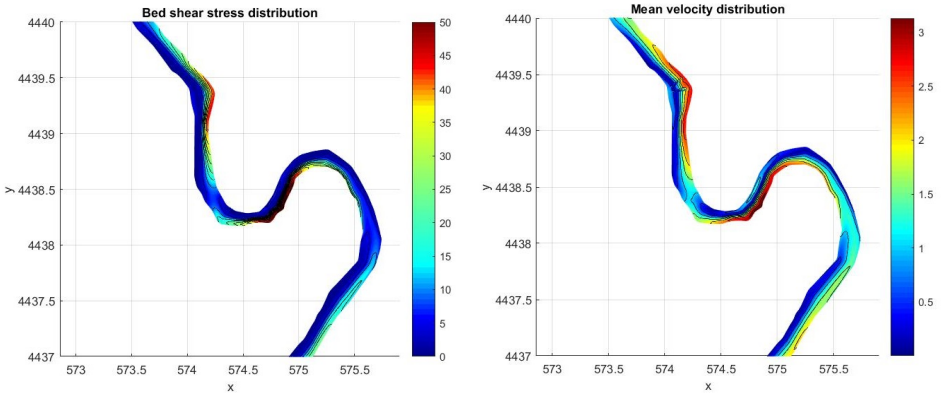


(a) Bed shear stress distribution in Pascal.

(b) Mean velocity distribution in m/s.

Figure 4.8: Hydraulic simulations results using a simple model for the 1976 Sacramento river configuration. (The axes coordinates are georeferenced with the UTM system).

embayment's area this favored a progressive erosion of the outer bank and, consequently, meander migration, see the dashed line in Fig. 4.6A and in Fig. 4.5. This concentration of shear stress also favors the exchange of momentum between the main channel and the floodplain. The different simulations that were made reveal that this shear stress concentration pattern is achieved during an entirely bank full condition.

The 2D hydrodynamic model is applied to analyze the 1976 configuration. The numerical grid is made up of about 30,000 nodes and 55,000 triangular elements, to cover a reach of about 13 km closed downstream at the bridge of Los Molinos. Given the absence of a comprehensive set of channel-bed elevation data, the bathymetry within the main channel is provided by the linearized morphodynamic model of Frascati and Lanzoni (2013), validated by comparison with the bathymetric survey used in the "Sacramento and San Joaquin River Basins Comprehensive Study" conducted in 2001 by the California Department of Water Resources. Also, the results from that study, which implemented a one-dimensional hydraulic model of the Sacramento River, were used to extract a rating curve for the downstream section of the numerical grid and to calibrate the resistance parameters of the present 2D model.

Fig. 4.9 shows the 2D flow field computed for a total discharge of 3000 $m^3/s$. The discharge confined within the upstream bend is 2760 $m^3/s$, while

the remaining fraction flows over the floodplain. A discharge of 340 $^{m^3}/_{s}$ flows in correspondence of the embayment preluding the chute formation. It can be noted that the constrained width of the main channel nearby the apex of the upstream bend acts to concentrate the water flux and to increase the flow velocity (Fig. 4.9B), generating a jet of water directed against the right bank at the inflection point, exactly were the embayment formed.

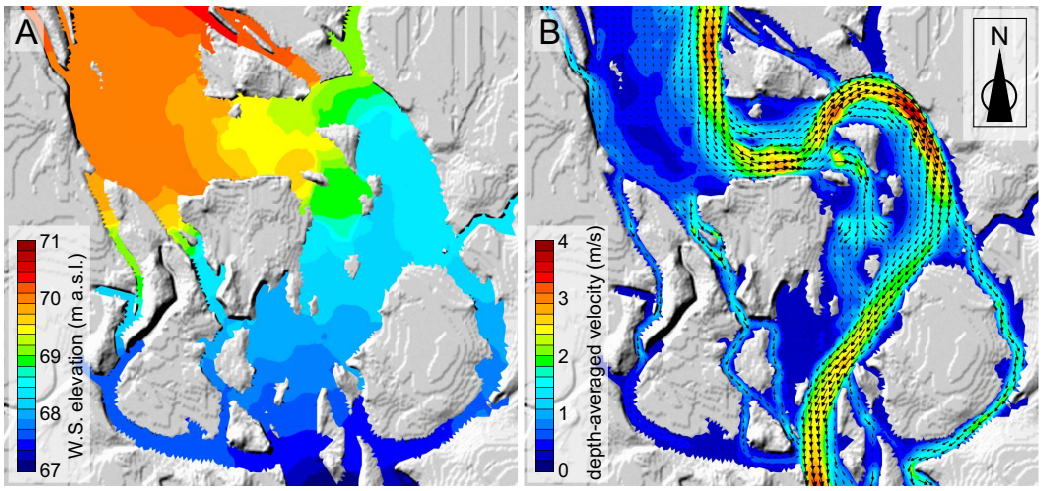


Figure 4.9: Sacramento River in 1976. Model results in terms of water surface elevation (A) and depth-averaged flow velocity (B), for a total discharge of 3,000 $^{m^3}/_{s}$. The flow is from North to South.

As a result, the incision of the considered chute turns out to be mainly driven by the inertia of the incoming channelized flow, which is predominant concerning the effects exerted by the floodplain characteristics (topography, vegetation, etc.). The prevailing of an inertia-dominated mechanism of chute formation is supported by the following reasons. The additional simulation carried out by switching off the advective terms in the 2D hydrodynamic model indicates that the maximum flow velocity downstream of the encroachment is reduced by more than 20 percent (from 2.9 to 2.3 $^{m}/_{s}$), and the discharge through the developing chute decreases by 30 percent (from 340 to 240 $^{m^3}/_{s}$). On the other hand, the chute that formed in 1976 followed the paleo-meander only in its first segment (i.e., for about 300 m). The inertia of the flow led to the formation a straight chute, irrespective of the preferential paleo-meander pathway, bending to the right.

To sum up, the initiation of the 1976 chute cutoff is due to the concomitant presence of two principal factors:

i) a concentration of flow velocities (due to the relatively narrow channel width just upstream of the chute incision) directed against the outer bank, and

ii) the presence of an embayment associated to a paleo-meander.

Also, the embayment acts to enlarge the channel width, thus reducing the flow velocity at the center of the main channel (Fig. 4.9). This reduction enhances sediment deposition and, consequently, the formation of a central-bar (Seminara, 2006) or a plug-bar (Eekhout and Hoitink, 2015), which facilitates the discharge diversion through the forming chute.

The energy of the flood, as it interacts with the variable topography, is reflected in the variability of the free-surface slope (Fig. 4.9A and Fig. 4.10). It is worth noting that the upstream and the downstream ends of the chute coincides with a local maximum and minimum of the free-surface elevation, respectively. This confirms that local differences in the shape of the floodwater surface determine how a chute progressively advances (Constantine et al., 2010). To gain insight into the mechanism that led to the chute incision and the abandon of the active bend, the bottom topography was artificially modified by progressively advancing the embayment eastward, the direction in which the chute formed. Model results reported in Fig. 4.11, show that a significant fraction of the discharge initially flowing within the main channel bend is progressively diverted along the forming chute. This causes, regarding maximum velocities, a reduction within the main channel and a substantial increase along the chute (red dashed line in Fig. 4.11). The apparent consequences are the progressive abandon of the former reach and an acceleration of the chute incision, due to the increased transport capacity.

Besides the numerical assessment of the hydrodynamics that likely determined the inception of the 1976 chute cutoff, was also carried out a partial assessment of the cutoff occurred in the same bend in 1995 (dashed line in Fig. 4.6B). Based on the available streamflow data, recorded by the USGS gauge station n. 11389500 (see Fig. 4.13), and on a close inspection of satellite photographs (see Fig. 4.12), whose availability is by far higher in 1995 than in 1976, this second cutoff appears to be triggered by a first flood (peak discharge of 2670 $^{m^3}/_s$ occurred in January, and developed entirely during a second flood (peak discharge of 3030 $^{m^3}/_s$ occurred in March. This seems to confirm the fact that the occurrence of subsequent floods (i.e., the discharge variability) plays a significant role in chute formation (McGowen and Garner, 1970). This suggests that, as was mentioned before, the discharge that

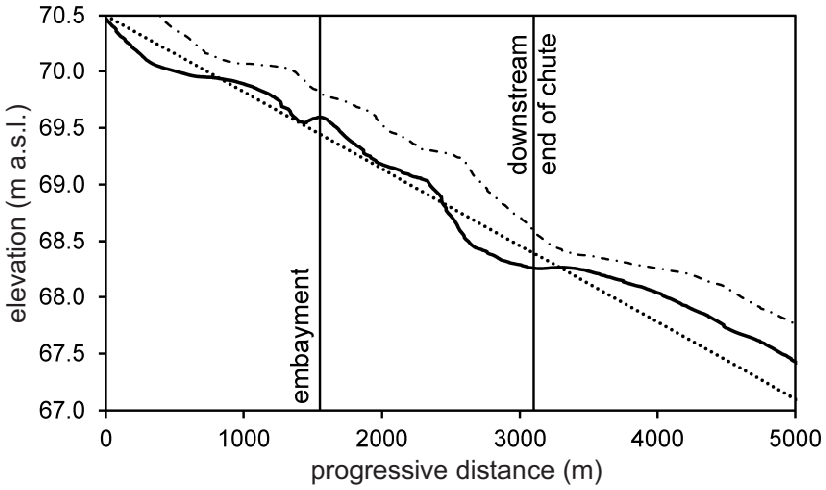


Figure 4.10: Sacramento River (California, USA). Water surface (solid line) and total head (dash dotted line) profile along the main channel center line. The dotted lines denote the mean slope of the river.

produces the chute cutoff in the river topographic configuration of 1976 may be triggered during the flood cycle from December 1979 to February 1980.

Again the model of Frascati and Lanzoni (2013) was applied using the configuration from 1994 as planimetric input data (see Fig. 4.13 a), and for the slope, sediment and depth-width relationship, mentioned previously. The model parameters were chosen to obtain full bank condition. The cross sections were discretized every 10 meters, and each cross section is dived in 200 points, equally spaced among them. For the flow discharged was selected the maximum hydrograph found between the configurations in which the chute occurred (see Fig. 4.13). It was not possible to implement the 2D hydrodynamic model due to the lack of a floodplain topographic information since the data available of the flood plain for this period is just after the chute cutoff process (see Fig. 4.6 B).

Fig. 4.8 show the bead mean shear stress and velocity flow field computed with the model of Frascati and Lanzoni (2013), in these results, there is a more precise concentration of shear stress and velocity where the chute channel forms, even if there is not a 2 D simulation to take in account the exchange of momentum between the main channel and the floodplain, is possible to intuit, that this factor and the embayment formation play an essential role for the chute channel formation.

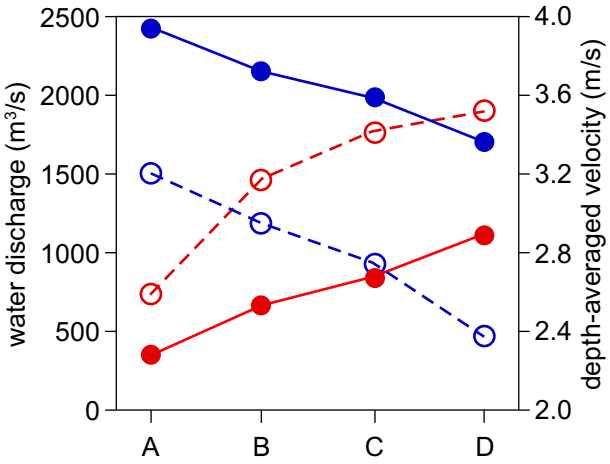


Figure 4.11: Water discharge (solid lines) and maximum depth-averaged velocity (dashed lines) in the main channel (blue lines) and the forming chute (red lines) just downstream of the embayment, respectively. Results are obtained considering different size of the embayment: original configuration referring to 1976 (A), embayments elongated eastward of about 200 m (C), 250 m (C), and 400 m (D).

Finally it could say, as was reported in Constantine et al. (2010), the formation of this second cutoff was preceded as well by the erosion of an embayment just downstream of the upstream bend, whose curvature significantly increased in the years between 1976 and 1995 due to the erosion of the outer bank (see Fig. 4.3A therein). Accordingly, the formation of this second chute cutoff likely followed the same dynamics of the previous cutoff.

### 4.4.2 Cecina River

The Cecina River is a gravel bed river in central Italy, with a catchment of about 900 $km^2$ and a total length of about 80 km. The Cecina River is highly ephemeral, with a flashy character, since flood flows are induced mainly by intense cloudbursts (Bartholdy and Billi, 2002). Bed material exhibits a general, though irregular, downstream decrease regarding median diameter, D50 (Billi and Paris, 1992). At the study reach (Fig. 4.15), which is located approximately 55 km from the source and 25 km from the outlet, D50 ranges between 15 and 30 mm, the bed elevation ranges between 34 and 38 m a.s.l., and the mean slope is about 1.85·10-3 (Fig. 4.16). Here, the Cecina River exhibited a remarkable increase of sinuosity starting from the

(a) 10/28/1994. (b) 03/051995. (c) 05/24/1995 (d) 03/23/1996

Figure 4.12: LandsatLook images from the Sacramento river. a) image from October 28, 1994 with a discharge of 132 $^{m^3}/_s$, b) image from March 5, 1995 with a discharge of 2675 $^{m^3}/_s$, c) image from May 24, 1995 with a discharge of 3030 $^{m^3}/_s$, d) image from March 23, 1996 with a discharge of 220 $^{m^3}/_s$

1990s (Bartholdy and Billi, 2002). During the 1950s and 1960s, a deficit in sediment supply due to change in land use in the upstream part of the basin was exacerbated by extensive mining of bed material, which was ultimately forbidden in 1978. The reduction in sediment supply formed a relatively straight, deep channel with alternate bars. After 1978, a consistent sediment load supply re-established due to the ceasing of mining and to bank erosion associated with channel widening (Rinaldi et al., 2008; Luppi et al., 2009; Nardi and Rinaldi, 2010; Rinaldi and Nardi, 2013).

Two consecutive meanders developed in the recent years (Fig. 4.15) due to a pronounced bank erosion process. Nardi et al. (2013) performed numerical simulations mainly focused on the bank erosion process related to the elongation of the first of these two meanders. The rapidity of the process, and in particular the erosion of the outer (left) bank of the first bend, led to an incomplete growth of the point bar in terms of ground elevation, as well as robust vegetation was unable to cover, and thus to protect, the newly formed bar (Fig. 4.15, panel F). In addition, the analysis of both the aerial images (Fig. 4.15, panel F) and the Digital Elevation Model (DEM) derived from a LiDAR survey (Fig. 4.16), suggests that the flow was unable to remove from the main channel bed the whole material eroded from the bank and thus to maintain the main channel sufficiently deep. This occurrence is also related to the lack of a fully developed point bar on the inside of the bend, which during flood events lets the incoming flow to expand over the inside of the bend, thus reducing the mean velocity of the in-channel stream flow (Fig. 4.18), its erosive power and sediment transport capacity. Also, the

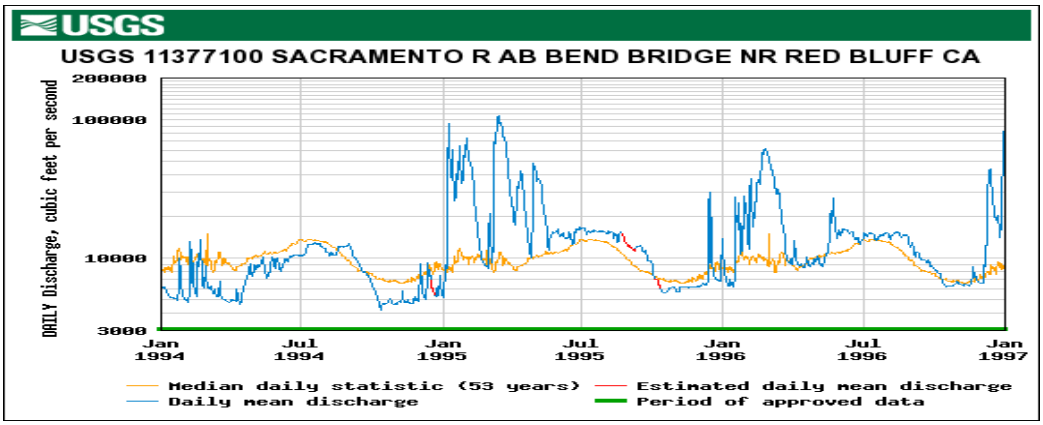


Figure 4.13: Hydro-graph from gauge station USGS no.11377100 in the period that correspond to a chute cutoff

inside of the first bend is characterized by a clear pattern of both topography and vegetation (Fig. 4.16 and Fig. 4.17), which determines the presence of preferential pathways for overflow.

In was in this context that, approximately between 2011 and 2013, the elongated meander underwent a chute cutoff (Fig. 4.15, panel G). The mechanism that led to the formation of the chute can be ascribed to both the extreme variability of flow regimes, which cause the rapid erosion of the outer bank of the bend first and to insufficient removal of the eroded material from the channel bed.

The hydrodynamic conditions responsible for the cutoff occurrence are assessed using the 2DEF hydrodynamic model, which is first applied to analyze the river configuration referring to 2008 (Fig. 4.16), and then to a geometry referring to, approximately, the year 2010. This last configuration, whose model topography is shown in Fig. 4.17 was reconstructed based on the DEM of 2008 and the aerial image of 2010 to "update" the path of the main channel. The 2008 configuration was set up for gathering a complete picture of the river, whereas only results referring to 2010 are shown and commented from now on. The numerical grid is made up of about 26,000 nodes and 51,000 triangular elements, to cover a reach long about 4 km (from 1 Km upstream to 3 km downstream the chute). The topography is assigned to the model elements based on a. Given that the topographical survey was conducted during a low-flow period, most parts of the main channel was covered by DTM data, and results from the model of Frascati and Lanzoni (2013) was used to estimate the bathymetry only in limited segments of the

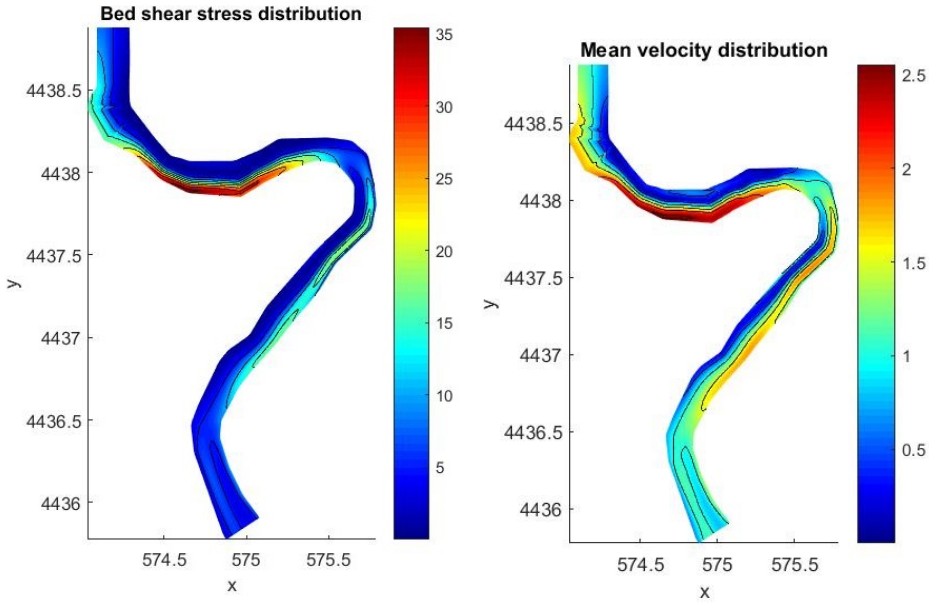


(a) Bed shear stress distribution in Pascal.

(b) Mean velocity distribution in m/s.

Figure 4.14: Hydraulic simulations results using a simple model for the 1994 Sacramento river configuration.. (The axes coordinates are georeferenced with the UTM system).

river.

The rating curve prescribes at the downstream section of the numerical grid is estimated by enforcing uniform flow conditions. Anyhow, preliminary tests showed that the distance between the area of interest and the closing section of the model is large enough so that errors in the downstream boundary condition are unable to affect the flow field where chute cutoff occurred. The resistance parameters of the 2DEF model were assumed based on granulometric and morphological characteristics of the considered reach(Nardi et al., 2013). Although the model is not properly calibrated against measured data, a set of preliminary simulations showed that the main conclusions that can be drawn from the modeling study remain the same by changing the resistance parameters within a reasonable range. Hence, and only in this view, the model results are to be considered as qualitative.

The model is forced with a total discharge in the range between 5 and 600 $m^3/s$ (Nardi et al., 2013). The model results show that the hydrodynamic

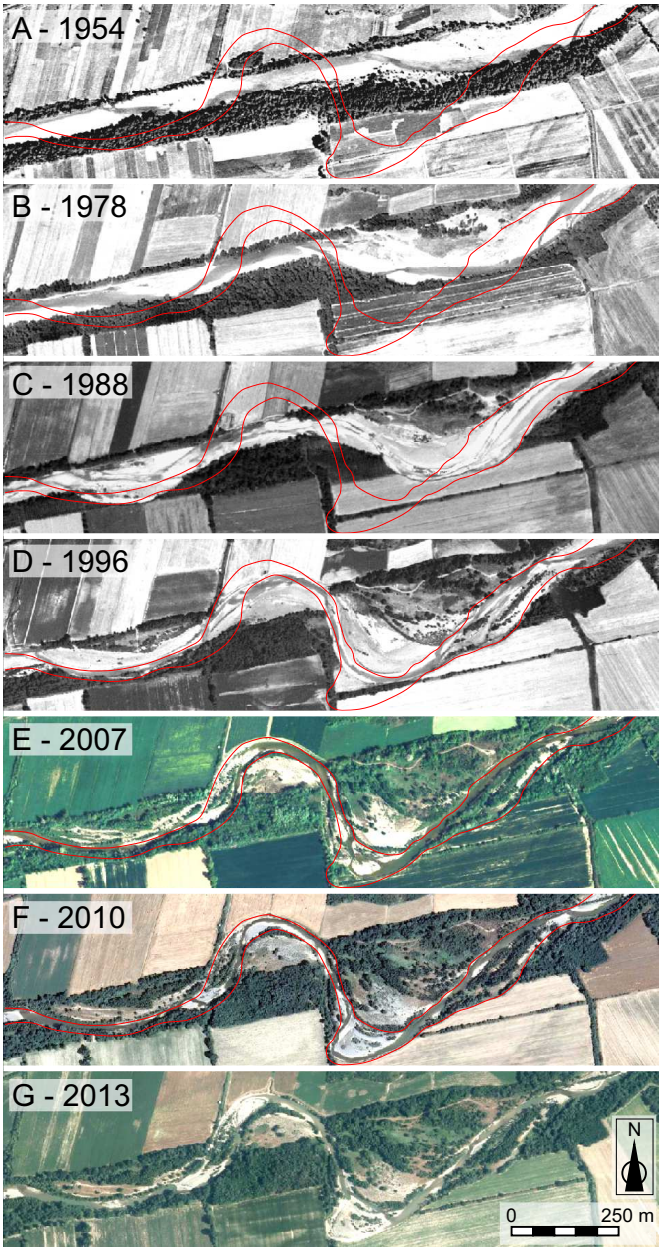


Figure 4.15: Cecina River (Tuscany, Italy). Historical aerial images are showing the recent evolution of the main channel. For comparison purposes, the red lines denote the channel banks of the 2013 configuration. Water flows from right to left.

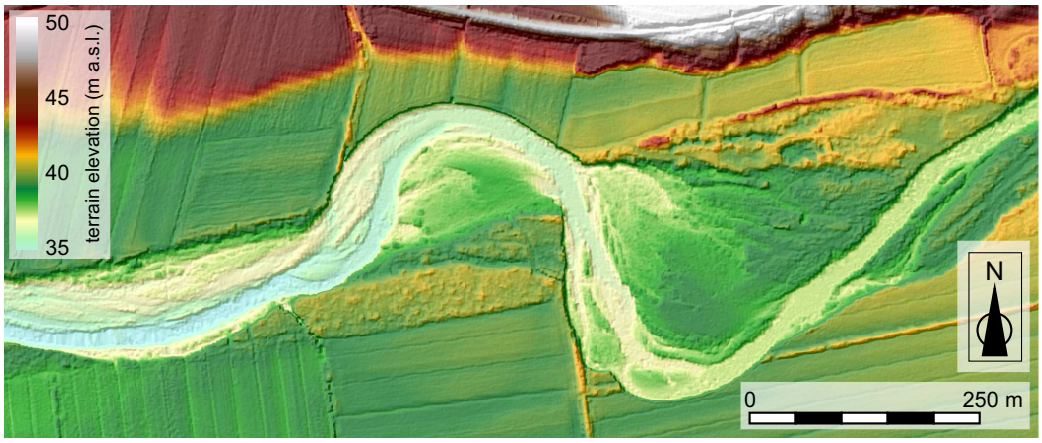


Figure 4.16: Cecina River. Digital Terrain Model (resolution of 1x1 m) derived by a LiDAR survey (data source: "Ministero dell'Ambiente e della tutela del Territorio e del Mare – Rilievi Lidar", courtesy of the Tuscany Region). The survey refers to year 2008.

flow field drastically changes with increasing discharge (Fig. 4.18), mostly regarding velocity pattern in the downstream part of the bend and on the point-bar. The most interesting and not obvious feature is that the flow velocity does not increase monotonically with the total discharge. Consider in particular points P1 and P2, placed where the chute has then occurred (Fig. 4.18); the flow velocity initially increases as the inside of the bend is flooded, and suddenly drops as the discharge surpass a sort of threshold (100 $^{m^3}/_s$ in our simulations, see Fig. 4.19). This occurrence is mainly due to the backwater effects and to the spreading of streamflow throughout the inside of the bend (Fig. 4.18), which effectively counteract the advective inertia of the incoming flow.

The mechanisms that here led to the chute incision is not related to the power of the upstream flow, which is indeed uncorrelated with the velocity in the inside of the bend for the significant values of the discharge (Fig. 4.19). Instead, the gradient advantage owed by paths on the point-bar and the poorly developed (and little conveying) main channel caused the incision of a chute for flow rates significant enough to affect the point bar, but relatively small if compared with the major floods of the Cecina River.

An analysis of the discharge time series, provided by the Hydrological Service of Tuscany Region (www.sir.toscana.it) for the Ponte di Monterufoli gauging section that is located few kilometers downstream of the study reach, shows that the two major floods in the period 2010-2013 were char-

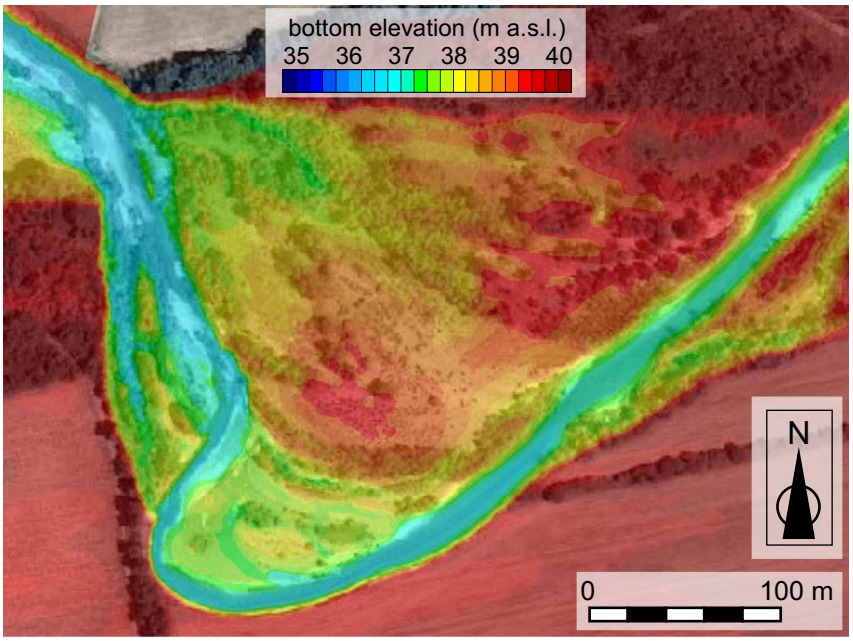


Figure 4.17: Cecina River. Bottom elevation of the numerical grid, reconstructed from the LiDAR survey (2008), the 2010 aerial image (shaded in background), and the model of Frascati and Lanzoni (2013). Water flows from right to left.

acterized by a maximum discharge of about 220 and 170 $^{m^3}/_s$, respectively. Such values are significantly less than the flood waves occurred just before (6th January 2010, peak discharge of 340 $^{m^3}/_s$) and after (21st October 2013, peak discharge of 540 $^{m^3}/_s$) this 3-year period.

### 4.4.3 Chixoy River

The Chixoy river (see Fig. 4.4) also knows as Negro river (due to the significant amount of suspending sediment that the river transport) collects water from Sierra de Los Cuchumatanes and the Sierra Madre at the northwest of Guatemala, whit a drain area of 10,909 $Km^2$, a mean annual discharge of 494 $^{m^3}/_s$ that flows over 418 Km to then became the Usumacinta river winch is the frontier between Guatemala and Mexico (according to the national hydrological service of Guatemala: Instituto Nacional de Sismología, Vulcanología, Meteorología e Hidrología -INSIVUMEH- http://insivumeh.gob.gt/hidrologia.html). The hydrologic regimen was mod-

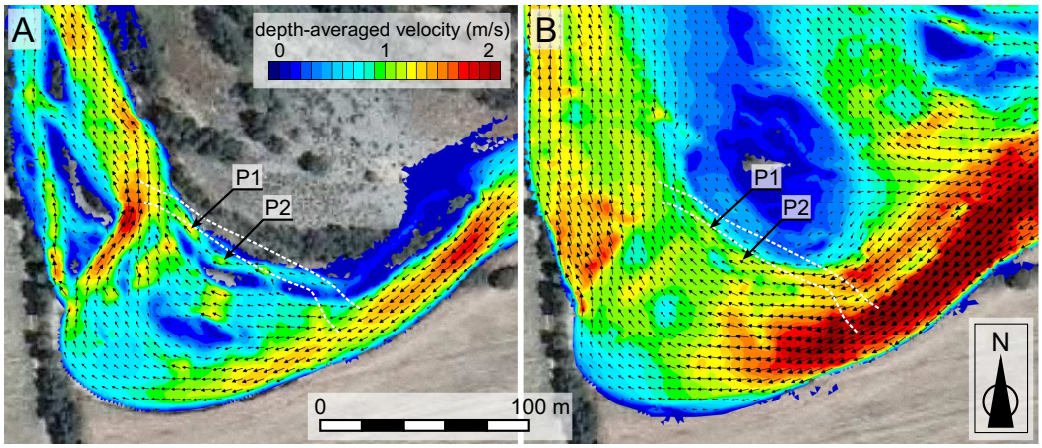


Figure 4.18: Cecina River. Model results in terms of depth-averaged velocity for a total water discharge of 40 $m^3/s$ (A) and 200 $m^3/s$ (B), respectively. The white dashed lines denote the location of the chute occurred between 2010 and 2013.

ified at the beginning of the 80s due to the construction of the Chixoy dam (upstream of our study area), which is the biggest dam in Guatemala supplying almost 1/3 of the electricity demand in Guatemala.

The Chixoy river is almost static in most of its course, but present a high-velocity meandering migration area, in 2010 was in this area where a chute cutoff was observed as can be seen in Fig. 4.20 ( unfortunately due to the high cloudiness that characterizes the area was not possible to obtain the images during all chute cutoff process). According to the available data from the gauge station INSIVUMEH Playa Grande (active since 2014), which is a few kilometers upstream from the area of interest, there is a relationship width to depth of around 23.5 m/m, a water surface slope of 0.000056 m/m and a sediment size that goes from 0.05 to 2 mm.

Also in the case of the Chixoy river, there is no available topographic data from the floodplain that correspond to the chute cutoff period, for that reason it was not possible to implement the 2D hydraulic model. For the discharge, the proceeding was the same as of the Sacramento River, analyzing the discharge hydrograph for the period between the satellite images (see Fig. 4.20). Using the gauge station INDE no.01.08.04H (see Fig. 4.21), that is upstream from the point of interest, choosing the biggest discharge record during this period. To apply the model of Frascati and Lanzoni (2013), planimetric input data was obtained from the satellite image of 2010 (see.

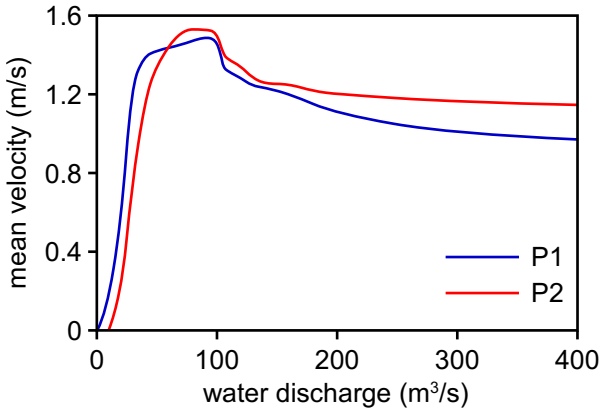


Figure 4.19: Cecina River. Depth-averaged velocity for different values of the total discharge at points P1 and P2 (see the black arrows in Fig 4.18), located where the chute later formed.

(a) May 10, 2010 (b) April 27, 2011 (c) March 28, 2012

Figure 4.20: LandsatLook images from the Chixoy river. (a) image from May 10, 2010 with a discharge of 353 $^{m^3}/_s$, (b) image from April 27, 2011 with two discharges before the image of 793 $^{m^3}/_s$ and 910 $^{m^3}/_s$, (c) image from March 28, 2012 with a discharge of 158 $^{m^3}/_s$.

Fig. 4.20(a)), using the slope, sediment and depth-width relationship, mentioned previously. The model parameters were chosen to obtain bank full condition that corresponds to the selected discharge. The cross sections were discretized every 10 meters, and each cross section is dived in 200 points, equally spaced among them.

Fig. 4.22 show respectably the bead average shear stress and velocity flow field computed with the model of Frascati and Lanzoni (2013). From these results is possible to see that, also in this study case, there is a concentration of shear stress and velocity where the chute channel forms. There are also other parts of the channel that present similar concentrations of velocity and shear stress in which the chute process did not appear, this suggest that

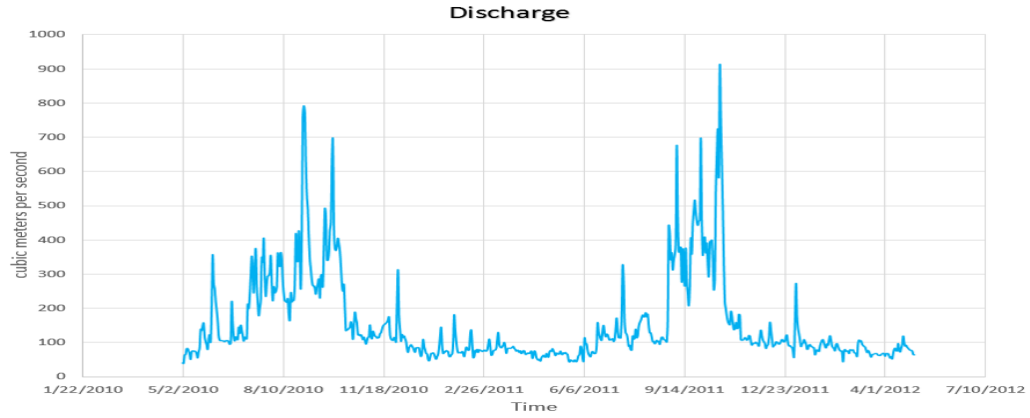


Figure 4.21: Daily discharge, river gauge station INDE no.01.08.04H, in the period that correspond to a chute cutoff.

in the case of the chute cutoff of 2010 in the Chixoy river, there are other mechanisms beyond the momentum exchange between the main channel and the floodplain. In this case, as was mention before the historical path of the river plays a crucial implication (see Fig. 4.4). When the channel presents the overbank flow and the exchange of momentum between the channel and the floodplain produced, the water reenters in a paleochannel that was not entirely closed as well as the floodplain in over this paleo channel was not wholly consolidated.

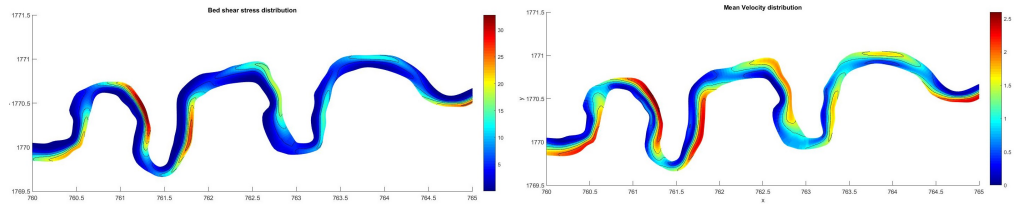


(a) Bed shear stress in Pascal. (b) Mean velocity distribution in m/s.

Figure 4.22: Hydraulic simulations results using a simple model for the Chixoy river. (The axes coordinates are georeferenced with the UTM system).

Is possible to argue that, the combination of this specific planimetric configuration (see Fig. 4.20(a)) which favor the concentration of shear stress and velocity (see Fig. 4.22) with the consequent exchange of momentum in specific zone neighbor to the paleochannel (see Fig. 4.4) and the sequence of floods (see Fig. 4.22) that affected during this specific channel configuration, all those together were the factors that trigger and ensure success of the chute

cutoff process.

## 4.5 Discussion

Hydrodynamic considerations and the numerical analyses highlight that the energy of the flow through the floodplain is due to two factors, which are distinct although interwoven: the advective inertia of upstream, in-channel flow, and the gradient of hydraulic head between the upstream and downstream ends of paths through the floodplain, also known as gradient advantage. The first factor dominates when the flow, coming from an upstream, relatively narrow bend, impinges the bank of the meander undergoing cutoff, first causing the incision of an embayment, and then the incision of the chute through the floodplain. When the second factor dominates, the chute forms either by progressive enlargement of existing swales or sloughs through the point/scroll bar or by headward incision of a gully.

Accordingly, based on these results and the literature review, two macro-groups are identified, in which the different mechanisms of chute formation can be grouped:

i) chute incision is driven by overbank flow occurring at the inflection point downstream of a relatively narrow meander bend, of which the Sacramento case study shown above is an illustrative example. In this case, the flow field within the main channel drives the erosion process due to advective inertia of in-channel stream flow;

ii) chutes, driven by the gradient advantage of a path through the inside of the bend, form owing to erosion of existing preferential pathways through the point/scrollbar.

In both the macro-groups, the occurrence of overflow is needed for the chute to form, but the total discharge plays an entirely different role in the two cases. The difference can be grasped from Fig. 4.23, which reports the free-surface gradient through the inside of the bend, where a chute subsequently formed, for increasing total discharges. In the Sacramento River, the gradient shows a general increase for increasing discharge, because the upstream flow is directed against the upstream end of the chute, so that the advective inertia of the flow results in a rise in free-surface elevation close

to the bank where the embayment then forms. Contrarily, in the Cecina River the increasing of discharge leads to a marked, monotonic decrease of the gradient through the floodplain; here, the upstream flow is not directed toward the inside of the bend, and backwater effects act to kill the gradient also for moderate discharges.

It is worth noting that, in rivers where the regular shape of meanders prevents the in-channel stream flow to decisively impinge against the downstream bank at the inflection point, the incision of chutes can be forced only because by gradient advantage (macro-group 2) and not by the advective inertia of the upstream in-channel flow. Accordingly, is possible to conjecture that chutes can assume a direction different to that of point/scrollbar swales or sloughs only if they own to the first of the two macro-group, i.e., if they are forced by the inertia of the upstream flow.

Chute cutoffs of both the two macro-groups can be detected in the reach of the Allier River depicted in Fig. 4.1; magenta and blue circles, denote chute channels mainly forced by the inertia of the in-channel flow and by gradient advantage, respectively. By looking at the Strickland River in the reach of Fig. 4.2, it appears that chutes only formed following scroll-bar ridge and swales, no matter the gradient advantage associated with short paths through the floodplain. Indeed, many locations in this reach are characterized by a sensibly higher gradient advantage than those where chute cutoffs occurred where, in fact, no preferential pathways are provided by ridge and swales topography.

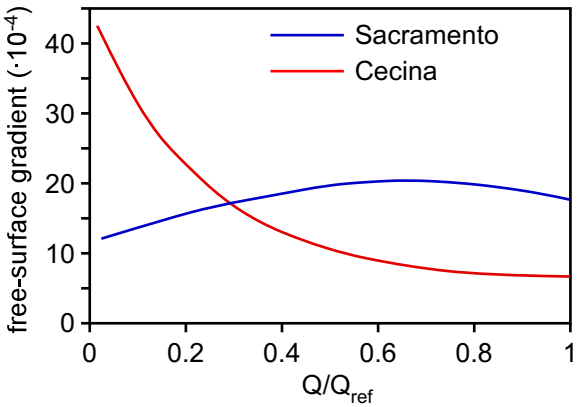


Figure 4.23: Free surface gradient between the upstream and downstream ends of the chute. The total discharge, Q, is scaled with a reference value, Qref, equal to 3,000 and 600 $^{m^3}/_s$ for the Sacramento and the Cecina Rivers, respectively.

In conclusion, as it was widely recognized, the floodplain topography plays a significant role in controlling not only the patterns of meander migration (e.g., (Bogoni et al., 2017)) but also the occurrence of chute cutoffs. In the case studies here analyzed, was observed that chutes typically form in correspondence of topographic lows, that are the remainder of paleo-meander cutoffs (i.e., segment of the main channel abandoned due to the occurrence of antecedent cutoffs) or result from the ridge and swale sequence characterizing scroll bars, possibly reinforced by the presence of a vegetation cover. Scroll patterned point bars are typical of medium-energy noncohesive floodplains (Nanson and Croke, 1992) and consist of heterolithic stratification of interbedded sand and mud deposits with lateral accretion surfaces. On the other hand, paleo-meander cutoffs can form up to the 75 percent of channel reaches within a floodplain (David et al., 2016); they are lower in elevation and likely different regarding stratigraphy, concerning the surrounding floodplain. Hence, they are preferential pathways for overbank flow, and prone to erosion given that the presence of less consolidated sediment deposits concerning the adjacent floodplain.

Also, the hydrodynamic flow field within the main channel can play a crucial role in the occurrence of chute cutoff. The application of the mathematical model developed by Frascati and Lanzoni (2013) to different rivers revealed that a significant concentration of both flow velocity and bottom shear stresses is always found in the main channel close to the bank which corresponds to the upstream section of chute cutoff up to be incised. The analysis of the chute initiation in the Sacramento River described in the previous Section, confirms that advective inertia of in-channel flow crucially affects the flow rate, the magnitude and the direction of velocity over the floodplain near the bank, where the chute incision occurred. Then, the inertia of the flow within the main channel, and not only the water surface elevation (Constantine et al., 2010), is an essential factor controlling chute formation. However, it must be stressed that similar or even higher values of velocity and shear stresses are contextually found in other parts of the same river, where chute incisions did not form. This is apparently due to the multiplicity of factors that control, often inhibiting, the development of chute channels.

## 4.6 Conclusions

This chapter focused on the formation of chute cutoffs in meandering rivers. A comprehensive review of the literature, focusing on the mechanisms of chute formation and the many controlling factors, pointed out the complexity of the subject.

The numerical analyses carried out in the present study, which was mostly concentrated on the hydrodynamic forcing responsible for chutes initiation, allowed to distinguish between hydraulically driven and topographically driven chute cutoffs. In the first case, the incision on the floodplain is primarily determined by the flow field within the main channel, upstream of the chute to be formed; in the second case, the incision is mainly determined by the gradient advantage and the flow field over the floodplain. In hydraulically dominated cutoffs, the mainstream is usually directed towards the outer bank due to pronounced channel curvature, thus significantly increasing the water level against the outer bank and promoting the formation of embayments as precursors of chute incisions. This mechanism is fostered by hydrodynamic conditions (e.g., backwater effects) and by sediment dynamics (e.g., deposition and formation of plug- or central-bars within the main channel). In topographically driven chute cutoffs, a significant role is played by the gradient advantage of flow paths through the floodplain concerning the main channel, and to the presence of ridge and swales topography or paleo-channels.

In any case, the presence of preferential pathways on the floodplain has a significant influence on the formation of chutes. This implies that to accurately model chute cutoff inception, the actual configuration of the floodplain must be accounted for, and the flow field within the main channel and over the adjacent areas have to be jointly solved. The presence of several controlling factors, interplaying and competing together, dramatically increases the complexity of the problem. Heterogeneity of the floodplain associated with sediment sorting and preserved sedimentary landforms, as well as vegetation encroachment may act either to enhance or to inhibit the occurrence of chute cutoffs.

Reliable predictions of chute cutoffs can be achieved by accurately modeling both the hydrodynamic flow field and the bed evolution within the main channel and over the floodplain. The flow field within the main channel, in fact, can significantly affect the overland flow on the floodplain. Also, the possible formation of plug- and central-bars within the main channel can

play a significant role in bifurcation dynamics and, thus, in controlling the incision of chutes. Floodplain heterogeneity, on the other hand, can also have an essential impact on cutoff occurrence. The knowledge gathered from this modeling approach may be used not only to assess local behaviors but also to develop a general, physics-based statistical framework to be inserted in long-term meander evolution models.

# Part III

# General conclusions

# Chapter 5

# General conclusions and future work

In this thesis, a low computational cost, physics-statistics based model has been developed for simulating erosion and accretion process that occur at the channel banks of meandering rivers. The model, taking advantage of the statistical characterization of along channel width variations observed in a wide sample of the river throughout all the world, mutually constrains bank erosion and accretion occurring at the channel banks to restrict width variations within a meaningful range of values.

The analysis of planform river configurations extracted from satellite images indicates that, for a given river, the normalized distribution of channel widths remains almost the same throughout time, and is best fitted by a General Extreme Value (GEV) probability distribution. Major variations in this width distribution are observed after cutoff events. However, after each cutoff, the river tends to progressively recover the pre-event width distribution.

A physics-statistically based numerical model, in which erosion and accretion rates are constrained according to the observed width distribution, allows stable long-term simulations of the meandering river evolution. The model has been tested concerning the Ucayali river, providing reasonable mid- and long-term results, with realistic values of the cross-section width. The model also seems to provide a realistic reproduction of the width-slope trajectories determined by the progressive river elongation as meanders grow and the abrupt channel shortening consequent to neck cutoffs.

Model application, as well as the interpretation of simulation results, must always carefully consider the intrinsic limitations of the modeling framework, mainly due to the linearized description of the flow field and the simplified treatment of bank collapse processes.

The two-dimensional description of the in-channel flow within meandering rivers provides useful information to locate the triggering of possible chute cutoffs. However, the analysis of some case studies has disclosed the complexity of physical processes leading to chute cutoff. The in-channel flow undoubtedly plays an important role but is only one of the mechanism that favor chute cutoffs. Indeed, the floodplain topography and texture are often crucial for the chute development. In this sense, a significant role is likely played by old abandoned channels.

The modeling framework developed in the present thesis can be used to inquire into the effects of width variations on the meandering and floodplain evolution. Another possible improvement is related to the coupling of the in-channel hydraulic model with a suitably simplified two-dimensional model of the floodplain overflow, with the aim of further addressing the hydraulically induced inception of chute cutoffs.

# Part IV

# Appendix

# Appendix A

# Complementary figures and tables of chapter 2

| No. | Name | Wavelength | Resolution | Use |
|---|---|---|---|---|
| 1 | Ultra Blue (Coastal/Aerosol) | 0.435 - 0.451 | 30 | Coastal areas and shallow water observations; aerosol, dust, smoke detection studies. |
| 2 | Blue | 0.452 - 0.512 | 30 | Bathymetric mapping; soil/vegetation discrimination, forest type mapping, and identifying manmade features. |
| 3 | Green | 0.533 - 0.590 | 30 | Peak vegetation; plant vigor assessments. |
| 4 | Red | 0.636 - 0.673 | 30 | Vegetation type identification; soils and urban features. |
| 5 | Near Infrared (NIR) | 0.851 - 0.879 | 30 | Vegetation detection and analysis; shoreline mapping and biomass content. |
| 6 | Shortwave Infrared 1 (SWIR 1) | 1.566 - 1.651 | 30 | Vegetation moisture content/drought analysis; burned and fireaffected areas; detection of active fires |
| 7 | Shortwave Infrared 2 (SWIR 2) | 2.107 - 2.294 | 30 | Additional detection of active fires (especially at night); plant moisture/drought analysis |
| 8 | Panchromatic | 0.503 - 0.676 | 15 | Sharpening multispectral imagery to higher resolution |
| 9 | Cirrus | 1.363 - 1.384 | 30 | Cirrus cloud detection |
| 10 | Thermal Infrared 1 (TIRS 1) | 10.60 - 11.19 | 100* | Ground temperature mapping and soil moisture estimations. |
| 11 | Thermal Infrared 2 (TIRS 2) | 11.50 - 12.51 | 100* | Ground temperature mapping and soil moisture estimations. |

Table A.1: Landsat 8 OLI and TIRS bands information. (Wavelength in micrometers, resolution in meters * TIRS bands are acquired at 100 meter resolution, but are re-sampled to 30 meter in delivered data product. Adapted from Tables 1 and 2 of (U.S. Geological Survey, 2015))

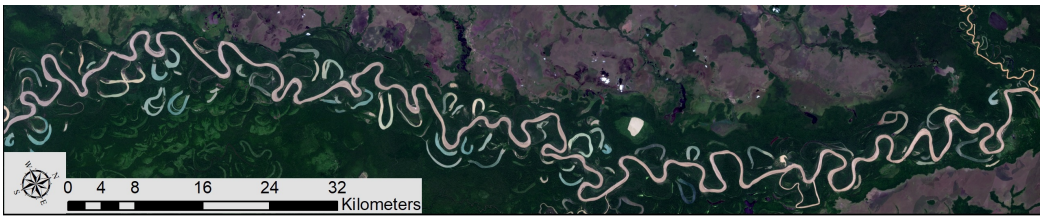


(a) Multispectral image.

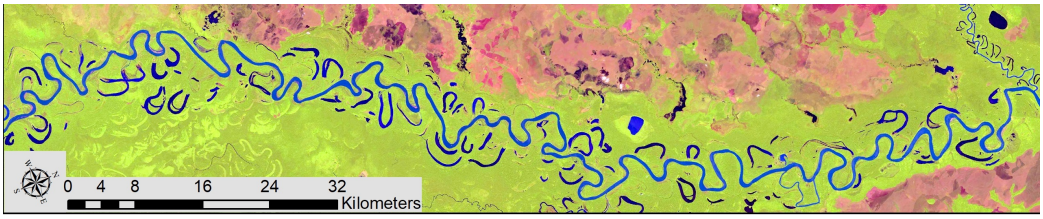


(b) Landsat look image.

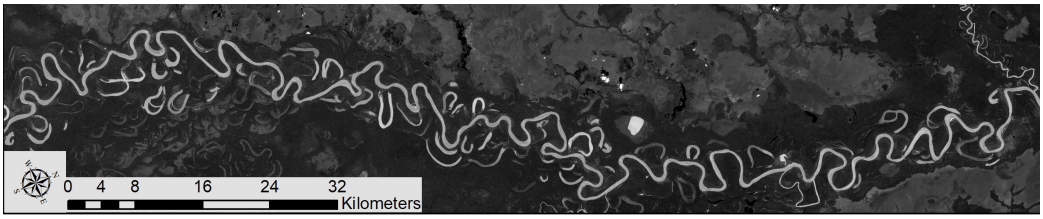


(c) Green band.

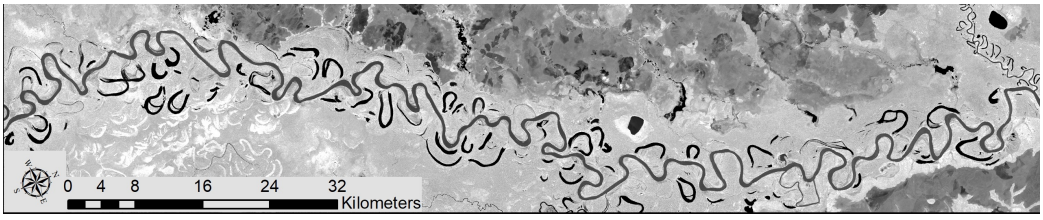


(d) NIR band.

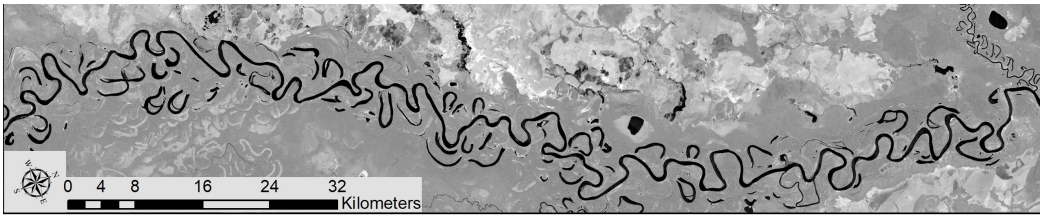


(e) SWIR1 band.

Figure A.1: Landsat 8 products for the Beni river.

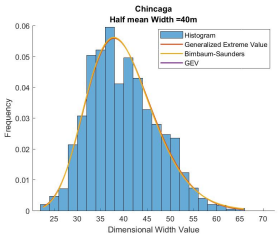


(1)

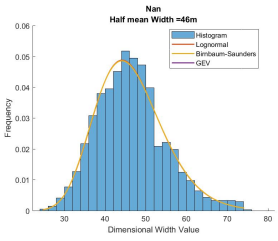


(2)

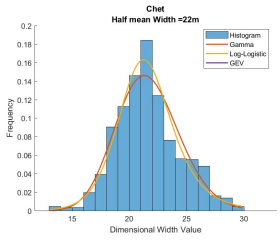


(3)

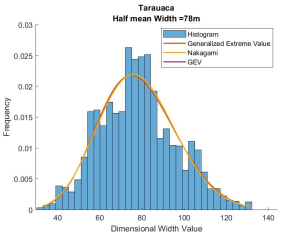


(4)

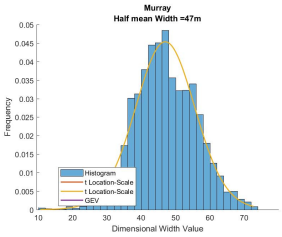


(5)

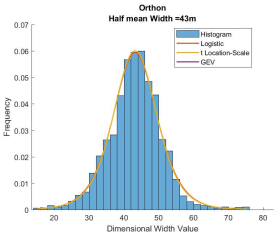


(6)

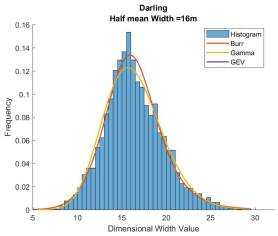


(7)

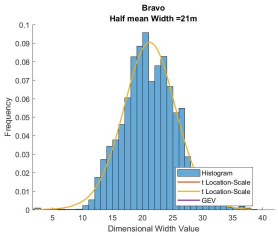


(8)

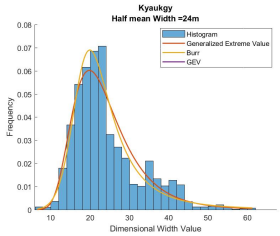


(9)

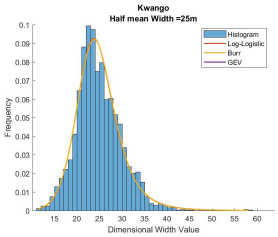


(10)

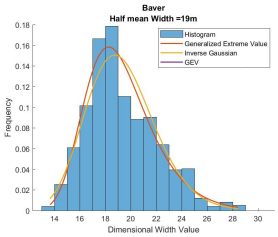


(11)

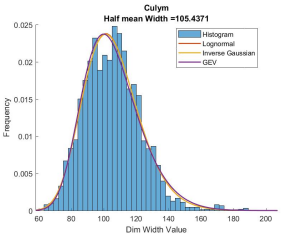


(12)

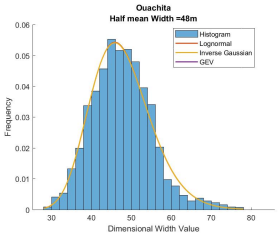


(13)

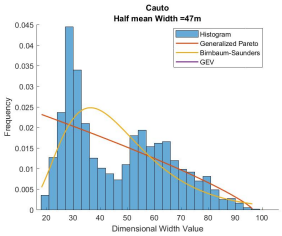


(14)

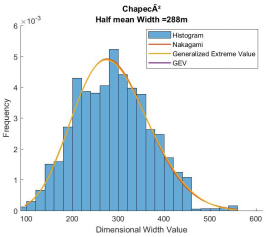


(15)

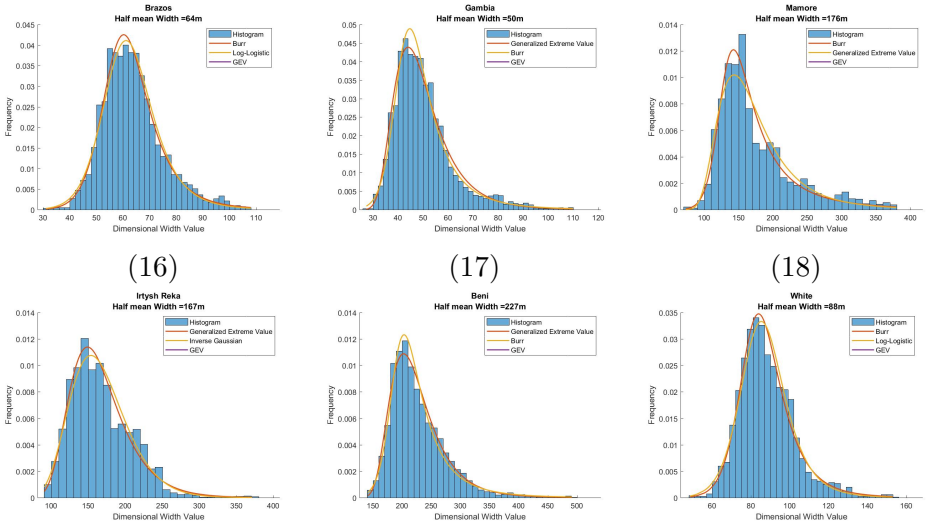


Figure A.2: Histogram, fist and second best fit PDF and GEV plot for each river in the dimensional.

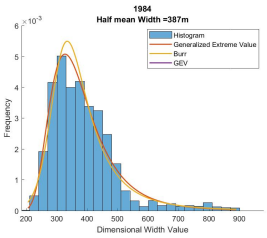


(1)

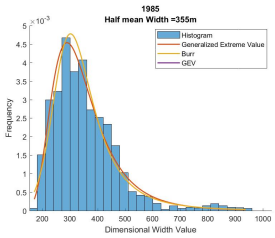


(2)

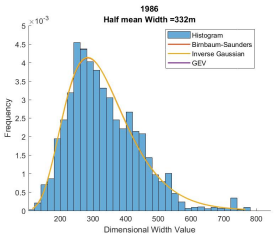


(3)

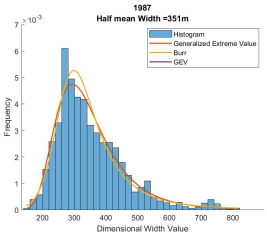


(4)

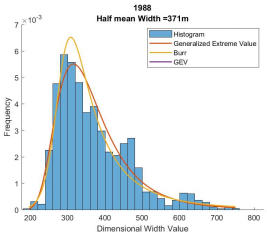


(5)

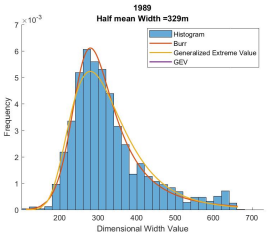


(6)

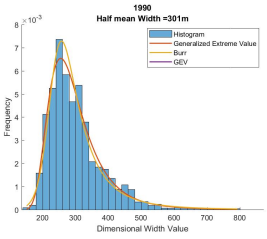


(7)

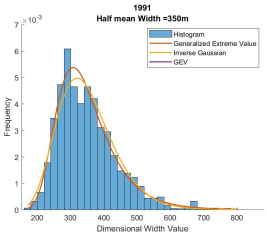


(8)

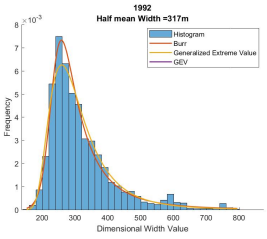


(9)

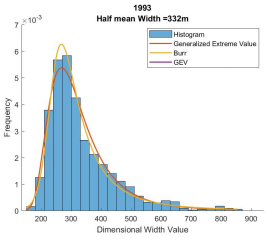


(10)

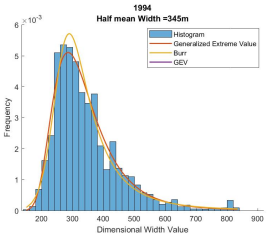


(11)

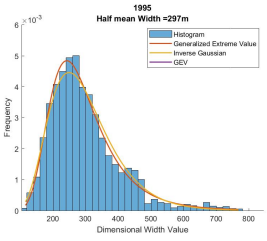


(12)

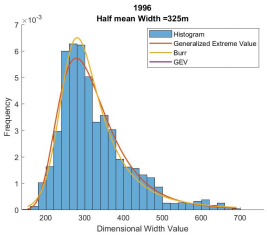


(13)

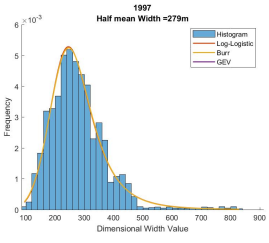


(14)

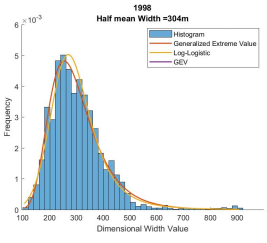


(15)

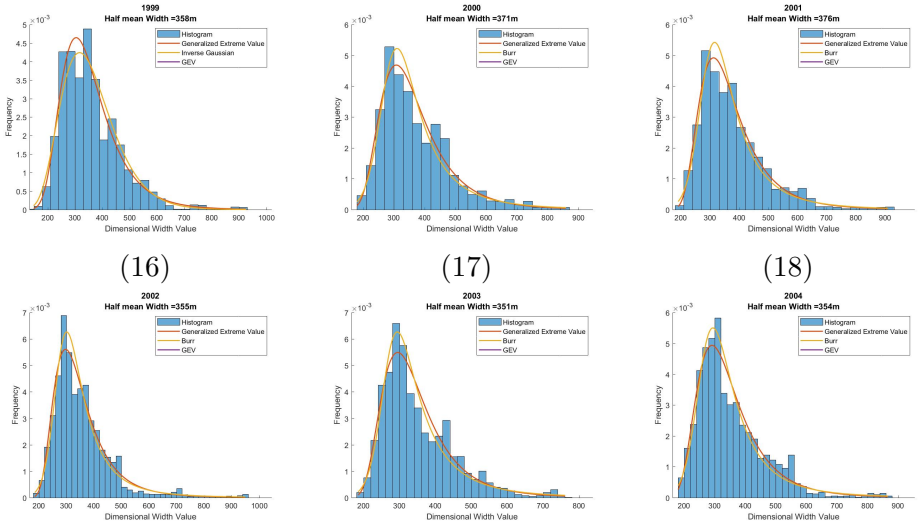


Figure A.3: Histogram, fist and second best fit PDF and GEV plot for each river in the no dimensional.

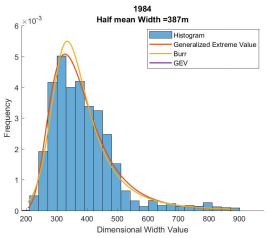


(1)

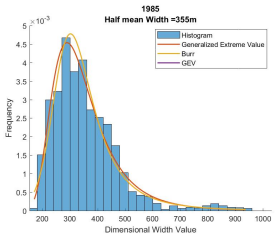


(2)

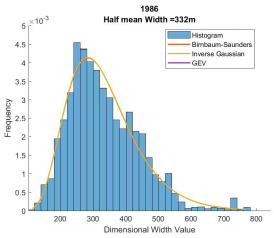


(3)

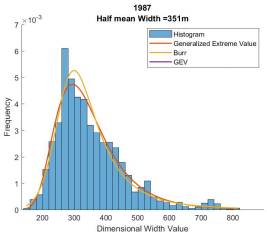


(4)

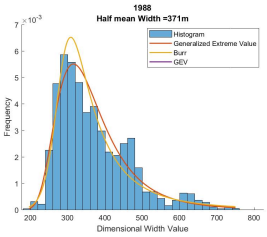


(5)

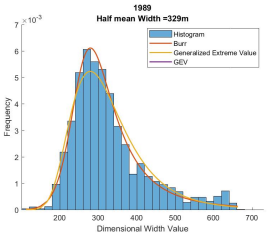


(6)

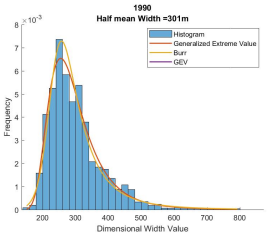


(7)

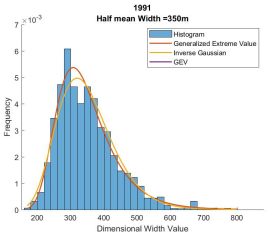


(8)

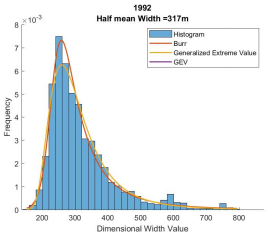


(9)

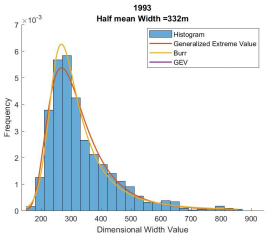


(10)

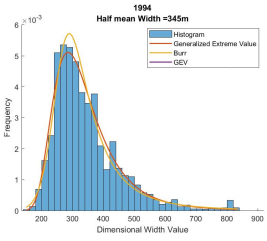


(11)

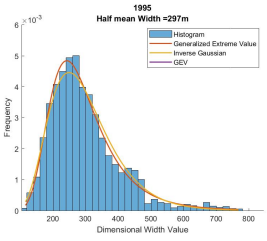


(12)

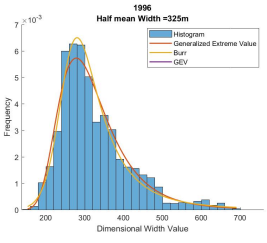


(13)

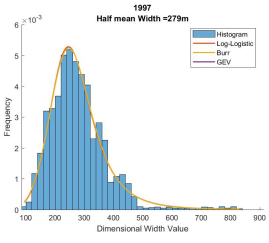


(14)

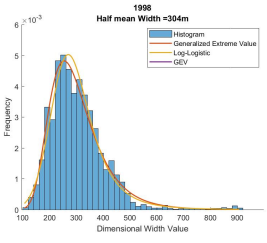


(15)

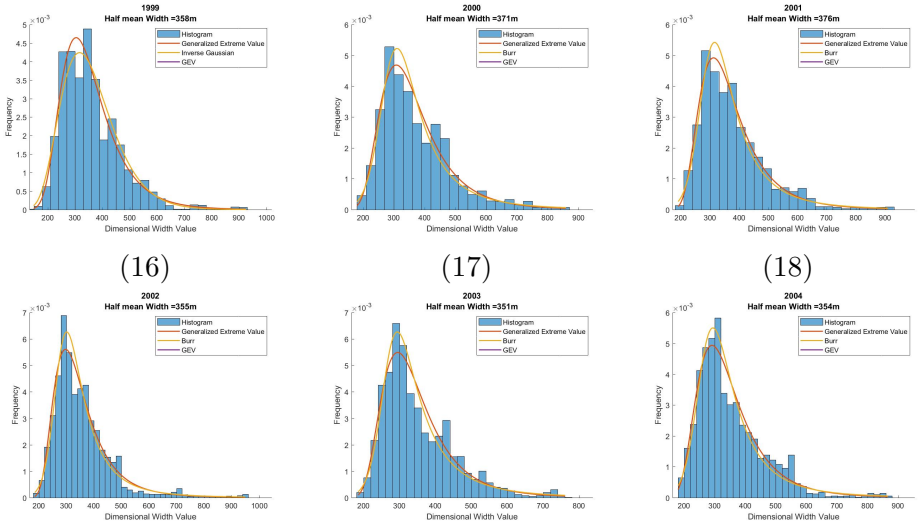


Figure A.4: Histogram, fist and second best fit PDF and GEV plot for each river in the no dimensional.

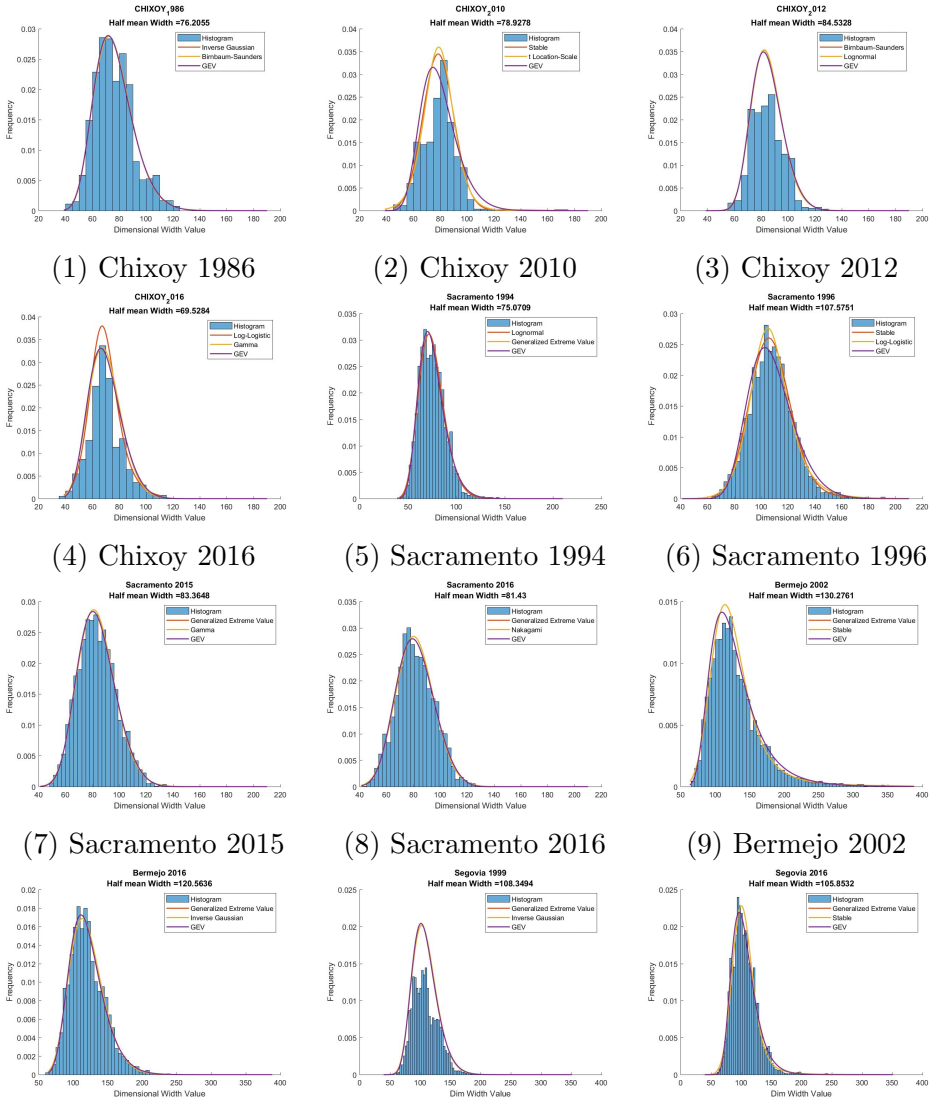


(1) Chixoy 1986 (2) Chixoy 2010 (3) Chixoy 2012

(4) Chixoy 2016 (5) Sacramento 1994 (6) Sacramento 1996

(7) Sacramento 2015 (8) Sacramento 2016 (9) Bermejo 2002

(10) Bermejo 2016 (11) Segovia 1999 (12) Segovia 2016

Figure A.5: Histogram, fist and second best fit PDF and GEV plot for each river in every analyzed year for the dimensional case.

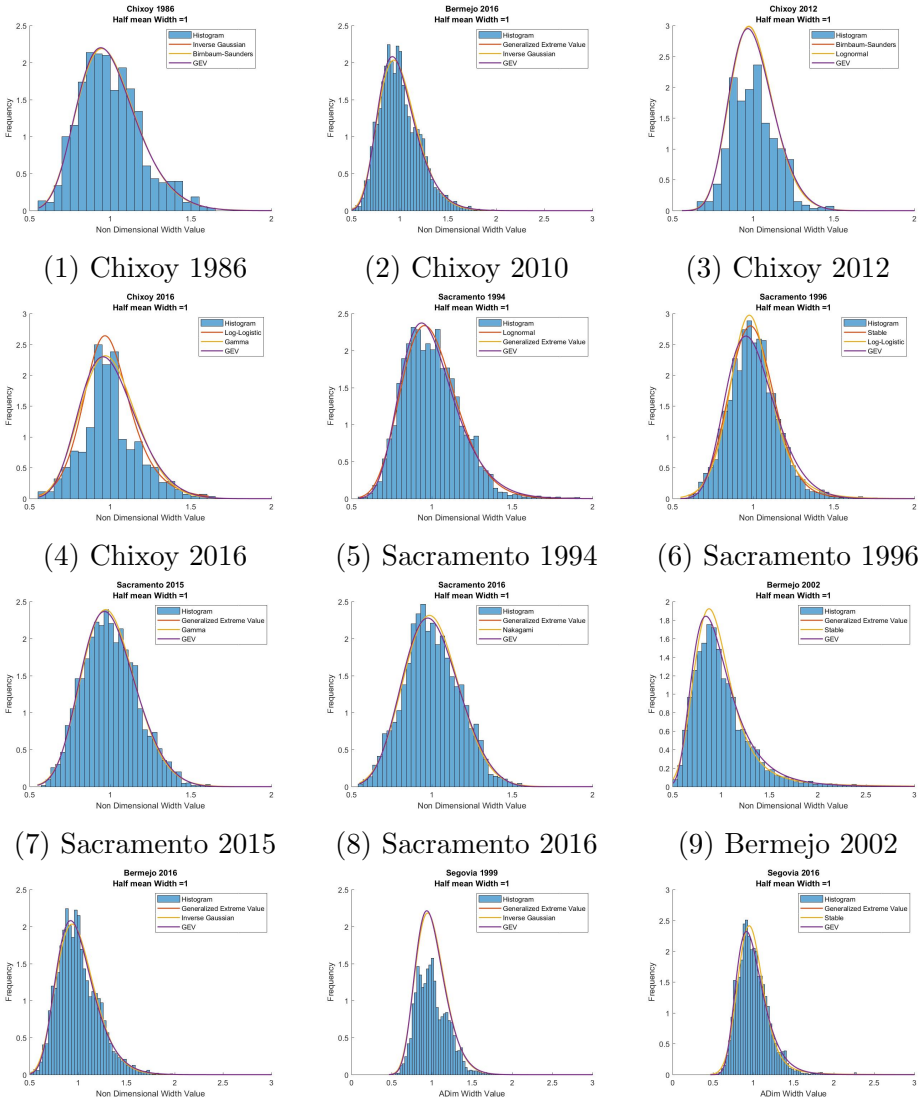


(1) Chixoy 1986 (2) Chixoy 2010 (3) Chixoy 2012

(4) Chixoy 2016 (5) Sacramento 1994 (6) Sacramento 1996

(7) Sacramento 2015 (8) Sacramento 2016 (9) Bermejo 2002

(10) Bermejo 2016 (11) Segovia 1999 (12) Segovia 2016

Figure A.6: Histogram, fist and second best fit PDF and GEV plot for each river in every analzyed year for the dimensionless case.

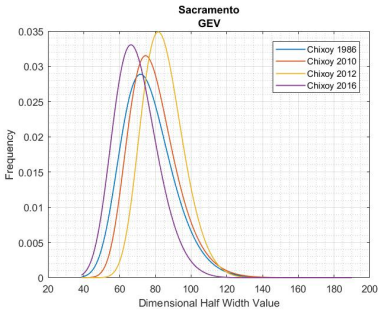


(1) Chixoy dimensional

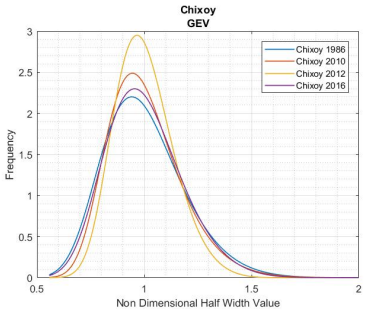


(2) Chixoy dimensionless

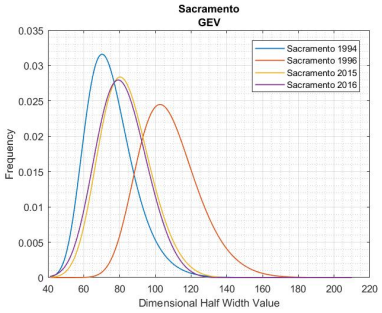


(3) Sacramento dimensional

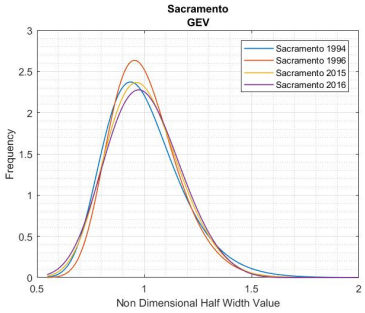


(4) Sacramento dimensionless

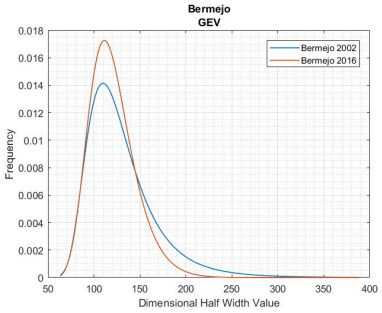


(5) Bermejo dimensional

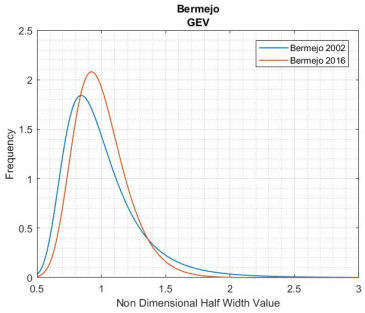


(6) Bermejo dimensionless

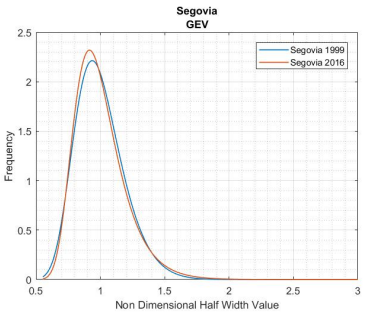


(7) Segovia dimensional

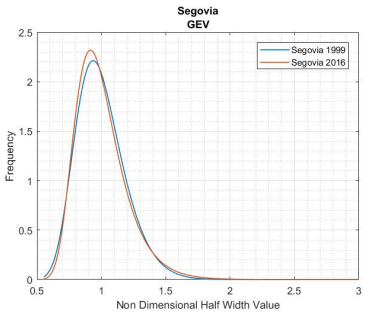


(8) Segovia dimensionless

Figure A.7: Dimensional and dimensionless GEV for each river through time.

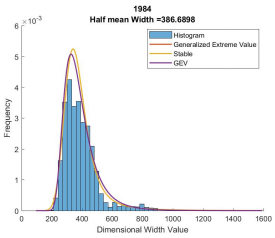


(a) 1984

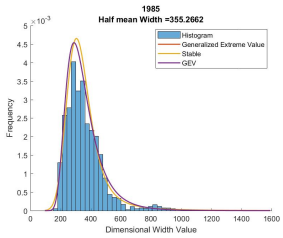


(b) 1985

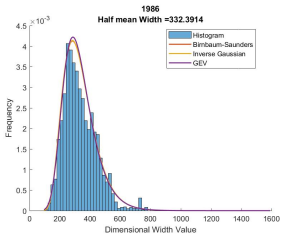


(c) 1986

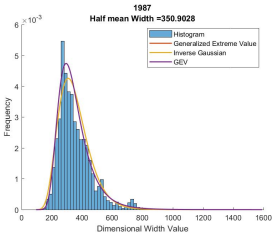


(d) 1987

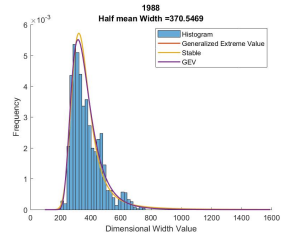


(e) 1988

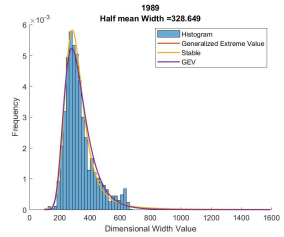


(f) 1989

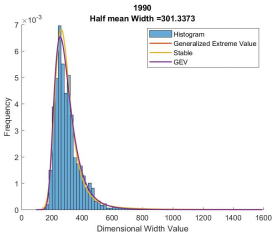


(g) 1990

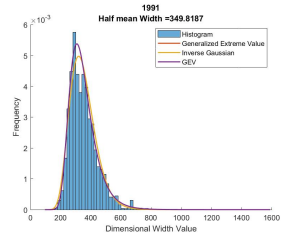


(h) 1991

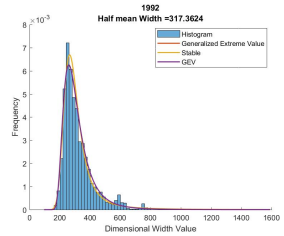


(i) 1992

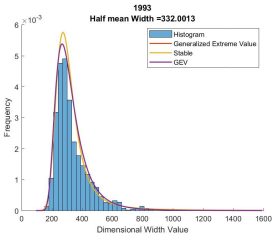


(j) 1993

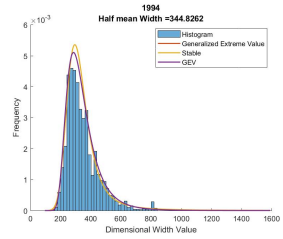


(k) 1994

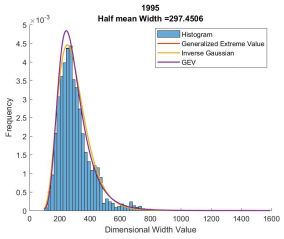


(l) 1995

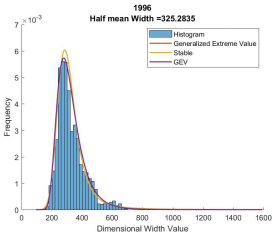


(m) 1996

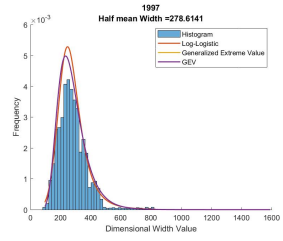


(n) 1997

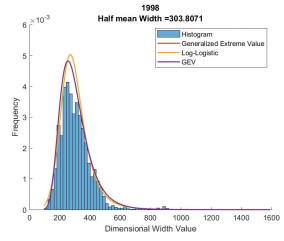


(o) 1998

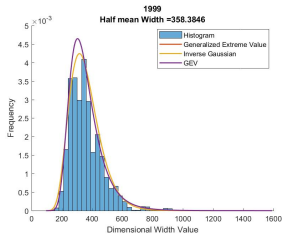


(p) 1999

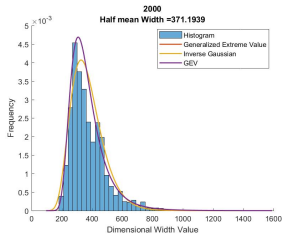


(q) 2000

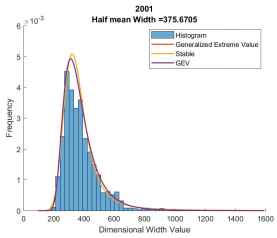


(r) 2001

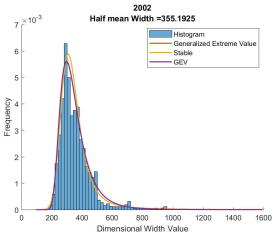


(s) 2002

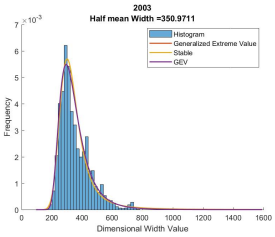


(t) 2003

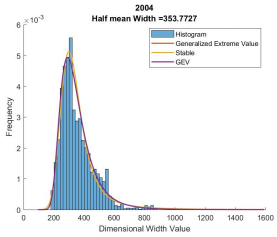


(u) 2004

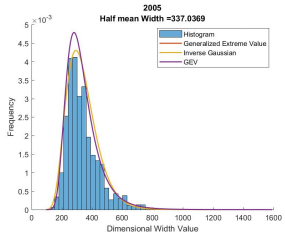


(v) 2005

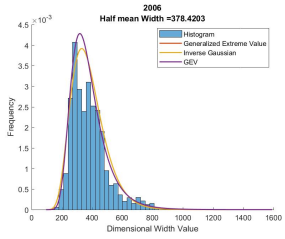


(w) 2006

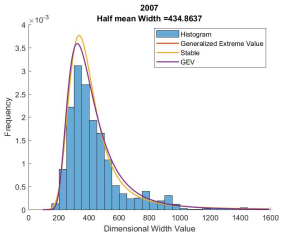


(x) 2007

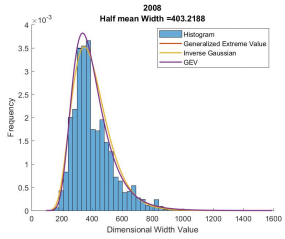


(y) 2008

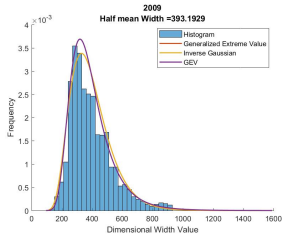


(z) 2009

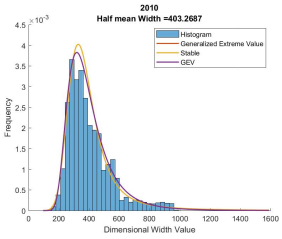


(aa) 2010

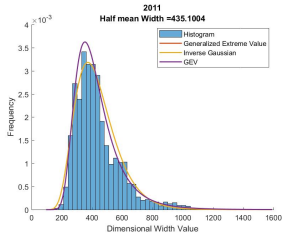


(ab) 2011

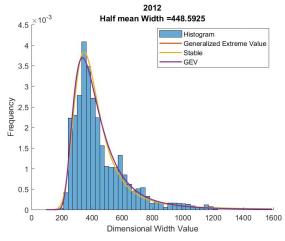


(ac) 2012

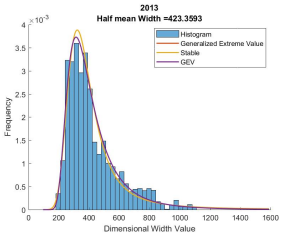


(ad) 2013

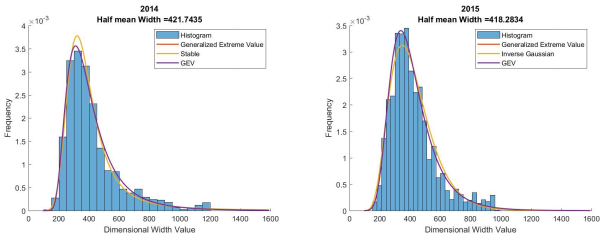


(ae) 2014 (af) 2015

Figure A.8: Ucayali's histogram, fist and second best fit PDF and GEV plot for each river in the dimensional case.

| No | River Name | Region | Country |
|---|---|---|---|
| 1 | Chinchaga | Alberta | Canada |
| 2 | Nan | Uttaradit | Thailandia |
| 3 | Chèt | Chèt | Russia |
| 4 | Tarauacà | Envira (Amazonas) | Brazil |
| 5 | Murray | ew South Wales /Victoria | Australia |
| 6 | Orthon | Pando | Bolivia |
| 7 | Darling | New South Wales | Australia |
| 8 | Bravo | Border | Mexico-USA |
| 9 | Kyaukgy | Toungoo | Myanmar |
| 10 | Kwango | Holò | Angola |
| 11 | Beaver | Alberta | Canada |
| 12 | Čulym | Oblast' di Tomsk | Russia |
| 13 | Ouachita | Arkansas | USA |
| 14 | Cauto | Provincia de Granma | Cuba |
| 15 | Chapecò | Santa Catarina/Rio Grande do Sul | Brazil |
| 16 | Brazos | Texas | USA |
| 17 | Gambia | Konkouli | Gambia-Senegal |
| 18 | Mamore | Chocabamba/Beni | Bolivia |
| 19 | Irtysh Reka | Oblast' di Omsk | Russia |
| 20 | Beni | Beni/La Paz | Bolivia |
| 21 | White | Arkansas | USA |
| 22 | Chixoy* | Quiche | Guatemala |
| 23 | Sacramento* | California | USA |
| 24 | Bermejo* | Provincia del Chaco | Argentina |
| 25 | Segovia* | Border | Honduras-Nicaragua |
| 26 | Ucayali* | Arequipa | Peru |

Table A.2: Studied rivers (* indicate those rivers that were analyzed in more than one temporal instant).

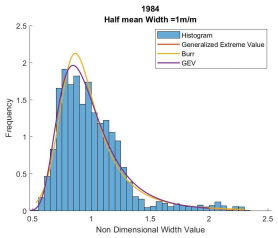


(a) 1984

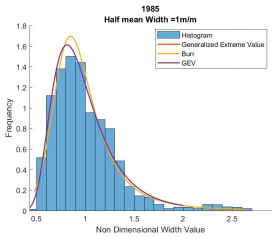


(b) 1985

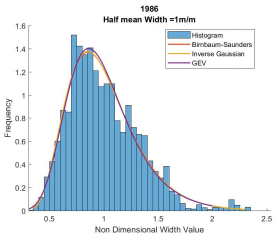


(c) 1986

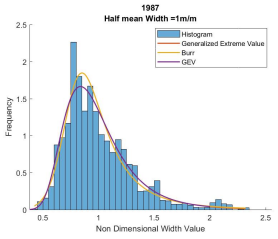


(d) 1987

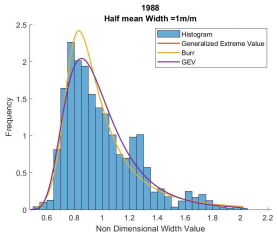


(e) 1988

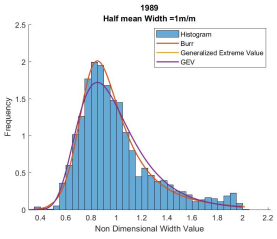


(f) 1989

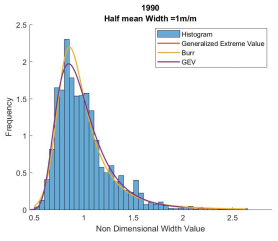


(g) 1990

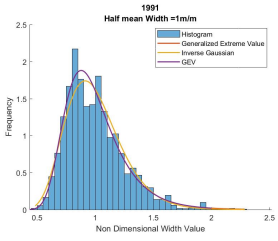


(h) 1991

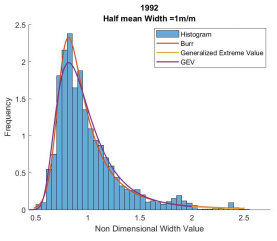


(i) 1992

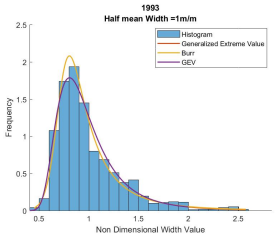


(j) 1993

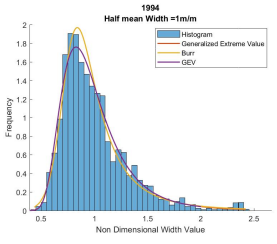


(k) 1994

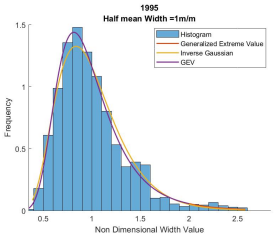


(l) 1995

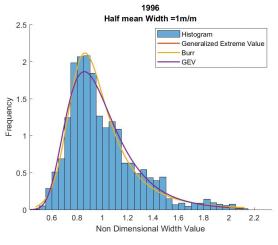


(m) 1996

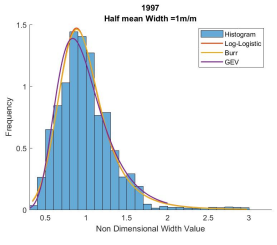


(n) 1997

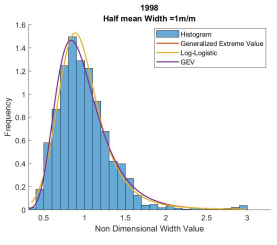


(o) 1998

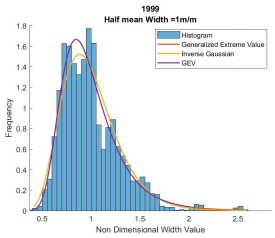


(p) 1999

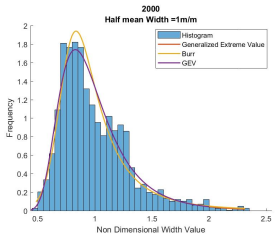


(q) 2000

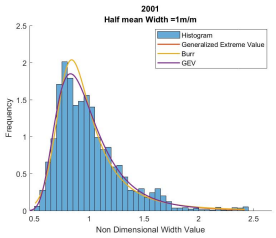


(r) 2001

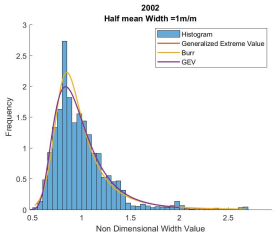


(s) 2002

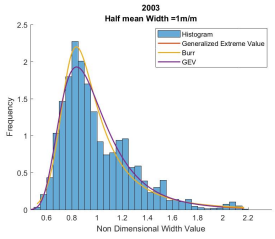


(t) 2003

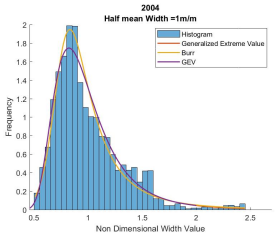


(u) 2004

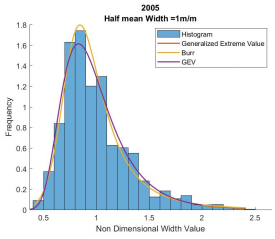


(v) 2005

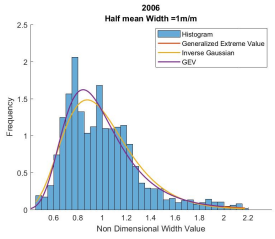


(w) 2006

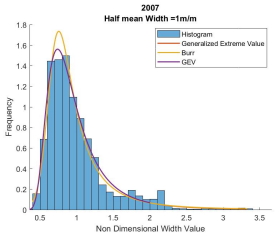


(x) 2007

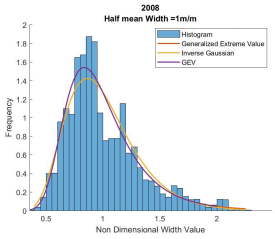


(y) 2008

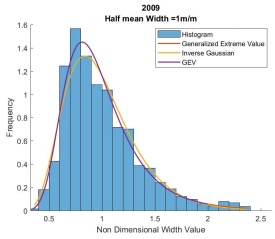


(z) 2009

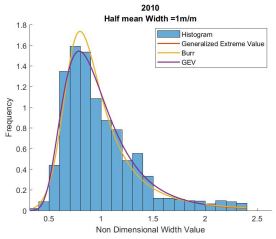


(aa) 2010

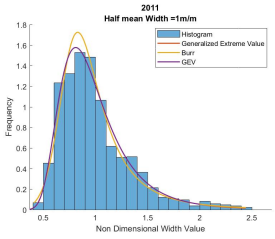


(ab) 2011

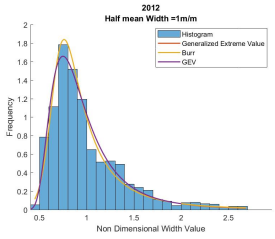


(ac) 2012

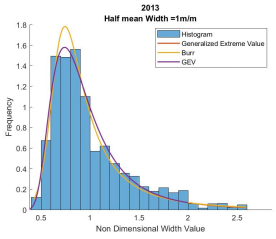


(ad) 2013

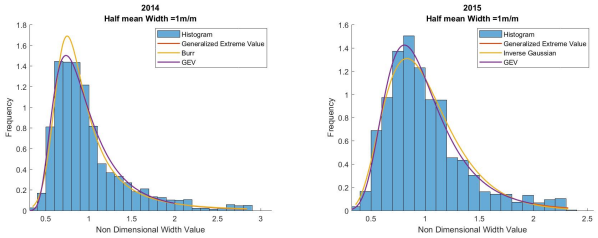


(ae) 2014 (af) 2015

Figure A.9: Ucayali's histogram, fist and second best fit PDF and GEV plot for each river in the no dimensional case.

| No | River Name | Upstream point | | Dowstream point | |
|---|---|---|---|---|---|
| | | Latitutde | Longitude | Latitutde | Longitude |
| 1 | Chinchaga | 058°35'58.53"N | 118°20'34.15"W | 058°52'13.50"N | 118°18'56.78"W |
| 2 | Nan | 016°53'54.61"N | 100°13'48.75"E | 016°31'07.99"N | 100°19'32.48"E |
| 3 | Chèt | 056°55'16.56"N | 087°30'37.70"E | 056°52'50.83"N | 087°15'58.27"E |
| 4 | Tarauacà | 007°26'44.20"S | 070°02'04.42"W | 006°52'42.25"S | 069°46'28.45"W |
| 5 | Murray | 034°43'43.52"S | 143°13'05.36"E | 034°35'01.49"S | 142°47'12.69"E |
| 6 | Orthon | 010°59'44.62"S | 067°25'57.52"W | 010°48'55.17"S | 066°01'44.72"W |
| 7 | Darling | 030°21'44.88"S | 145°32'39.59"E | 030°43'10.95"S | 144°47'32.35"E |
| 8 | Bravo | 026°03'31.89"N | 098°12'02.34"W | 025°57'07.02"N | 097°08'59.76"W |
| 9 | Kyaukgy | 018°11'14.44"N | 096°47'27.08"E | 017°57'29.42"N | 096°50'56.53"E |
| 10 | Kwango | 009°46'12.16"S | 018°35'43.26"E | 009°37'57.45"S | 018°23'32.45"E |
| 11 | Beaver | 054°16'59.22"N | 110°06'11.59"W | 054°15'16.85"N | 109°57'40.14"W |
| 12 | Čulym | 057°19'18.14"N | 090°22'33.72"E | 057°28'57.05"N | 089°21'57.95"E |
| 13 | Ouachita | 033°17'29.89"N | 092°28'10.53"W | 033°04'17.15"N | 092° 7'45.77"W |
| 14 | Cauto | 020°34'08.38"N | 076°45'51.73"W | 020°33'08.36"N | 077°13'47.38"W |
| 15 | Chapecò | 027°08'20.30"S | 053°02'35.92"W | 027°35'01.85"S | 054°46'36.55"W |
| 16 | Brazos | 030°19'29.62"N | 096°08'57.03"W | 029°32'29.93"N | 095°37'29.71"W |
| 17 | Gambia | 013°03'32.72"N | 013°19'15.50"W | 013°32'37.35"N | 014°34'06.50"W |
| 18 | Mamore | 016°44'03.25"S | 064°46'48.39"W | 015°48'29.03"S | 064°46'23.46"W |
| 19 | Irtysh Reka | 057°39'06.24"N | 071°39'25.23"E | 057°56'45.13"N | 069°40'29.10"E |
| 20 | Beni | 013°35'52.61"S | 067°21'43.81"W | 012°33'55.71"S | 066°57'55.81"W |
| 21 | White | 035°38'28.88"N | 091°25'23.60"W | 035°10'55.05"N | 091°25'34.58"W |
| 22 | Chixoy | 016°01'19.85"N | 090°35'42.25"W | 015°59'59.95"N | 090°29'42.50"W |
| 23 | Sacramento | 040°09'11.49"N | 122°11'59.71"W | 039°12'36.18"N | 121°59'20.73"W |
| 24 | Bermejo | 024°49'03.37"S | 061°08'06.32"W | 025°45'36.70"S | 059°56'50.41"W |
| 25 | Segovia | 014°40'02.56"N | 084°24'09.34"W | 014°59'48.61"N | 083°12'30.22"W |
| 26 | Ucayali | 009°47'13.71"S | 074°09'13.00"W | 009°22'48.78"S | 074°21'09.83"W |

Table A.3: Coordinates of studied rivers (* indicate those rivers that were analyzed in more than one temporal instant).

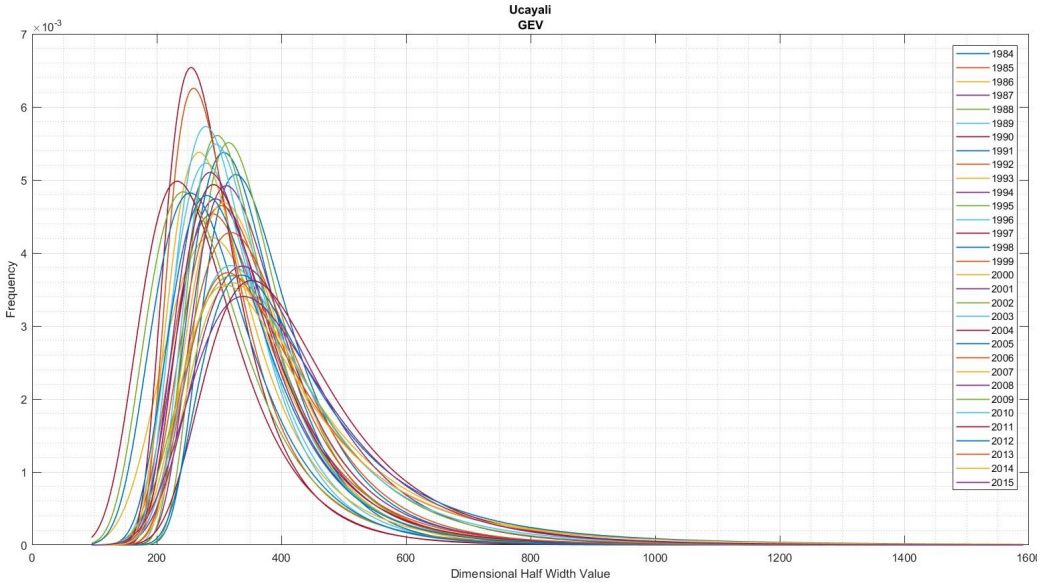


(a) Dimensional

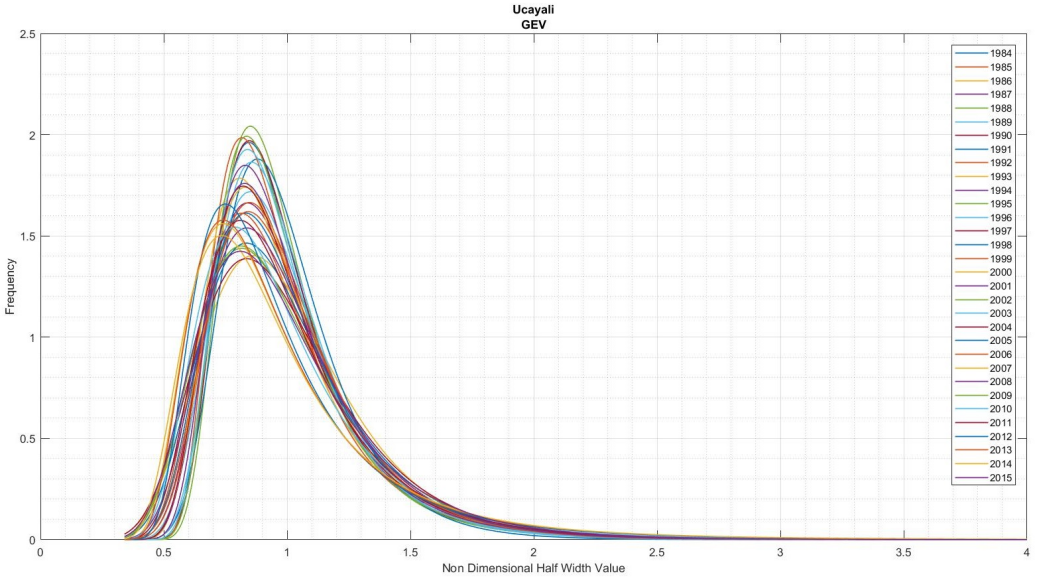


(b) Dimensionless

Figure A.10: Ucayali's GEV for the dimensional and non dimensio.

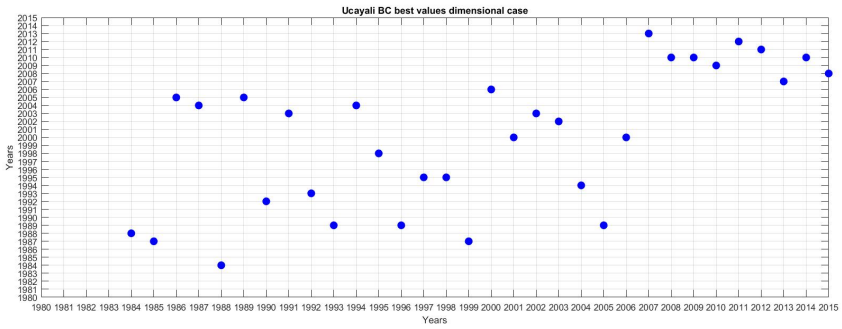


(a) Best BC dimensional case.

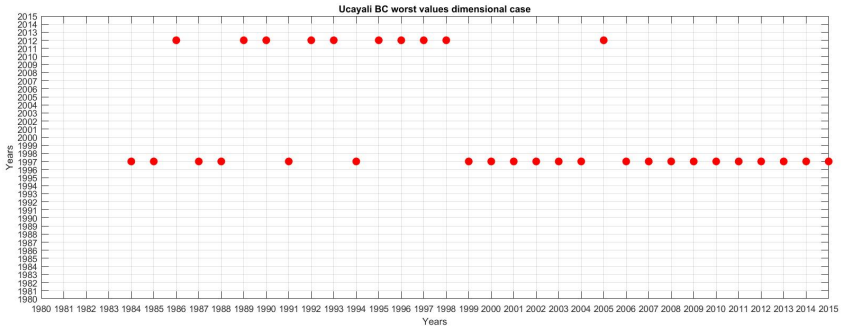


(b) Worst BC dimensional case.

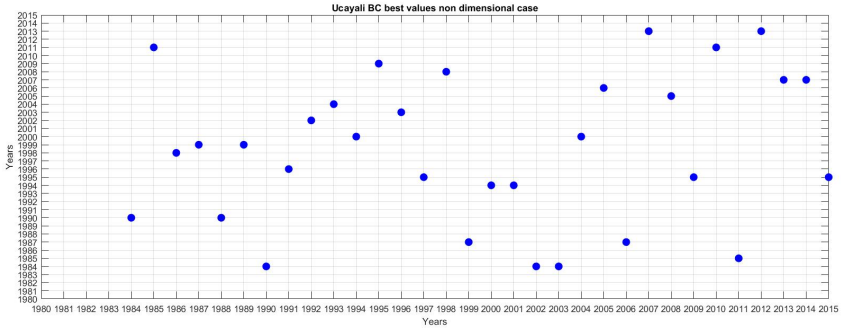


(c) Best BC dimensionless case.l

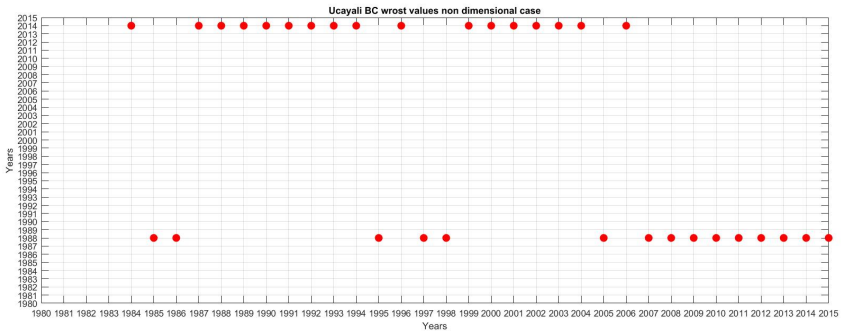


(d) Worst BC dimensionless case.

Figure A.11: Ucayali's best and worst BC couples for the dimensional and dimensionless case.

| River | Count | Average (m) | Stnd. Dev. | Coeff. of Var. | Min. (m) | Max. (m) | Range (m) | Stnd. skewness | Stnd. kurtosis |
|---|---|---|---|---|---|---|---|---|---|
| Chincaga | 4921 | 39.86 | 7.33 | 18.40% | 22.65 | 65.86 | 43.21 | 11.62 | -2.78 |
| Nan | 4592 | 46.44 | 8.51 | 18.31% | 24.71 | 74.17 | 49.46 | 14.45 | 5.03 |
| Chet | 1677 | 21.66 | 2.75 | 12.71% | 13.05 | 29.86 | 16.81 | 4.72 | 1.08 |
| Tarauaca | 8496 | 75.47 | 18.11 | 23.99% | 24.63 | 132.40 | 107.77 | 11.86 | -1.03 |
| Murray | 5222 | 47.45 | 9.21 | 19.40% | 10.53 | 75.68 | 65.15 | 0.32 | 3.06 |
| Orthon | 18261 | 45.60 | 7.95 | 17.43% | 15.00 | 82.16 | 67.15 | 13.49 | 34.11 |
| Darling | 8699 | 15.55 | 3.14 | 20.21% | 5.50 | 29.26 | 23.76 | 20.03 | 11.92 |
| Bravo | 12688 | 20.19 | 8.98 | 44.46% | 1.89 | 73.83 | 71.94 | 104.57 | 162.76 |
| Kyaukgy | 3528 | 24.24 | 8.60 | 35.48% | 6.53 | 61.26 | 54.72 | 28.37 | 15.09 |
| Kwango | 3178 | 24.87 | 5.12 | 20.60% | 11.29 | 58.03 | 46.74 | 22.09 | 39.50 |
| Baver | 985 | 19.31 | 2.77 | 14.33% | 13.66 | 28.43 | 14.77 | 8.64 | 1.14 |
| Culym | 6953 | 107.24 | 19.62 | 18.29% | 42.92 | 188.52 | 145.60 | 10.09 | 17.81 |
| Ouachita | 4232 | 47.66 | 7.60 | 15.95% | 28.13 | 77.96 | 49.83 | 14.28 | 10.43 |
| Cauto | 5564 | 50.14 | 20.23 | 40.34% | 18.30 | 116.31 | 98.01 | 11.80 | -12.67 |
| Chapecò | 16547 | 256.04 | 82.66 | 32.28% | 97.15 | 560.59 | 463.43 | 30.22 | 1.42 |
| Brazos | 12058 | 64.26 | 11.18 | 17.39% | 31.04 | 126.17 | 95.13 | 37.32 | 30.30 |
| Gambia | 17948 | 59.47 | 16.42 | 27.61% | 27.40 | 197.15 | 169.75 | 134.19 | 327.14 |
| Mamore | 11742 | 168.78 | 48.33 | 28.63% | 72.97 | 496.88 | 423.90 | 72.76 | 85.77 |
| Irtysh Reka | 8585 | 164.93 | 44.36 | 26.90% | 79.16 | 397.79 | 318.63 | 43.64 | 46.60 |
| Beni | 4343 | 227.06 | 47.88 | 21.09% | 141.24 | 490.93 | 349.69 | 39.96 | 48.87 |
| White | 2230 | 88.19 | 14.36 | 16.29% | 48.64 | 153.03 | 104.40 | 19.39 | 19.32 |

Table A.4: General statistic values of the dimensional half width for the river group 1.

| River | Count | Stnd. Dev. | Coeff. Var. | Min. | Max. | Range | Stnd. skewness | Stnd. kurtosis |
|---|---|---|---|---|---|---|---|---|
| Chincaga | 4921 | 0.18 | 18.40% | 0.57 | 1.65 | 1.08 | 11.62 | -2.78 |
| Nan | 4592 | 0.18 | 18.31% | 0.53 | 1.60 | 1.06 | 14.45 | 5.03 |
| Chet | 1677 | 0.13 | 12.71% | 0.60 | 1.38 | 0.78 | 4.72 | 1.08 |
| Tarauaca | 8496 | 0.24 | 23.99% | 0.33 | 1.75 | 1.43 | 11.86 | -1.03 |
| Murray | 5222 | 0.19 | 19.40% | 0.22 | 1.59 | 1.37 | 0.32 | 3.06 |
| Orthon | 18261 | 0.17 | 17.43% | 0.33 | 1.80 | 1.47 | 13.49 | 34.11 |
| Darling | 8699 | 0.20 | 20.21% | 0.35 | 1.88 | 1.53 | 20.03 | 11.92 |
| Bravo | 12688 | 0.44 | 44.46% | 0.09 | 3.66 | 3.56 | 104.57 | 162.76 |
| Kyaukgy | 3528 | 0.35 | 35.48% | 0.27 | 2.53 | 2.26 | 28.37 | 15.09 |
| Kwango | 3178 | 0.21 | 20.60% | 0.45 | 2.33 | 1.88 | 22.09 | 39.50 |
| Baver | 985 | 0.14 | 14.33% | 0.71 | 1.47 | 0.76 | 8.64 | 1.14 |
| Culym | 6953 | 0.18 | 18.29% | 0.40 | 1.76 | 1.36 | 10.09 | 17.81 |
| Ouachita | 4232 | 0.16 | 15.95% | 0.59 | 1.64 | 1.05 | 14.28 | 10.43 |
| Cauto | 5564 | 0.40 | 40.34% | 0.36 | 2.32 | 1.95 | 11.80 | -12.66 |
| Chapecò | 16547 | 0.32 | 32.28% | 0.38 | 2.19 | 1.81 | 30.22 | 1.42 |
| Brazos | 12058 | 0.17 | 17.39% | 0.48 | 1.96 | 1.48 | 37.32 | 30.30 |
| Gambia | 17948 | 0.28 | 27.61% | 0.46 | 3.32 | 2.85 | 134.19 | 327.14 |
| Mamore | 11742 | 0.29 | 28.63% | 0.43 | 2.94 | 2.51 | 72.76 | 85.77 |
| Irtysh Reka | 8585 | 0.27 | 26.90% | 0.48 | 2.41 | 1.93 | 43.64 | 46.60 |
| Beni | 4343 | 0.21 | 21.09% | 0.62 | 2.16 | 1.54 | 39.96 | 48.87 |
| White | 2330 | 0.16 | 16.29% | 0.55 | 1.74 | 1.18 | 19.39 | 19.32 |

Table A.5: General statistics values for the dimensionless half width of the river group 1.

| River | Location estimates | | | | Scale estimates | | | | Standard | | Winsorized | |
|---|---|---|---|---|---|---|---|---|---|---|---|---|
| | Sample mean | Sample median | Trimmed mean | Winsorize mean | Sample std. dev. | MAD /0.6745 | Sbi | Winsorized sigma | Lower Limit | Upper Limit | Lower Limit | Upper Limit |
| Chincaga | 39.86 | 39.02 | 39.41 | 39.67 | 7.33 | 7.56 | 7.46 | 8.08 | 39.65 | 40.06 | 39.40 | 39.94 |
| Nan | 46.44 | 45.92 | 45.90 | 46.08 | 8.51 | 7.95 | 8.39 | 8.73 | 46.20 | 46.69 | 45.78 | 46.38 |
| Chet | 21.66 | 21.46 | 21.51 | 21.61 | 2.75 | 2.50 | 2.75 | 2.88 | 21.53 | 21.79 | 21.44 | 21.77 |
| Tarauaca | 75.47 | 74.39 | 74.46 | 74.99 | 18.11 | 17.91 | 18.28 | 19.30 | 75.08 | 75.85 | 74.50 | 75.48 |
| Murray | 47.45 | 46.84 | 47.33 | 47.39 | 9.21 | 9.42 | 9.24 | 9.68 | 47.20 | 47.70 | 47.07 | 47.70 |
| Orthon | 45.60 | 45.42 | 45.49 | 45.51 | 7.95 | 7.05 | 7.60 | 7.52 | 45.48 | 45.71 | 45.38 | 45.64 |
| Darling | 15.55 | 15.26 | 15.36 | 15.43 | 3.14 | 2.86 | 3.07 | 3.15 | 15.48 | 15.61 | 15.36 | 15.51 |
| Bravo | 20.19 | 18.26 | 18.53 | 18.86 | 8.98 | 6.30 | 6.21 | 6.81 | 20.03 | 20.34 | 18.71 | 19.00 |
| Kyaukgy | 24.24 | 22.14 | 22.83 | 23.65 | 8.60 | 6.50 | 7.75 | 8.82 | 23.96 | 24.53 | 23.31 | 24.00 |
| Kwango | 24.87 | 24.19 | 24.53 | 24.69 | 5.12 | 4.47 | 4.79 | 4.86 | 24.69 | 25.05 | 24.48 | 24.89 |
| Baver | 19.31 | 18.66 | 19.05 | 19.18 | 2.77 | 2.52 | 2.76 | 2.89 | 19.14 | 19.49 | 18.96 | 19.40 |
| Culym | 107.24 | 106.93 | 106.62 | 106.77 | 19.62 | 18.73 | 18.88 | 19.40 | 106.78 | 107.70 | 106.23 | 107.32 |
| Ouachita | 47.66 | 47.26 | 47.32 | 47.34 | 7.60 | 7.31 | 7.40 | 7.66 | 47.43 | 47.89 | 47.07 | 47.62 |
| Cauto | 50.14 | 50.81 | 48.54 | 49.23 | 20.23 | 27.33 | 20.84 | 24.72 | 49.61 | 50.68 | 48.46 | 50.01 |
| Chapecò | 256.04 | 248.80 | 249.84 | 251.43 | 82.66 | 88.75 | 83.05 | 91.25 | 254.78 | 257.30 | 249.76 | 253.09 |
| Brazos | 64.26 | 62.86 | 63.25 | 63.58 | 11.18 | 10.19 | 10.62 | 10.80 | 64.06 | 64.46 | 63.35 | 63.81 |
| Gambia | 59.47 | 56.90 | 57.24 | 57.67 | 16.42 | 11.26 | 12.30 | 12.64 | 59.23 | 59.71 | 57.45 | 57.89 |
| Mamore | 168.78 | 156.91 | 160.47 | 162.86 | 48.33 | 37.41 | 39.66 | 42.35 | 167.90 | 169.65 | 161.95 | 163.78 |
| Irtysh Reka | 164.93 | 156.65 | 159.96 | 161.98 | 44.36 | 39.99 | 41.18 | 44.58 | 163.99 | 165.87 | 160.86 | 163.11 |
| Beni | 227.06 | 216.19 | 220.22 | 222.73 | 47.88 | 39.13 | 41.53 | 44.84 | 225.64 | 228.49 | 221.13 | 224.32 |
| White | 88.19 | 86.06 | 86.86 | 87.22 | 14.36 | 12.58 | 13.17 | 13.46 | 87.60 | 88.77 | 86.57 | 87.87 |

Table A.6: Dimensional width outlier Identification (trimming: 15% confidence intervals for the mean 95%).

| River | Location estimates | | | | Scale estimates | | | | Standard | | Winsorized | |
|---|---|---|---|---|---|---|---|---|---|---|---|---|
| | Sample mean | Sample median | Trimmed mean | Winsorize mean | Sample std. dev. | MAD /0.6745 | Sbi | Winsorized sigma | Lower Limit | Upper Limit | Lower Limit | Upper Limit |
| Chincaga | 1 | 0.979 | 0.989 | 0.995 | 0.184 | 0.190 | 0.187 | 0.203 | 0.995 | 1.005 | 0.988 | 1.002 |
| Nan | 1 | 0.989 | 0.988 | 0.992 | 0.183 | 0.171 | 0.181 | 0.188 | 0.995 | 1.005 | 0.986 | 0.999 |
| Chet | 1 | 0.991 | 0.993 | 0.997 | 0.127 | 0.116 | 0.127 | 0.133 | 0.994 | 1.006 | 0.990 | 1.005 |
| Tarauaca | 1 | 0.986 | 0.987 | 0.994 | 0.240 | 0.237 | 0.242 | 0.256 | 0.995 | 1.005 | 0.987 | 1.000 |
| Murray | 1 | 0.987 | 0.997 | 0.999 | 0.194 | 0.198 | 0.195 | 0.204 | 0.995 | 1.005 | 0.992 | 1.005 |
| Orthon | 1 | 0.996 | 0.998 | 0.998 | 0.174 | 0.155 | 0.167 | 0.165 | 0.997 | 1.003 | 0.995 | 1.001 |
| Darling | 1 | 0.982 | 0.988 | 0.993 | 0.202 | 0.184 | 0.198 | 0.202 | 0.996 | 1.004 | 0.988 | 0.998 |
| Bravo | 1 | 0.904 | 0.918 | 0.934 | 0.445 | 0.312 | 0.308 | 0.337 | 0.992 | 1.008 | 0.927 | 0.941 |
| Kyaukgy | 1 | 0.913 | 0.942 | 0.976 | 0.355 | 0.268 | 0.320 | 0.364 | 0.988 | 1.012 | 0.961 | 0.990 |
| Kwango | 1 | 0.972 | 0.986 | 0.992 | 0.206 | 0.180 | 0.193 | 0.196 | 0.993 | 1.007 | 0.984 | 1.001 |
| Baver | 1 | 0.966 | 0.986 | 0.993 | 0.143 | 0.131 | 0.143 | 0.150 | 0.991 | 1.009 | 0.982 | 1.004 |
| Culym | 1 | 0.997 | 0.994 | 0.996 | 0.183 | 0.175 | 0.176 | 0.181 | 0.996 | 1.004 | 0.991 | 1.001 |
| Ouachita | 1 | 0.992 | 0.993 | 0.993 | 0.159 | 0.153 | 0.155 | 0.161 | 0.995 | 1.005 | 0.988 | 0.999 |
| Cauto | 1 | 1.013 | 0.968 | 0.982 | 0.403 | 0.545 | 0.416 | 0.493 | 0.989 | 1.011 | 0.966 | 0.997 |
| Chapecò | 1 | 0.972 | 0.976 | 0.982 | 0.323 | 0.347 | 0.324 | 0.356 | 0.995 | 1.005 | 0.975 | 0.988 |
| Brazos | 1 | 0.978 | 0.984 | 0.989 | 0.174 | 0.159 | 0.165 | 0.168 | 0.997 | 1.003 | 0.986 | 0.993 |
| Gambia | 1 | 0.957 | 0.963 | 0.970 | 0.276 | 0.189 | 0.207 | 0.213 | 0.996 | 1.004 | 0.966 | 0.973 |
| Mamore | 1 | 0.930 | 0.951 | 0.965 | 0.286 | 0.222 | 0.235 | 0.251 | 0.995 | 1.005 | 0.960 | 0.970 |
| Irtysh Reka | 1 | 0.950 | 0.970 | 0.982 | 0.269 | 0.242 | 0.250 | 0.270 | 0.994 | 1.006 | 0.975 | 0.989 |
| Beni | 1 | 0.952 | 0.970 | 0.981 | 0.211 | 0.172 | 0.183 | 0.197 | 0.994 | 1.006 | 0.974 | 0.988 |
| White | 1 | 0.976 | 0.985 | 0.989 | 0.163 | 0.143 | 0.149 | 0.153 | 0.993 | 1.007 | 0.982 | 0.996 |

Table A.7: Dimensionless width outlier Identification (trimming: 15% confidence intervals for the mean 95%).

| River | Normal Distribution | | | | | | Log-Normal Distribution | | | | | |
|---|---|---|---|---|---|---|---|---|---|---|---|---|
| | Max to mean | Min to mean | Max to Min | $\lambda 1$ | $\lambda 2$ | # outliers | Max to mean | Min to mean | Max to Min | $\lambda 1$ | $\lambda 2$ | # outliers |
| Chincaga | 3.55 | 2.35 | 5.89 | 4.41 | 8.30 | 0 | 2.82 | 2.98 | 5.81 | 4.41 | 8.30 | 0 |
| Nan | 3.26 | 2.56 | 5.82 | 4.39 | 8.27 | 0 | 2.66 | 3.37 | 6.04 | 4.39 | 8.27 | 0 |
| Chet | 2.98 | 3.13 | 6.10 | 4.16 | 7.76 | 0 | 2.58 | 3.91 | 6.49 | 4.16 | 7.76 | 0 |
| Tarauaca | 2.91 | 2.50 | 5.41 | 4.41 | 8.30 | 0 | 2.27 | 3.50 | 5.76 | 4.41 | 8.30 | 0 |
| Murray | 2.85 | 4.04 | 6.90 | 4.41 | 8.30 | 0 | 2.34 | 4.38 | 9.39 | 4.41 | 8.30 | 19 |
| Orthon | 4.18 | 3.65 | 7.83 | 4.41 | 8.30 | 0 | 3.17 | 4.40 | 8.50 | 4.41 | 8.30 | 23 |
| Darling | 3.92 | 3.29 | 7.21 | 4.41 | 8.30 | 0 | 2.97 | 4.24 | 8.16 | 4.41 | 8.30 | 5 |
| Bravo | 3.68 | 4.21 | 7.89 | 4.41 | 8.30 | 0 | 2.78 | 4.41 | 12.53 | 4.41 | 8.30 | 15 |
| Kyaukgy | 4.30 | 2.06 | 6.36 | 4.34 | 8.14 | 0 | 2.97 | 3.79 | 6.76 | 4.34 | 8.14 | 0 |
| Kwango | 6.47 | 2.65 | 9.12 | 4.31 | 8.09 | 11 | 4.29 | 3.81 | 8.10 | 4.31 | 8.09 | 2 |
| Baver | 3.30 | 2.04 | 5.34 | 4.04 | 7.48 | 0 | 2.84 | 2.41 | 5.25 | 4.04 | 7.48 | 0 |
| Culym | 4.76 | 2.36 | 7.12 | 4.41 | 8.30 | 10 | 3.64 | 2.95 | 6.59 | 4.41 | 8.30 | 0 |
| Ouachita | 3.99 | 2.57 | 6.56 | 4.38 | 8.23 | 0 | 3.19 | 3.25 | 6.44 | 4.38 | 8.23 | 0 |
| Cauto | 2.69 | 1.54 | 4.23 | 4.41 | 8.30 | 0 | 2.00 | 2.14 | 4.14 | 4.41 | 8.30 | 0 |
| Chapecò | 3.36 | 2.38 | 5.73 | 4.41 | 8.30 | 0 | 2.36 | 3.51 | 5.87 | 4.41 | 8.30 | 0 |
| Brazos | 3.86 | 2.83 | 6.69 | 4.41 | 8.30 | 0 | 3.10 | 3.99 | 7.09 | 4.41 | 8.30 | 0 |
| Gambia | 4.93 | 1.89 | 6.82 | 4.41 | 8.30 | 23 | 3.68 | 2.65 | 6.34 | 4.41 | 8.30 | 0 |
| Mamore | 3.59 | 1.81 | 5.40 | 4.41 | 8.30 | 0 | 2.80 | 2.87 | 5.67 | 4.41 | 8.30 | 0 |
| Irtysh Reka | 5.05 | 1.88 | 6.94 | 4.41 | 8.30 | 21 | 3.54 | 2.50 | 6.04 | 4.41 | 8.30 | 0 |
| Beni | 5.51 | 1.79 | 7.30 | 4.38 | 8.24 | 21 | 4.08 | 2.35 | 6.43 | 4.38 | 8.24 | 0 |
| White | 4.53 | 2.75 | 7.29 | 4.24 | 7.93 | 10 | 3.60 | 3.72 | 7.31 | 4.24 | 7.93 | 0 |

Table A.8: Grubbs outlier test for the half mean width ($\lambda 1$ correspond to the relation of maximum and minimum values test, $\lambda 2$ correspond to the maximum to minimum values test) for both normal and log normal distribution assumption.

| River | Normal Distribution | | | | Log-Normal Distribution | | | |
|---|---|---|---|---|---|---|---|---|
| | Z of max value | Z of min value | $\lambda$ | # outlier | Z of max value | Z of min value | $\lambda$ | # outlier |
| Chincaga | 3.55 | 2.44 | 4.26 | 0 | 2.84 | 2.98 | 4.26 | 0 |
| Nan | 3.26 | 2.72 | 4.24 | 0 | 2.70 | 3.37 | 4.24 | 0 |
| Chet | 2.98 | 3.13 | 4.01 | 0 | 2.69 | 3.91 | 4.01 | 0 |
| Tarauaca | 2.92 | 2.56 | 4.26 | 0 | 2.44 | 3.50 | 4.26 | 0 |
| Murray | 2.85 | 4.04 | 4.26 | 0 | 2.51 | 7.17 | 4.26 | 21 |
| Orthon | 4.19 | 3.76 | 4.26 | 0 | 3.31 | 5.47 | 4.26 | 32 |
| Darling | 3.92 | 3.33 | 4.26 | 0 | 3.02 | 5.22 | 4.26 | 5 |
| Bravo | 3.68 | 4.21 | 4.26 | 0 | 2.83 | 9.97 | 4.26 | 17 |
| Kyaukgy | 4.30 | 2.26 | 4.18 | 5 | 3.01 | 3.79 | 4.18 | 0 |
| Kwango | 6.47 | 2.90 | 4.16 | 11 | 4.29 | 3.87 | 4.16 | 4 |
| Baver | 3.30 | 2.30 | 3.87 | 0 | 2.84 | 2.48 | 3.87 | 0 |
| Culym | 4.76 | 2.56 | 4.26 | 11 | 3.64 | 3.03 | 4.26 | 0 |
| Ouachita | 3.99 | 2.79 | 4.22 | 0 | 3.20 | 3.25 | 4.22 | 0 |
| Cauto | 2.69 | 1.57 | 4.26 | 0 | 2.01 | 2.14 | 4.26 | 0 |
| Chapecò | 3.36 | 2.43 | 4.26 | 0 | 2.53 | 3.52 | 4.26 | 0 |
| Brazos | 3.86 | 3.06 | 4.26 | 0 | 3.13 | 3.99 | 4.26 | 0 |
| Gambia | 4.93 | 2.11 | 4.26 | 27 | 3.69 | 2.85 | 4.26 | 0 |
| Mamore | 3.59 | 1.95 | 4.26 | 0 | 2.81 | 2.87 | 4.26 | 0 |
| Irtysh Reka | 5.05 | 2.04 | 4.26 | 23 | 3.54 | 2.58 | 4.26 | 0 |
| Beni | 5.51 | 2.05 | 4.23 | 28 | 4.08 | 2.57 | 4.23 | 0 |
| White | 4.53 | 3.06 | 4.08 | 12 | 3.62 | 3.72 | 4.08 | 0 |

Table A.9: Extreme Studentized deviate test for the half mean width for both normal and log normal distribution assumption.

| River | Kimber's test | | | Walsh's test | |
|---|---|---|---|---|---|
| | S | s | # outliers | # lower outliers | # upper outliers |
| Chincaga | 3.36E-04 | 3.08E-03 | 0 | 0 | 0 |
| Nan | 3.48E-04 | 3.29E-03 | 0 | 0 | 0 |
| Chet | 8.22E-04 | 8.38E-03 | 0 | 0 | 0 |
| Tarauaca | 3.41E-04 | 3.08E-03 | 0 | 0 | 0 |
| Murray | 3.15E-04 | 3.08E-03 | 0 | 1 | 0 |
| Orthon | 3.55E-04 | 3.08E-03 | 0 | 0 | 0 |
| Darling | 3.64E-04 | 3.08E-03 | 0 | 1 | 0 |
| Bravo | 3.65E-04 | 3.08E-03 | 0 | 4 | 0 |
| Kyaukgy | 7.16E-04 | 4.20E-03 | 0 | 0 | 0 |
| Kwango | 7.34E-04 | 4.63E-03 | 0 | 0 | 0 |
| Baver | 1.49E-03 | 1.37E-02 | 0 | 0 | 0 |
| Culym | 3.63E-04 | 3.08E-03 | 0 | 0 | 0 |
| Ouachita | 3.87E-04 | 3.55E-03 | 0 | 0 | 0 |
| Cauto | 4.19E-04 | 3.08E-03 | 0 | 0 | 0 |
| Chapecò | 3.94E-04 | 3.08E-03 | 0 | 0 | 0 |
| Brazos | 3.45E-04 | 3.08E-03 | 0 | 0 | 0 |
| Gambia | 4.44E-04 | 3.08E-03 | 0 | 1 | 0 |
| Mamore | 4.38E-04 | 3.08E-03 | 0 | 0 | 0 |
| Irtysh Reka | 4.52E-04 | 3.08E-03 | 0 | 0 | 0 |
| Beni | 4.98E-04 | 3.46E-03 | 0 | 0 | 0 |
| White | 7.45E-04 | 6.18E-03 | 0 | 1 | 0 |

Table A.10: Kimber's (columns 3-4) and Walsh's (columns 5-6) tests for the half mean width value. (S is the likelihood ratio test statistic, s is the critical value for a specific significance level).

| River | Best PDF | Dimensional case | | | Dimensionless case | | |
|---|---|---|---|---|---|---|---|
| | | BIC | GEV BIC | Diff % | BIC | GEV BIC | Diff % |
| Chincaga | GEV | 3.34E+04 | 3.34E+04 | 0.00% | -2.87E+03 | -2.87E+03 | 0.0% |
| Nan | Log Normal | 3.25E+04 | 3.25E+04 | 0.02% | -2.75E+03 | -2.74E+03 | 0.2% |
| Chet | Gamma | 8.15E+03 | 8.16E+03 | 0.07% | -2.16E+03 | -2.16E+03 | 0.2% |
| Tarauaca | GEV | 4.24E+04 | 4.24E+04 | 0.00% | -4.52E+02 | -4.52E+02 | 0.0% |
| Murray | T-location scale | 3.56E+04 | 3.57E+04 | 0.11% | -2.27E+03 | -2.23E+03 | 1.7% |
| Orthon | Logistic | 3.39E+04 | 3.44E+04 | 1.42% | -3.18E+03 | -2.69E+03 | 15.4% |
| Darling | Burr | 2.56E+04 | 2.56E+04 | 0.07% | -1.89E+03 | -1.87E+03 | 1.0% |
| Bravo | T-location scale | 2.90E+04 | 2.91E+04 | 0.40% | -1.09E+03 | -9.77E+02 | 10.5% |
| Kyaukgy | GEV | 2.43E+04 | 2.43E+04 | 0.00% | 1.77E+03 | 1.77E+03 | 0.0% |
| Kwango | Log logistic | 1.91E+04 | 1.92E+04 | 0.54% | -1.32E+03 | -1.21E+03 | 7.9% |
| Baver | GEV | 4.73E+03 | 4.73E+03 | 0.00% | -1.10E+03 | -1.10E+03 | 0.0% |
| Culym | Log Normal | 4.19E+04 | 4.19E+04 | 0.09% | -3.98E+03 | -3.95E+03 | 0.9% |
| Ouachita | Log Normal | 2.90E+04 | 2.90E+04 | 0.10% | -3.69E+03 | -3.66E+03 | 0.7% |
| Cauto | GEV | 4.15E+04 | 4.15E+04 | 0.00% | 3.66E+03 | 3.66E+03 | 0.0% |
| Chapecò | GEV | 5.71E+04 | 5.71E+04 | 0.00% | 1.37E+03 | 1.37E+03 | 0.0% |
| Brazos | Burr | 3.75E+04 | 3.76E+04 | 0.06% | -3.33E+03 | -3.30E+03 | 0.7% |
| Gambia | GEV | 3.70E+04 | 3.70E+04 | 0.00% | -1.60E+03 | -1.60E+03 | 0.0% |
| Mamore | GEV | 5.18E+04 | 5.18E+04 | 0.00% | 9.53E+02 | 9.53E+02 | 0.0% |
| Irtysh Reka | GEV | 4.97E+04 | 4.97E+04 | 0.00% | -6.52E+02 | -6.52E+02 | 0.0% |
| Beni | GEV | 4.47E+04 | 4.47E+04 | 0.00% | -2.44E+03 | -2.44E+03 | 0.0% |
| White | Burr | 1.88E+04 | 1.88E+04 | 0.17% | -2.12E+03 | -2.09E+03 | 1.5% |

Table A.11: Best fitting PDF and compare with the GEV based on BIC for the dimensional and dimensionless case.

| Id | River | Year |
|---|---|---|
| 22.1 | Chixoy | 1986 |
| 22.2 | Chixoy | 2010 |
| 22.3 | Chixoy | 2012 |
| 22.4 | Chixoy | 2016 |
| 23.1 | Sacramento | 1994 |
| 23.2 | Sacramento | 1996 |
| 23.3 | Sacramento | 2015 |
| 23.4 | Sacramento | 2016 |
| 24.1 | Bermejo | 2002 |
| 24.2 | Bermejo | 2016 |
| 25.1 | Segovia | 1999 |
| 25.2 | Segovia | 2016 |
| 26.1-26.32 | Ucayali | 1984-2015 |

Table A.12: Years under analysis for the different rivers.

| River | Count | Stnd. Dev. | Coeff. Var. | Min. | Max. | Range | Stnd. skewness | Stnd. kurtosis |
|---|---|---|---|---|---|---|---|---|
| Chixoy 1986 | 1604 | 0.21 | 20.95% | 0.58 | 2.21 | 1.63 | 20.58 | 31.68 |
| Chixoy 2010 | 846 | 0.18 | 18.50% | 0.59 | 2.02 | 1.43 | 17.42 | 37.73 |
| Chixoy 2012 | 792 | 0.14 | 13.58% | 0.66 | 1.46 | 0.80 | 3.23 | 0.51 |
| Chixoy 2016 | 822 | 0.17 | 17.42% | 0.57 | 1.61 | 1.03 | 6.09 | 5.01 |
| Sacramento 1994 | 7753 | 0.18 | 18.08% | 0.55 | 1.93 | 1.37 | 27.20 | 24.21 |
| Sacramento 1996 | 5026 | 0.15 | 15.34% | 0.60 | 1.74 | 1.14 | 16.23 | 17.78 |
| Sacramento 2015 | 5112 | 0.17 | 16.85% | 0.59 | 1.62 | 1.03 | 8.72 | -1.76 |
| Sacramento 2016 | 7667 | 0.17 | 17.25% | 0.55 | 1.55 | 0.99 | 6.57 | -4.12 |
| Bermejo 2002 | 1749 | 0.30 | 30.34% | 0.47 | 2.25 | 1.78 | 20.52 | 14.46 |
| Bermejo 2016 | 1916 | 0.20 | 19.77% | 0.49 | 1.63 | 1.14 | 3.19 | 0.05 |
| Segovia 1999 | 6914 | 0.19 | 19.11% | 0.56 | 1.75 | 1.20 | 18.98 | 2.58 |
| Segovia 2016 | 10350 | 0.20 | 19.91% | 0.55 | 2.28 | 1.73 | 54.71 | 89.66 |

Table A.13: General statistic values of the dimensionless half width for the river groups 2

| River | Source | Sum of Squares | Df | Mean Square | F-Ratio | P-Value |
|---|---|---|---|---|---|---|
| Chixoy | Between groups | 9.90E+04 | 3 | 3.30E+04 | 162.33 | 0 |
| | Within groups | 8.25E+05 | 4060 | 2.03E+02 | | |
| Sacramento | Between groups | 3.43E+06 | 3 | 1.14E+06 | 5493.83 | 0 |
| | Within groups | 5.32E+06 | 25554 | 2.08E+02 | | |
| Bermejo | Between groups | 1.00E+05 | 1 | 1.00E+05 | 80.91 | 0 |
| | Within groups | 4.53E+06 | 3663 | 1.24E+03 | | |
| Segovia | Between groups | 2.58E+04 | 1 | 2.58E+04 | 58.96 | 0 |
| | Within groups | 7.56E+06 | 17262 | 4.38E+02 | | |

Table A.14: ANOVA table each river group.

| Rivers | Method | Tukey HSD | Scheffe | Bonferroni |
|---|---|---|---|---|
| | Difference | +/- Limits | +/- Limits | +/- Limits |
| Chixoy 1986 - Chixoy 2010 | -3.31 | 1.56 | 1.69 | 1.60 |
| Chixoy 1986 - Chixoy 2012 | -7.90 | 1.59 | 1.73 | 1.63 |
| Chixoy 1986 - Chixoy 2016 | 7.21 | 1.57 | 1.71 | 1.61 |
| Chixoy 2010 - Chixoy 2012 | -4.59 | 1.81 | 1.97 | 1.86 |
| Chixoy 2010 - Chixoy 2016 | 10.52 | 1.79 | 1.95 | 1.84 |
| Chixoy 2012 - Chixoy 2016 | 15.11 | 1.82 | 1.99 | 1.87 |
| Sacramento 1994 - Sacramento 1996 | -32.47 | 0.67 | 0.73 | 0.69 |
| Sacramento 1994 - Sacramento 2015 | -8.29 | 0.67 | 0.73 | 0.69 |
| Sacramento 1994 - Sacramento 2016 | -6.32 | 0.60 | 0.65 | 0.61 |
| Sacramento 1996 - Sacramento 2015 | 24.18 | 0.74 | 0.80 | 0.76 |
| Sacramento 1996 - Sacramento 2016 | 26.15 | 0.67 | 0.73 | 0.69 |
| Sacramento 2015 - Sacramento 2016 | 1.97 | 0.67 | 0.73 | 0.69 |
| Bermejo 2002 - Bermejo 2016 | 10.46 | 2.28 | 2.28 | 2.28 |
| Segovia 1999 - Segovia 2016 | 2.50 | 0.64 | 0.64 | 0.64 |

Table A.15: Multiple range test for mean differences at 5% of statically significantly different.

| River group | Test | Value | P-Value | Comparison | $\sigma 1$ | $\sigma 2$ | F-Ratio | P-Value |
|---|---|---|---|---|---|---|---|---|
| Chixoy | Bartlett's | 155.91 | 0.000 | 1986 / 2010 | 16.09 | 14.81 | 1.18 | 0.007 |
| | Levene's | 28.94 | 0.000 | 1986 / 2012 | 16.09 | 11.50 | 1.96 | 0.000 |
| | | | | 1986 / 2016 | 16.09 | 12.12 | 1.76 | 0.000 |
| | | | | 2010 / 2012 | 14.81 | 11.50 | 1.66 | 0.000 |
| | | | | 2010 / 2016 | 14.81 | 12.12 | 1.50 | 0.000 |
| | | | | 2012 / 2016 | 11.50 | 12.12 | 0.90 | 0.140 |
| Sacramento | Bartlett's | 271.35 | 0.000 | 1994 / 1996 | 13.58 | 16.50 | 0.68 | 0.000 |
| | Levene's | 56.92 | 0.000 | 1994 / 2015 | 13.58 | 14.06 | 0.93 | 0.007 |
| | | | | 1994 / 2016 | 13.58 | 14.05 | 0.93 | 0.003 |
| | | | | 1996 / 2015 | 16.50 | 14.06 | 1.38 | 0.000 |
| | | | | 1996 / 2016 | 16.50 | 14.05 | 1.38 | 0.000 |
| | | | | 2015 / 2016 | 14.06 | 14.05 | 1.00 | 0.974 |
| Bermejo | Bartlett's | 453.23 | 0.000 | 2002 / 2016 | 43.02 | 25.97 | 2.74 | 0.000 |
| | Levene's | 256.26 | 0.000 | | | | | |
| Segovia | Bartlett's | 2.53 | 0.111 | 1999 / 2016 | 20.71 | 21.08 | 0.97 | 0.112 |
| | Levene's | 11.31 | 0.001 | | | | | |

Table A.16: Variance check.

| River group | Test | Test statistic | P-Value | Grand median | Comparison | Difference | +/- Limits |
|---|---|---|---|---|---|---|---|
| Chixoy | Kruskal-Wallis | 559.50 | 0 | | 1986 / 2010 | -328.74 | 131.53 |
| | Mood's | 505.97 | 0 | 76.34 | 1986 / 2012 | -767.80 | 134.44 |
| | | | | | 1986 / 2016 | 558.88 | 132.78 |
| | | | | | 2010 / 2012 | -439.07 | 153.05 |
| | | | | | 2010 / 2016 | 887.62 | 151.60 |
| | | | | | 2012 / 2016 | 1326.68 | 154.13 |
| Sacramento | Kruskal-Wallis | 8941.33 | 0 | | 1994 / 1996 | -12411.90 | 352.51 |
| | Mood's | 5790.09 | 0 | 82.67 | 1994 / 2015 | -3866.16 | 350.70 |
| | | | | | 1994 / 2016 | -3022.47 | 313.51 |
| | | | | | 1996 / 2015 | 8545.76 | 386.66 |
| | | | | | 1996 / 2016 | 9389.44 | 353.28 |
| | | | | | 2015 / 2016 | 843.69 | 351.48 |
| Bermejo | Kruskal-Wallis | 20.40 | 6E-06 | | 2002 / 2016 | 158.07 | 68.59 |
| | Mood's | 2.07 | 0.15 | 132.99 | | | |
| Segovia | Kruskal-Wallis | 76.80 | 0 | | 1999 / 2016 | 678.41 | 151.72 |
| | Mood's | 62.26 | 0 | 104.33 | | | |

Table A.17: Median check.

| River | Kimber's test | | | Walsh's test | |
|---|---|---|---|---|---|
| | S | s | # outliers | # Lower outliers | # Upper outliers |
| Chixoy 1986 | 1.37E-03 | 8.74E-03 | 0 | 0 | 0 |
| Chixoy 2010 | 2.39E-03 | 1.58E-02 | 0 | 0 | 0 |
| Chixoy 2012 | 1.84E-03 | 1.67E-02 | 0 | 0 | 0 |
| Chixoy 2016 | 1.95E-03 | 1.62E-02 | 0 | 0 | 0 |
| Sacramento 1994 | 2.48E-04 | 2.02E-03 | 0 | 1 | 0 |
| Sacramento 1996 | 3.47E-04 | 3.02E-03 | 0 | 0 | 0 |
| Sacramento 2015 | 3.17E-04 | 2.97E-03 | 0 | 0 | 1 |
| Sacramento 2016 | 2.02E-04 | 2.04E-03 | 0 | 0 | 0 |
| Bermejo 2002 | 1.29E-03 | 8.06E-03 | 0 | 0 | 0 |
| Bermejo 2016 | 8.50E-04 | 7.41E-03 | 0 | 0 | 0 |
| Segovia 1999 | 2.54E-04 | 2.24E-03 | 0 | 1 | 0 |
| Segovia 2016 | 2.20E-04 | 1.54E-03 | 0 | 0 | 0 |

Table A.18: Non normal test for river group 2 (see also Table A.10).

| River | Best PDF | Dimensional case | | | Dimensionless case | | |
|---|---|---|---|---|---|---|---|
| | | BIC | GEV BIC | Diff % | BIC | GEV BIC | Diff % |
| Chixoy 1986 | Inv Gauss | 8.60E+03 | 8.61E+03 | 0.05% | -5.56E+02 | -5.52E+02 | 0.82% |
| Chixoy 2010 | Stable | 6.82E+03 | 6.89E+03 | 0.98% | -7.57E+02 | -6.71E+02 | 11.37% |
| Chixoy 2012 | Bim-Saund | 6.06E+03 | 6.07E+03 | 0.13% | -9.07E+02 | -8.99E+02 | 0.89% |
| Chixoy 2016 | Log Logistic | 6.39E+03 | 6.41E+03 | 0.35% | -5.51E+02 | -5.29E+02 | 4.11% |
| Sacramento 1994 | GEV | 6.19E+04 | 6.19E+04 | 0.00% | -5.10E+03 | -5.10E+03 | 0.00% |
| Sacramento 1996 | Log Logistic | 4.23E+04 | 4.23E+04 | 0.17% | -4.77E+03 | -4.69E+03 | 1.53% |
| Sacramento 2015 | GEV | 4.15E+04 | 4.15E+04 | 0.00% | -3.78E+03 | -3.78E+03 | 0.00% |
| Sacramento 2016 | GEV | 6.22E+04 | 6.22E+04 | 0.00% | -5.24E+03 | -5.24E+03 | 0.00% |
| Bermejo 2002 | GEV | 1.77E+04 | 1.77E+04 | 0.00% | 3.83E+02 | 3.83E+02 | 0.00% |
| Bermejo 2016 | GEV | 1.79E+04 | 1.79E+04 | 0.00% | -7.69E+02 | -7.69E+02 | 0.00% |
| Segovia 1999 | GEV | 6.11E+04 | 6.11E+04 | 0.00% | -3.68E+03 | -3.68E+03 | 0.00% |
| Segovia 2016 | GEV | 9.07E+04 | 9.07E+04 | 0.00% | -5.78E+03 | -5.78E+03 | 0.00% |

Table A.19: Multi river best PDF fitting and compare with GEV based on BIC for the dimensional and dimensionless case.

| River group | Comparison | Dimensional | | Dimensionless | |
|---|---|---|---|---|---|
| | | BC | BDC | BC | BDC |
| Chixoy | 1986 / 2010 | 0.005 | 0.995 | 0.005 | 0.995 |
| | 1986 / 2012 | 0.027 | 0.973 | 0.027 | 0.973 |
| | 1986 / 2016 | 0.002 | 0.998 | 0.002 | 0.998 |
| | 2010 / 2012 | 0.012 | 0.988 | 0.012 | 0.988 |
| | 2010 / 2016 | 0.003 | 0.997 | 0.003 | 0.997 |
| | 2012 / 2016 | 0.018 | 0.982 | 0.018 | 0.982 |
| Sacramento | 1994 / 1996 | 0.606 | 0.546 | 0.005 | 0.995 |
| | 1994 / 2015 | 0.048 | 0.953 | 0.004 | 0.996 |
| | 1994 / 2016 | 0.031 | 0.969 | 0.006 | 0.994 |
| | 1996 / 2015 | 0.336 | 0.715 | 0.004 | 0.997 |
| | 1996 / 2016 | 0.402 | 0.669 | 0.007 | 0.993 |
| | 2015 / 2016 | 0.003 | 0.997 | 0.002 | 0.998 |
| Bermejo | 2002 / 2016 | 0.022 | 0.979 | 0.021 | 0.979 |
| Segovia | 1999 / 2016 | 0.004 | 0.996 | 0.002 | 0.998 |

Table A.20: Bhattacharyya coefficient and Bhattacharyya coefficient distance for dimensional and dimensionless case.

| Year | Count | Average (m) | Stnd. Dev. | Coeff. of Var. | Min. (m) | Max. (m) | Range (m) | Stnd. skewness | Stnd. kurtosis |
|---|---|---|---|---|---|---|---|---|---|
| 1984 | 3552 | 386.69 | 111.20 | 28.76% | 204.96 | 889.49 | 684.54 | 41.64 | 49.41 |
| 1985 | 3616 | 355.27 | 123.50 | 34.76% | 170.36 | 937.28 | 766.93 | 42.75 | 55.57 |
| 1986 | 3751 | 332.39 | 107.87 | 32.45% | 114.16 | 765.44 | 651.28 | 22.15 | 14.13 |
| 1987 | 3760 | 350.90 | 109.63 | 31.24% | 149.04 | 814.16 | 665.12 | 32.96 | 27.62 |
| 1988 | 3834 | 370.55 | 97.42 | 26.29% | 196.20 | 749.61 | 553.41 | 28.51 | 13.98 |
| 1989 | 3989 | 328.65 | 98.51 | 29.97% | 111.98 | 663.16 | 551.18 | 31.57 | 16.90 |
| 1990 | 3964 | 301.34 | 84.81 | 28.14% | 151.37 | 792.48 | 641.12 | 40.15 | 47.76 |
| 1991 | 3966 | 349.82 | 89.54 | 25.60% | 169.71 | 799.52 | 629.81 | 28.96 | 25.42 |
| 1992 | 4035 | 317.36 | 100.90 | 31.79% | 152.11 | 794.39 | 642.28 | 45.14 | 46.21 |
| 1993 | 3520 | 332.00 | 112.42 | 33.86% | 150.01 | 855.28 | 705.27 | 40.18 | 41.38 |
| 1994 | 3607 | 344.83 | 109.35 | 31.71% | 150.04 | 834.66 | 684.62 | 38.24 | 40.78 |
| 1995 | 3715 | 297.45 | 107.26 | 36.06% | 115.80 | 767.53 | 651.73 | 34.10 | 32.37 |
| 1996 | 3759 | 325.28 | 90.27 | 27.75% | 153.47 | 690.39 | 536.93 | 31.08 | 21.71 |
| 1997 | 3408 | 278.61 | 99.24 | 35.62% | 95.48 | 829.34 | 733.87 | 39.70 | 66.17 |
| 1998 | 3456 | 303.81 | 105.55 | 34.74% | 106.08 | 906.75 | 800.66 | 43.29 | 77.61 |
| 1999 | 3518 | 358.39 | 109.07 | 30.43% | 148.62 | 925.82 | 777.20 | 33.38 | 39.80 |
| 2000 | 3600 | 371.19 | 114.83 | 30.94% | 180.35 | 859.15 | 678.80 | 31.54 | 24.16 |
| 2001 | 3676 | 375.67 | 113.68 | 30.26% | 190.92 | 909.00 | 718.08 | 36.64 | 38.07 |
| 2002 | 3828 | 355.19 | 108.01 | 30.41% | 185.24 | 949.44 | 764.20 | 53.27 | 83.80 |
| 2003 | 3956 | 350.97 | 99.41 | 28.32% | 184.64 | 761.08 | 576.44 | 32.25 | 23.01 |
| 2004 | 4012 | 353.77 | 112.16 | 31.71% | 180.38 | 866.65 | 686.27 | 36.85 | 36.63 |
| 2005 | 3416 | 337.04 | 109.26 | 32.42% | 138.61 | 813.87 | 675.26 | 31.29 | 24.81 |
| 2006 | 3473 | 378.42 | 117.44 | 31.03% | 172.12 | 823.45 | 651.34 | 27.96 | 19.00 |
| 2007 | 3463 | 434.86 | 188.82 | 43.42% | 173.53 | 1446.39 | 1272.86 | 45.80 | 56.25 |
| 2008 | 3553 | 403.22 | 130.82 | 32.44% | 160.04 | 908.46 | 748.43 | 26.46 | 13.82 |
| 2009 | 3681 | 393.19 | 139.89 | 35.58% | 142.93 | 929.84 | 786.91 | 29.63 | 19.65 |
| 2010 | 3739 | 403.27 | 149.13 | 36.98% | 140.81 | 966.47 | 825.66 | 35.20 | 26.04 |
| 2011 | 3835 | 435.10 | 150.88 | 34.68% | 178.06 | 1063.88 | 885.82 | 35.07 | 28.93 |
| 2012 | 3948 | 448.59 | 179.01 | 39.90% | 202.68 | 1205.40 | 1002.73 | 41.06 | 35.64 |
| 2013 | 4036 | 423.36 | 171.73 | 40.56% | 180.80 | 1097.18 | 916.38 | 35.58 | 21.38 |
| 2014 | 4159 | 421.74 | 186.40 | 44.20% | 146.70 | 1198.46 | 1051.76 | 45.93 | 44.43 |
| 2015 | 3998 | 418.28 | 152.84 | 36.54% | 150.34 | 971.34 | 821.00 | 32.71 | 22.39 |

Table A.21: General statistic values of the dimensional half width from the Ucayali river.

| River | Count | Stnd. Dev. | Coeff. Var. | Min. | Max. | Range | Stnd. skewness | Stnd. kurtosis |
|---|---|---|---|---|---|---|---|---|
| 1984 | 3552 | 0.29 | 28.76% | 0.53 | 2.30 | 1.77 | 41.64 | 49.41 |
| 1985 | 3616 | 0.35 | 34.76% | 0.48 | 2.64 | 2.16 | 42.75 | 55.57 |
| 1986 | 3751 | 0.32 | 32.45% | 0.34 | 2.30 | 1.96 | 22.15 | 14.13 |
| 1987 | 3760 | 0.31 | 31.24% | 0.42 | 2.32 | 1.90 | 32.96 | 27.62 |
| 1988 | 3834 | 0.26 | 26.29% | 0.53 | 2.02 | 1.49 | 28.51 | 13.98 |
| 1989 | 3989 | 0.30 | 29.97% | 0.34 | 2.02 | 1.68 | 31.57 | 16.90 |
| 1990 | 3964 | 0.28 | 28.14% | 0.50 | 2.63 | 2.13 | 40.15 | 47.76 |
| 1991 | 3966 | 0.26 | 25.60% | 0.49 | 2.29 | 1.80 | 28.96 | 25.42 |
| 1992 | 4035 | 0.32 | 31.79% | 0.48 | 2.50 | 2.02 | 45.14 | 46.21 |
| 1993 | 3520 | 0.34 | 33.86% | 0.45 | 2.58 | 2.12 | 40.18 | 41.38 |
| 1994 | 3607 | 0.32 | 31.71% | 0.44 | 2.42 | 1.99 | 38.24 | 40.78 |
| 1995 | 3715 | 0.36 | 36.06% | 0.39 | 2.58 | 2.19 | 34.10 | 32.37 |
| 1996 | 3759 | 0.28 | 27.75% | 0.47 | 2.12 | 1.65 | 31.08 | 21.71 |
| 1997 | 3408 | 0.36 | 35.62% | 0.34 | 2.98 | 2.63 | 39.70 | 66.17 |
| 1998 | 3456 | 0.35 | 34.74% | 0.35 | 2.98 | 2.64 | 43.29 | 77.61 |
| 1999 | 3518 | 0.30 | 30.43% | 0.41 | 2.58 | 2.17 | 33.38 | 39.80 |
| 2000 | 3600 | 0.31 | 30.94% | 0.49 | 2.31 | 1.83 | 31.54 | 24.16 |
| 2001 | 3676 | 0.30 | 30.26% | 0.51 | 2.42 | 1.91 | 36.64 | 38.07 |
| 2002 | 3828 | 0.30 | 30.41% | 0.52 | 2.67 | 2.15 | 53.27 | 83.80 |
| 2003 | 3956 | 0.28 | 28.32% | 0.53 | 2.17 | 1.64 | 32.25 | 23.01 |
| 2004 | 4012 | 0.32 | 31.71% | 0.51 | 2.45 | 1.94 | 36.85 | 36.63 |
| 2005 | 3416 | 0.32 | 32.42% | 0.41 | 2.41 | 2.00 | 31.29 | 24.81 |
| 2006 | 3473 | 0.31 | 31.03% | 0.45 | 2.18 | 1.72 | 27.96 | 19.00 |
| 2007 | 3463 | 0.43 | 43.42% | 0.40 | 3.33 | 2.93 | 45.80 | 56.25 |
| 2008 | 3553 | 0.32 | 32.44% | 0.40 | 2.25 | 1.86 | 26.46 | 13.82 |
| 2009 | 3681 | 0.36 | 35.58% | 0.36 | 2.36 | 2.00 | 29.63 | 19.65 |
| 2010 | 3739 | 0.37 | 36.98% | 0.35 | 2.40 | 2.05 | 35.20 | 26.04 |
| 2011 | 3835 | 0.35 | 34.68% | 0.41 | 2.45 | 2.04 | 35.07 | 28.93 |
| 2012 | 3948 | 0.40 | 39.90% | 0.45 | 2.69 | 2.24 | 41.06 | 35.64 |
| 2013 | 4036 | 0.41 | 40.56% | 0.43 | 2.59 | 2.16 | 35.58 | 21.38 |
| 2014 | 4159 | 0.44 | 44.20% | 0.35 | 2.84 | 2.49 | 45.93 | 44.43 |
| 2015 | 3998 | 0.37 | 36.54% | 0.36 | 2.32 | 1.96 | 32.71 | 22.39 |

Table A.22: General statistic values of the dimensionless half width from the Ucayali river.

| Year | B | L | 1984 | 1985 | 1986 | 1987 | 1988 | 1989 | 1990 | 1991 | 1992 | 1993 | 1994 | 1995 | 1996 | 1997 | 1998 | 1999 | 2000 | 2001 | 2002 | 2003 | 2004 | 2005 | 2006 | 2007 | 2008 | 2009 | 2010 | 2011 | 2012 | 2013 | 2014 | 2015 |
|---|---|---|---|---|---|---|---|---|---|---|---|---|---|---|---|---|---|---|---|---|---|---|---|---|---|---|---|---|---|---|---|---|---|---|
| 1984 | 10 | 0 | | | 1 | 1 | | | | | | 1 | 1 | | | | | 1 | 1 | 1 | 1 | | 1 | 1 | | | | | | | | | | |
| 1985 | 0 | 0 | | | | | | | | | | | | | | | | | | | | | | | | | | | | | | | | |
| 1986 | 7 | 1 | 1 | | | 1 | | | | | | | 1 | 1 | | | 1 | 1 | | | 1 | | | 1 | | | | | | | | | | |
| 1987 | 7 | 2 | 1 | | 1 | | | | | | | 1 | 1 | 1 | | 1 | | 1 | | | 1 | | 1 | 1 | | | | | | | | | | |
| 1988 | 3 | 0 | | | | | | 1 | | | | | | | | 1 | | | | | | 1 | | | | | | | | | | | | |
| 1989 | 3 | 1 | | | | 1 | 1 | | | | 1 | | | | | 1 | | | | | | 1 | | | | | | | | | | | | |
| 1990 | 0 | 0 | | | | | | | | | | | | | | | | | | | | | | | | | | | | | | | | |
| 1991 | 1 | 0 | | | | | | | | | | | | | 1 | | | | | | | | | | | | | | | | | | | |
| 1992 | 2 | 1 | | | | | | 1 | | | | | | | | 1 | | | | | | 1 | | | | | | | | | | | | |
| 1993 | 6 | 2 | | | | | | | | | | | 1 | | | | | 1 | 1 | 1 | | | 1 | 1 | | | | | | | | | | |
| 1994 | 5 | 4 | | | 1 | 1 | | | | | | 1 | | 1 | | | 1 | 1 | | | 1 | | 1 | 1 | | | | | | | | | | |
| 1995 | 4 | 3 | | | 1 | 1 | | | | | | 1 | 1 | | | | 1 | 1 | | | 1 | | | 1 | | | | | | | | | | |
| 1996 | 0 | 1 | | | | | | | | 1 | | | | | | | | | | | | | | | | | | | | | | | | |
| 1997 | 1 | 3 | | | | | 1 | 1 | | | 1 | | | | | | | | | | | 1 | | | | | | | | | | | | |
| 1998 | 2 | 2 | | | 1 | | | | | | | | | 1 | | | | 1 | | | 1 | | | | | | | | | | | | | |
| 1999 | 3 | 7 | 1 | | 1 | 1 | | | | | | 1 | 1 | 1 | | | 1 | | | | 1 | | 1 | 1 | | | | | | | | | | |
| 2000 | 3 | 2 | 1 | | | | | | | | | 1 | | | | | | | | 1 | | | 1 | | | | | | | | | | | |
| 2001 | 3 | 2 | 1 | | | | | | | | | 1 | | | | | | | 1 | | | | 1 | | 1 | | | | | | | | | | |
| 2002 | 7 | 1 | 1 | | 1 | 1 | | | | | | | 1 | 1 | | | 1 | 1 | | | | | | 1 | | | | | | | | | | |
| 2003 | 4 | 0 | | | | | 1 | 1 | | | 1 | | | | | 1 | | | | | | | | | | | | | | | | | | |
| 2004 | 7 | 1 | 1 | | | 1 | | | | | | 1 | 1 | | | | | 1 | 1 | | | | | 1 | | | | | | | | | | |
| 2005 | 9 | 0 | 1 | | 1 | 1 | | | | | | 1 | 1 | 1 | | | | 1 | | | 1 | | 1 | | | | | | | | | | | |
| 2006 | 2 | 0 | | | | | | | | | | | | | | | | | 1 | 1 | | | | | | | | | | | | | | |
| 2007 | 0 | 1 | | | | | | | | | | | | | | | | | | | | | | | | | | | | | | | 1 | |
| 2008 | 0 | 0 | | | | | | | | | | | | | | | | | | | | | | | | | | | | | | | | |
| 2009 | 0 | 0 | | | | | | | | | | | | | | | | | | | | | | | | | | | | | | | | |
| 2010 | 2 | 0 | | | | | | | | | | | | | | | | | | | | | | | | | | | 1 | 1 | | | | 1 |
| 2011 | 1 | 1 | | | | | | | | | | | | | | | | | | | | | | | | | | | 1 | | | | | 1 |
| 2012 | 0 | 0 | | | | | | | | | | | | | | | | | | | | | | | | | | | | | | | | |
| 2013 | 0 | 0 | | | | | | | | | | | | | | | | | | | | | | | | | | | | | | | | |
| 2014 | 1 | 0 | | | | | | | | | | | | | | | | | | | | | | | | 1 | | | | | | | | |
| 2015 | 2 | 0 | | | | | | | | | | | | | | | | | | | | | | | | | | | 1 | 1 | | | | |

Table A.23: Ucayali variance check (B is for Bartlett and L for Levene tests. The number indicates the amount of pairs that show non statistically significant differences between the variance).

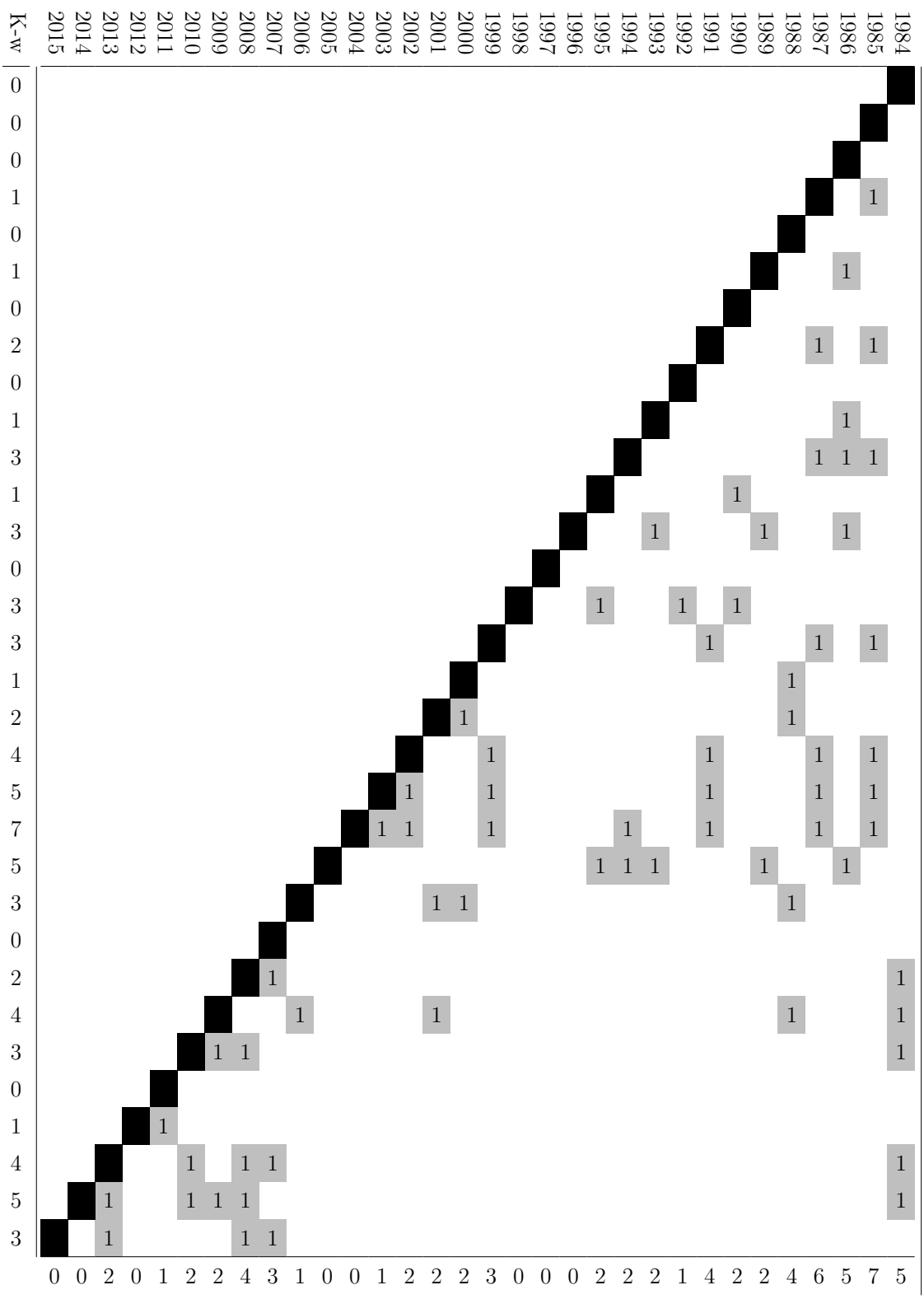


Table A.24: Ucayali median check (K-W is for Kruskal-Wallis Test. The number indicates the amount of pairs that show non statistically significant differences between the medians).

| Ucayali | | Dimensional case | | | Dimensionless case | | |
|---|---|---|---|---|---|---|---|
| Year | Best PDF | BIC | GEV BIC | Diff. % | BIC | GEV BIC | Diff. % |
| 1984 | GEV | 4.22E+04 | 4.22E+04 | 0.00% | -1.28E+02 | -1.28E+02 | 0.00% |
| 1985 | GEV | 4.37E+04 | 4.37E+04 | 0.00% | 1.28E+03 | 1.28E+03 | 0.00% |
| 1986 | Bir.-Saun. | 4.53E+04 | 4.53E+04 | 0.04% | 1.70E+03 | 1.72E+03 | 1.13% |
| 1987 | GEV | 4.50E+04 | 4.50E+04 | 0.00% | 8.91E+02 | 8.91E+02 | 0.00% |
| 1988 | GEV | 4.49E+04 | 4.49E+04 | 0.00% | -4.09E+02 | -4.09E+02 | 0.00% |
| 1989 | GEV | 4.68E+04 | 4.68E+04 | 0.00% | 6.16E+02 | 6.16E+02 | 0.00% |
| 1990 | GEV | 4.51E+04 | 4.51E+04 | 0.00% | -1.74E+02 | -1.74E+02 | 0.00% |
| 1991 | GEV | 4.62E+04 | 4.62E+04 | 0.00% | -3.07E+02 | -3.07E+02 | 0.00% |
| 1992 | GEV | 4.67E+04 | 4.67E+04 | 0.00% | 1.85E+02 | 1.85E+02 | 0.00% |
| 1993 | GEV | 4.17E+04 | 4.17E+04 | 0.00% | 7.96E+02 | 7.96E+02 | 0.00% |
| 1994 | GEV | 4.28E+04 | 4.28E+04 | 0.00% | 6.63E+02 | 6.63E+02 | 0.00% |
| 1995 | GEV | 4.43E+04 | 4.43E+04 | 0.00% | 1.94E+03 | 1.94E+03 | 0.00% |
| 1996 | GEV | 4.35E+04 | 4.35E+04 | 0.00% | 3.37E+01 | 3.37E+01 | 0.00% |
| 1997 | Log loistic | 4.01E+04 | 4.02E+04 | 0.05% | 1.76E+03 | 1.78E+03 | 1.11% |
| 1998 | GEV | 4.10E+04 | 4.10E+04 | 0.00% | 1.52E+03 | 1.52E+03 | 0.00% |
| 1999 | GEV | 4.21E+04 | 4.21E+04 | 0.00% | 7.36E+02 | 7.36E+02 | 0.00% |
| 2000 | GEV | 4.33E+04 | 4.33E+04 | 0.00% | 7.16E+02 | 7.16E+02 | 0.00% |
| 2001 | GEV | 4.40E+04 | 4.40E+04 | 0.00% | 3.90E+02 | 3.90E+02 | 0.00% |
| 2002 | GEV | 4.48E+04 | 4.48E+04 | 0.00% | -1.21E+02 | -1.21E+02 | 0.00% |
| 2003 | GEV | 4.64E+04 | 4.64E+04 | 0.00% | 6.36E+01 | 6.36E+01 | 0.00% |
| 2004 | GEV | 4.79E+04 | 4.79E+04 | 0.00% | 8.57E+02 | 8.57E+02 | 0.00% |
| 2005 | GEV | 4.08E+04 | 4.08E+04 | 0.00% | 1.04E+03 | 1.04E+03 | 0.00% |
| 2006 | GEV | 4.22E+04 | 4.22E+04 | 0.00% | 9.35E+02 | 9.35E+02 | 0.00% |
| 2007 | GEV | 4.42E+04 | 4.42E+04 | 0.00% | 2.07E+03 | 2.07E+03 | 0.00% |
| 2008 | GEV | 4.39E+04 | 4.39E+04 | 0.00% | 1.30E+03 | 1.30E+03 | 0.00% |
| 2009 | GEV | 4.59E+04 | 4.59E+04 | 0.00% | 1.90E+03 | 1.90E+03 | 0.00% |
| 2010 | GEV | 4.67E+04 | 4.67E+04 | 0.00% | 1.81E+03 | 1.81E+03 | 0.00% |
| 2011 | GEV | 4.81E+04 | 4.81E+04 | 0.00% | 1.52E+03 | 1.52E+03 | 0.00% |
| 2012 | GEV | 5.02E+04 | 5.02E+04 | 0.00% | 1.98E+03 | 1.98E+03 | 0.00% |
| 2013 | GEV | 5.12E+04 | 5.12E+04 | 0.00% | 2.40E+03 | 2.40E+03 | 0.00% |
| 2014 | GEV | 5.30E+04 | 5.30E+04 | 0.00% | 2.75E+03 | 2.75E+03 | 0.00% |
| 2015 | GEV | 5.05E+04 | 5.05E+04 | 0.00% | 2.20E+03 | 2.20E+03 | 0.00% |

Table A.25: Ucayali's best fitting PDF and compare with the GEV based on BIC for dimensional and dimensionless case.

| Year | Dimensional case | | | | | | Dimensionless case | | | | | |
|---|---|---|---|---|---|---|---|---|---|---|---|---|
| | Worst Case | | | Best Case | | | Worst Case | | | Best Case | | |
| | BC | BDC | Year | BC | BDC | Year | BC | BDC | Year | BC | BDC | Year |
| 1984 | 0.785 | 0.242 | 1997 | 0.997 | 0.003 | 1988 | 0.947 | 0.054 | 2014 | 1.000 | 0.000 | 1990 |
| 1985 | 0.915 | 0.089 | 1997 | 0.999 | 0.001 | 1987 | 0.978 | 0.022 | 1988 | 1.000 | 0.000 | 2011 |
| 1986 | 0.891 | 0.115 | 2012 | 0.994 | 0.006 | 2005 | 0.965 | 0.036 | 1988 | 0.998 | 0.002 | 1998 |
| 1987 | 0.910 | 0.095 | 1997 | 0.999 | 0.001 | 2004 | 0.978 | 0.023 | 2014 | 1.000 | 0.000 | 1999 |
| 1988 | 0.807 | 0.214 | 1997 | 0.997 | 0.003 | 1984 | 0.936 | 0.066 | 2014 | 0.999 | 0.001 | 1990 |
| 1989 | 0.893 | 0.114 | 2012 | 0.998 | 0.002 | 2005 | 0.970 | 0.030 | 2014 | 1.000 | 0.000 | 1999 |
| 1990 | 0.820 | 0.198 | 2012 | 0.996 | 0.004 | 1992 | 0.946 | 0.056 | 2014 | 1.000 | 0.000 | 1984 |
| 1991 | 0.871 | 0.139 | 1997 | 0.997 | 0.003 | 2003 | 0.944 | 0.058 | 2014 | 0.999 | 0.001 | 1996 |
| 1992 | 0.864 | 0.146 | 2012 | 0.996 | 0.004 | 1993 | 0.955 | 0.046 | 2014 | 0.999 | 0.001 | 2002 |
| 1993 | 0.897 | 0.109 | 2012 | 0.997 | 0.003 | 1989 | 0.976 | 0.024 | 2014 | 0.999 | 0.001 | 2004 |
| 1994 | 0.910 | 0.094 | 1997 | 0.999 | 0.001 | 2004 | 0.973 | 0.028 | 2014 | 1.000 | 0.000 | 2000 |
| 1995 | 0.806 | 0.215 | 2012 | 0.998 | 0.002 | 1998 | 0.962 | 0.039 | 1988 | 0.999 | 0.001 | 2009 |
| 1996 | 0.886 | 0.121 | 2012 | 0.998 | 0.002 | 1989 | 0.954 | 0.047 | 2014 | 0.999 | 0.001 | 2003 |
| 1997 | 0.752 | 0.285 | 2012 | 0.995 | 0.005 | 1995 | 0.960 | 0.040 | 1988 | 0.999 | 0.001 | 1995 |
| 1998 | 0.827 | 0.190 | 2012 | 0.998 | 0.002 | 1995 | 0.969 | 0.031 | 1988 | 0.999 | 0.001 | 2008 |
| 1999 | 0.894 | 0.113 | 1997 | 0.999 | 0.001 | 1987 | 0.975 | 0.025 | 2014 | 1.000 | 0.000 | 1987 |
| 2000 | 0.861 | 0.149 | 1997 | 0.998 | 0.002 | 2006 | 0.974 | 0.026 | 2014 | 1.000 | 0.000 | 1994 |
| 2001 | 0.834 | 0.182 | 1997 | 0.998 | 0.002 | 2000 | 0.964 | 0.037 | 2014 | 0.999 | 0.001 | 1994 |
| 2002 | 0.854 | 0.157 | 1997 | 0.999 | 0.001 | 2003 | 0.947 | 0.054 | 2014 | 1.000 | 0.000 | 1984 |
| 2003 | 0.871 | 0.139 | 1997 | 0.999 | 0.001 | 2002 | 0.953 | 0.048 | 2014 | 1.000 | 0.000 | 1984 |
| 2004 | 0.896 | 0.109 | 1997 | 0.999 | 0.001 | 1994 | 0.975 | 0.025 | 2014 | 1.000 | 0.000 | 2000 |
| 2005 | 0.908 | 0.097 | 2012 | 0.998 | 0.002 | 1989 | 0.982 | 0.018 | 1988 | 1.000 | 0.000 | 2006 |
| 2006 | 0.863 | 0.147 | 1997 | 0.998 | 0.002 | 2000 | 0.980 | 0.021 | 2014 | 1.000 | 0.000 | 1987 |
| 2007 | 0.806 | 0.216 | 1997 | 0.996 | 0.004 | 2013 | 0.944 | 0.058 | 1988 | 0.997 | 0.003 | 2013 |
| 2008 | 0.831 | 0.185 | 1997 | 0.997 | 0.003 | 2010 | 0.977 | 0.024 | 1988 | 0.999 | 0.001 | 2005 |
| 2009 | 0.872 | 0.137 | 1997 | 0.998 | 0.002 | 2010 | 0.963 | 0.038 | 1988 | 0.999 | 0.001 | 1995 |
| 2010 | 0.845 | 0.168 | 1997 | 0.998 | 0.002 | 2009 | 0.965 | 0.036 | 1988 | 0.999 | 0.001 | 2011 |
| 2011 | 0.767 | 0.265 | 1997 | 0.995 | 0.005 | 2012 | 0.974 | 0.026 | 1988 | 1.000 | 0.000 | 1985 |
| 2012 | 0.752 | 0.285 | 1997 | 0.995 | 0.005 | 2011 | 0.957 | 0.044 | 1988 | 0.996 | 0.004 | 2013 |
| 2013 | 0.821 | 0.197 | 1997 | 0.996 | 0.004 | 2007 | 0.946 | 0.055 | 1988 | 0.997 | 0.003 | 2007 |
| 2014 | 0.843 | 0.170 | 1997 | 0.996 | 0.004 | 2010 | 0.936 | 0.066 | 1988 | 0.997 | 0.003 | 2007 |
| 2015 | 0.832 | 0.184 | 1997 | 0.997 | 0.003 | 2008 | 0.959 | 0.042 | 1988 | 0.999 | 0.001 | 1995 |

Table A.26: Ucayali's best and worst cases of the BC and BDC per year in the dimensional and dimensionless case.

# Appendix B

# Complementary threshold equations of chapter 3

The model include different equations for the erosion and deposition threshold, that as was mention before in the case of deposition is taken as the suspension movement threshold. Must of these equations are based in experimental data and the Shields diagram and the movability number $\Lambda$ .

### B.0.1 Erosion Thresholds

(Krey, 1925) proposed a simple empirical equations

$$\tau_c^*(d \geq 6mm) = 0.076(\gamma_s - \gamma)d \quad \text{(B.1)}$$

$$\tau_c^*(0.1 \leq d \geq 3mm) = 2.85 \times 10^{-4}(\gamma_s - \gamma)d^{1/3} \quad \text{(B.2)}$$

(Meyer-Peter and Müller, 1948) proposed for a completely turbulent flow and a sediment diameter between 0.4 to 30 mm

$$\tau_c^* = 0.047(\gamma_s - \gamma)d \quad \text{(B.3)}$$

(Brownlie, 1981)

$$\Theta_c = 0.22\widetilde{d}^{-0.6} + 0.06exp\left(-17.77\widetilde{d}^{-0.6}\right) \quad \text{(B.4)}$$

$$\widetilde{d} = d\left(\Delta g d\right)^{0.5}/\nu \quad \text{(B.5)}$$

(Van Rijn, 1984)

$$\Theta_c(4 < D_* \leq 4) = 0.24D_*^{-1} \quad \text{(B.6)}$$
$$\Theta_c(4 < D_* \leq 10) = 0.14D_*^{-0.64} \quad \text{(B.7)}$$
$$\Theta_c(10 < D_* \leq 20) = 0.04D_*^{-1} \quad \text{(B.8)}$$
$$\Theta_c(20 < D_* \leq 150) = 0.013D_*^{0.29} \quad \text{(B.9)}$$
$$\Theta_c(D_* > 150) = 0.055 \quad \text{(B.10)}$$
$$D_* = d\left(\Delta g/\nu^2\right)^{1/3} \quad \text{(B.11)}$$

(Soulsby and Whitehouse, 1997)

$$\Theta_c = \frac{0.3}{1 + 1.2D_*} + 0.055\left[1 - exp\left(-0.02D_*\right)\right] \quad \text{(B.12)}$$

(Wu and Wang, 1999)

$$\Theta_c(D_* < 1.5) = 0.126D_*^{-0.44} \quad \text{(B.13)}$$
$$\Theta_c(1.5 < D_* \leq 10) = 0.131D_*^{-0.55} \quad \text{(B.14)}$$
$$\Theta_c(10 < D_* \leq 20) = 0.0685D_*^{0.27} \quad \text{(B.15)}$$
$$\Theta_c(20 < D_* \leq 40) = 0.0173D_*^{0.19} \quad \text{(B.16)}$$
$$\Theta_c(40 < D_* \leq 150) = 0.0115D_*^{0.3} \quad \text{(B.17)}$$
$$\Theta_c(D_* > 150) = 0.052 \quad \text{(B.18)}$$

(Paphitis, 2001)

*In terms of* $D_*$

Lower limit

$$\Theta_c(0.1 < Re_* < 10^4) = \frac{0.165}{0.7 + 1.2D_*} + 0.030\,[1 - 0.57exp\,(-0.02D_*)] \quad \text{(B.19)}$$

Upper limit

$$\Theta_c(0.1 < Re_* < 10^4) = \frac{0.380}{1.2 + 1.2D_*} + 0.070\,[1 - 0.57exp\,(-0.02D_*)] \quad \text{(B.20)}$$

Mean threshold curve

$$\Theta_c(0.1 < Re_* < 10^4) = \frac{0.273}{1.0 + 1.2D_*} + 0.046\,[1 - 0.57exp\,(-0.02D_*)] \quad \text{(B.21)}$$

*In terms of* $\Lambda$

Lower limit

$$\Lambda(0.1 < Re_* < 10^5) = \frac{0.65}{Re_*} + 12exp(-2.5Re_*) + 0.01lnRe_* + 0.078 \quad \text{(B.22)}$$

Upper limit

$$\Lambda(0.1 < Re_* < 10^5) = \frac{0.88}{Re_*} + 14exp(-1.5Re_*) + 0.01lnRe_* + 0.180 \quad \text{(B.23)}$$

Mean threshold curve

$$\Lambda(0.1 < Re_* < 10^5) = \frac{0.75}{Re_*} + 14exp(-2.0Re_*) + 0.01lnRe_* + 0.115 \quad \text{(B.24)}$$

$$\Lambda = \frac{u_*}{w_s} \quad \text{(B.25)}$$

(Cheng, 2004)

$$\Theta_c(0.114 \leq D_* \leq 35.4 \rhd 0.02 \leq Re_* \leq 48.8) \;=\; 0.147D_*^{-0.29} \quad \text{(B.26)}$$

(Iwagaki, 1956)

$$\Theta_c\left(\widetilde{d} \leq 2.140\right) = 0.14 \tag{B.27}$$

$$\Theta_c\left(2.140 < \widetilde{d} \leq 54.02\right) = 0.195\widetilde{d}^{-7/16} \tag{B.28}$$

$$\Theta_c\left(54.20 < \widetilde{d} \leq 162.7\right) = 0.034 \tag{B.29}$$

$$\Theta_c\left(162.7 < \widetilde{d} \leq 671.0\right) = 0.00878\widetilde{d}^{3/11} \tag{B.30}$$

$$\Theta_c\left(\widetilde{d} > 671.0\right) = 0.05 \tag{B.31}$$

(Cao et al., 2006)

$$\Theta_c\left(\widetilde{d} \leq 6.61\right) = 0.1414\widetilde{d}^{-0.23} \tag{B.32}$$

$$\Theta_c\left(6.61 < \widetilde{d} \leq 282.84\right) = \frac{\left[1 + \left(0.0223\widetilde{d}\right)^{2.84}\right]^{0.35}}{3.09\widetilde{d}^{0.68}} \tag{B.33}$$

$$\Theta_c\left(\widetilde{d} \geq 282.84\right) = 0.045 \tag{B.34}$$

### B.0.2 Deposition Thresholds

(Sumer, 1986)

$$\Theta_c\left(R_* \leq 70\right) = \frac{17}{R_*} \tag{B.35}$$

$$\Theta_c\left(R_* > 70\right) = 0.27 \tag{B.36}$$

(Celik and Rodi, 1991)

$$\Theta_c\left(R_* \leq 0.6\right) = \frac{0.15}{R_*} \tag{B.37}$$

$$\Theta_c\left(R_* > 0.6\right) = 0.25 \tag{B.38}$$

(Nino et al., 2003)

$$\Lambda_c\left(1 \leq Re_p \leq 27.3\right) = 21.2Re_p^{-1.2} \tag{B.39}$$

$$\Lambda_c\left(Re_p > 27.3\right) = 0.4 \tag{B.40}$$

(Cheng, 2008)

$$\Theta_c = \frac{1.32Re_c^2}{\left[\left(\sqrt[3]{\alpha\left[Re_c - Re_c exp(-0.093Re_c^{1.3})\right]} + 5\right)^2 - 25\right]^{3/2}} \quad \text{(B.41)}$$

$$\alpha = -0.5\pi ln\left(4p_c - 4p_c^2\right) \quad \text{(B.42)}$$

$p_c$ = 0.01Suspension threshold

$p_c$ = $10^{-7}$Incipient sediment motion threshold

# Part V

# Bibliography

# Bibliography


Abizaid, C. (2005). An Anthropogenic Meander Cutoff along the Ucayali River , Peruvian. *American Geographical Society*, 95(1):122–135.

Aguinis, H., Gottfredson, R. K., and Joo, H. (2013). Best-Practice Recommendations for Defining, Identifying, and Handling Outliers. *Organizational Research Methods*, 16(2):270–301.

Ali, S. Z. and Dey, S. (2016). Hydrodynamics of sediment threshold. *Physics of Fluids*, 28(7):075103.

Asahi, K., Shimizu, Y., Nelson, J., and Parker, G. (2013). Numerical simulation of river meandering with self-evolving banks. *Journal of Geophysical Research: Earth Surface*, 118(4):2208–2229.

Bagnold, R. A. (1966). An Approach to the Sediment Transport Problem from General Physics.

Barsi, J. A., Lee, K., Kvaran, G., Markham, B. L., and Pedelty, J. A. (2014). The spectral response of the Landsat-8 operational land imager. *Remote Sensing*, 6(10):10232–10251.

Bartholdy, J. and Billi, P. (2002). Morphodynamics of a pseudomeandering gravel bar reach. *Geomorphology*, 42(3-4):293–310.

Bartlett, M. S. (1937). Properties of Sufficiency and Statistical Tests. *Proceedings of the Royal Society of London. Series A Mathematical and Physical Sciences*, 160(901):268–282.

Beheshti, A. A. and Ataie-Ashtiani, B. (2008). Analysis of threshold and incipient conditions for sediment movement. *Coastal Engineering*, 55(5):423–430.

Bertoldi, W., Siviglia, A., Tettamanti, S., Toffolon, M., Vetsch, D., and Francalanci, S. (2014). Modeling vegetation controls on fluvial morphological trajectories. *Geophysical Research Letters*, 41(20):7167–7175.

Bertoldi, W., Zanoni, L., Miori, S., Repetto, R., and Tubino, M. (2009). Interaction between migrating bars and bifurcations in gravel bed rivers. *Water Resources Research*, 45(6):1–12.

Bhattacharyya, A. (1943). On a Measure of Divergence between Two Multinomial Populations. *Sankhyā: The Indian Journal of Statistics (1933-1960)*, 7(4):401–406.

Billi, P. and Paris, E. (1992). Bed sediment characterisation in river engineering problems. In Bogen, J., Walling, D., and Day, T., editors, *Erosion and Sediment Transport Monitoring Programmes in River Basins*, pages 11–20, Wallingford. IAHS Press.

Bogoni, M., Putti, M., and Lanzoni, S. (2017). Modelingmeandermorphodynamics over self-formed heterogeneous floodplains. *Water Resources Research*, pages 5137–5157.

Bolla Pittaluga, M., Coco, G., and Kleinhans, M. G. (2015). A unified framework for stability of channel bifurcations in gravel and sand fluvial systems. *Geophysical Research Letters*, 42(18):7521–7536.

Bolla Pittaluga, M. and Seminara, G. (2011). Nonlinearity and unsteadiness in river meandering: A review of progress in theory and modelling. *Earth Surface Processes and Landforms*, 36(1):20–38.

Bose, S. K. and Dey, S. (2013). Sediment Entrainment Probability and Threshold of Sediment Suspension: An Exponential Based Approach. *Journal of Hydraulic Engineering*, 139(10):1099–1106.

Braudrick, C., Dietrich, W. E., Leverich, G., and Sklar, L. (2009). Experimental evidence for the conditions necessary to sustain meandering in coarse-bedded rivers. *Proceedings of the National Academy of Sciences of the United States of America*, 106(40):16936–16941.

Brice, J. C. (1975). Airphoto Interpretation of the Form and Behavior of Alluvial Rivers. Technical report, US Army Research Office, St Louis, MO.

Bridge, J. (2003). *Rivers and Floodplains: Forms, Processes, and Sedimentary Record.* Blackwell, Malden.

Bridge, J. S., Smith, N. D., Trent, F., Gabel, S. L., and Bernstein, P. (1986). Sedimentology and morphology of a low-sinuosity river: Calamus River, Nebraska Sand Hills. *Sedimentology*, 33(6):851–870.

Brierley, G. (1991). Floodplain sedimentology of the Squamish River, B.C.: relevance of element analysis. *Sedimentology*, 38:735–750.

Brownlie, W. R. (1981). Prediction of Flow Depth and Sediment Discharge in Open Channels. Report No. KH-R-43A. Technical Report November, W. M. Keck Laboratory of Hydraulics and Water Resources, Division of Engineering and Applied Science, California Institute of Technology, Pasadena, California.

Camporeale, C., Perona, P., Porporato, A., and Ridolfi, L. (2005). On the long-term behavior of meandering rivers. *Water Resources Research*, 41(12):W04109.

Camporeale, C., Perona, P., Porporato, A., and Ridolfi, L. (2007). Hierarchy of models for meandering rivers and related morphodynamic processes. *Reviews of Geophysics*, 45(1):1–28.

Camporeale, C., Perucca, E., and Ridolfi, L. (2008). Significance of cutoff in meandering river dynamics. *Journal of Geophysical Research: Earth Surface*, 113(1):1–11.

Campos, J. C., Sillero, N., and Brito, J. C. (2012). Normalized difference water indexes have dissimilar performances in detecting seasonal and permanent water in the Sahara-Sahel transition zone. *Journal of Hydrology*, 464-465(July 2017):438–446.

Cao, Z., Pender, G., and Meng, J. (2006). Explicit Formulation of the Shields Diagram for Incipient. *Journal of Hydraulic Engineering*, 132(October):1097–1099.

Celik, I. and Rodi, W. W. (1991). Suspended Sediment-Transport Capacity for Open Channel Flow. *Journal of Hydraulic Engineering*, 117(2):191–204.

Chang, T. and Toebes, G. (1970). A Statistical Comparison of Meandering Planforms in the Wabash Basin. *Water Resources Research*, 6(2):557–578.

Chatanantavet, P., Lamb, M. P., and Nittrouer, J. A. (2012). Backwater controls of avulsion location on deltas. *Geophysical Research Letters*, 39(1):2–7.

Chen, D. and Duan, J. G. (2006). Modeling width adjustment in meandering channels. *Journal of Hydrology*, 321:59–76.

Cheng, N.-S. (1997). Simplified Settling Velocity Formula for Sediment Particle. *Journal of Hydraulic Engineering*, 123(February):149–152.

Cheng, N.-S. (2004). Analysis of bedload transport in laminar flows. *Advances in Water Resources*, 27:937–942.

Cheng, N.-S. (2008). Comparison of Settling-Velocity-Based Formulas for Threshold of Sediment Motion. *Journal of Hydraulic Engineering-Asce*, 134(8):1136–1141.

Cheng, N.-S. and Chiew, Y.-M. (1999). Analysis of Initiation of Sediment Suspension from Bed Load. *Journal of Hydraulic Engineering*, 125(8):855–861.

Church, M. (2015). Channel Stability: Morphodynamics and the Morphology of Rivers. In Rowinski, P. and Radecki-Pawlik, A., editors, *Rivers-Physical, Fluvial and Environmental Processess*, chapter Channel St, pages 255–277. Springer International Publishing, Switzerland.

Constantine, C. R., Dunne, T., and Hanson, G. J. (2009). Examining the physical meaning of the bank erosion coefficient used in meander migration modeling. *Geomorphology*, 106(3-4):242–252.

Constantine, J. A., Dunne, T., Ahmed, J., Legleiter, C., and Lazarus, E. D. (2014). Sediment supply as a driver of river meandering and floodplain evolution in the Amazon Basin. *Nature Geoscience*, 7(12):899–903.

Constantine, J. A., McLean, S. R., and Dunne, T. (2010). A mechanism of chute cutoff along large meandering rivers with uniform floodplain topography. *Bulletin of the Geological Society of America*, 122(5-6):855–869.

Coomes, O. T., Abizaid, C., and Lapointe, M. (2009). Human Modification of a Large Meandering Amazonian River: Genesis, Ecological and Economic Consequences of The Masisea Cutoff on the Central Ucayali, Peru. *AMBIO: A Journal of the Human Environment*, 38(3):130–134.

D'Alpaos, L. and Defina, A. (2007). Mathematical modeling of tidal hydrodynamics in shallow lagoons: A review of open issues and applications to the Venice lagoon. *Computers and Geosciences*, 33(4):476–496.

Darby, S. E., Alabyan, A. M., and Van de Wiel, M. J. (2002). Numerical simulation of bank erosion and channel migration in meandering rivers. *Water Resources Research*, 38(9):2–1–2–21.

Darby, S. E. and Delbono, I. (2002). A model of equilibrium bed topography for meander bends with erodible banks. *Earth Surface Processes and Landforms*, 27(10):1057–1085.

Darby, S. E. and Thorne, C. R. (1996). Development and Testing of Riverbank-Stability Analysis. *Journal of Hydraulic Engineering*, 122(8):443–454.

David, S. R., Edmonds, D. A., and Letsinger, S. L. (2016). Controls on the occurrence and prevalence of floodplain channels in meandering rivers. *Earth Surface Processes and Landforms*, pages 1–13.

Defina, A. (2000). Two-dimensional shallow flow equations for partially dry areas. *Water Resources Research*, 36(11):3251.

Defina, A. (2003). Numerical experiments on bar growth. *Water Resources Research*, 39(4):1–12.

Dey, S. (1999). Sediment threshold. *Applied Mathematical Modelling*, 23(5):399–417.

Dey, S. (2014). *Fluvial Hydrodynamics*. Springer International Publishing, first edition.

Dey, S. and Papanicolaou, A. (2008). Sediment Threshold under Stream Flow: A State-of-the-Art Review. *Ksce Journal of Civil Engineering*, 12(1):45–60.

Dieras, P. L., Constantine, J. A., Hales, T. C., Piegay, H., and Riquier, J. (2013). The role of oxbow lakes in the off-channel storage of bed material along the Ain River, France. *Geomorphology*, 188:110–119.

Dunn, O. J. (1961). Multiple comparasions among means. *Journal of the American Statistical Association*, 56(293):52–64.

Dunne, T. and Aalto, R. (2013). Large River Floodplains. In Shroder, J., editor, *Treatise on Geomorphology*, chapter Large Rive, pages 645–678. Academic Press, first edit edition.

Dury, G. H., Sinker, C. A., and Pannett, D. J. (1972). Climatic Change and Arrested Meander Development on the River Severn. *Area*, 4(2):81–85.

Edwards, B. L., Keim, R. F., Johnson, E. L., Hupp, C. R., Marre, S., and King, S. L. (2016). Geomorphic adjustment to hydrologic modifications along a meandering river: Implications for surface flooding on a floodplain. *Geomorphology*, 269:149–159.

Eekhout, J. P. C. and Hoitink, A. J. F. (2015). Chute cutoff as a morphological response to stream reconstruction: The possible role of backwater. *Water Resources Research RESEARCH*, 51:3339–3352.

Eke, E. C. (2013). *Numerical modeling of river migration incorporating erosional and depositional bank processes*. PhD thesis, University of Illinois at Urbana-Champaign.

Eke, E. C., Czapiga, M. J., Viparelli, E., Shimizu, Y., Imran, J., Sun, T., Parker, G., and et Al, E. (2014a). Coevolution of width and sinuosity in meandering rivers. *Journal of Fluid Mechanics*, 760(May):127–174.

Eke, E. C., Parker, G., and Shimizu, Y. (2014b). Numerical modeling of erosional and depositional bank processes in migrating river bends with self-formed width: Morphodynamics of bar push and bank pull. *Journal of Geophysical Research : Earth Surface*, (2):1–29.

El Gammal, E. S. A. (2016). On The Chutes and Chute Cutoff along the River Nile Within Egypt. *Arabian Journal for Science and Engineering*, pages 1–14.

Erskine, W., McFadden, C., and Bishop, P. (1992). Alluvial cutoffs as indicators of former channel conditions. *Earth Surface Processes and Landforms*, 17(1):22–37.

Ettmer, B. and Alvarado-Ancieta, C. A. (2010). Morphological development of the Ucayali River , Peru without human impacts Basic results of topographical survey. *Waldökologie, Landschaftsforschung und Naturschutz*, 10:77–84.

Ferguson, R. I. (1976). Disturbed periodic model for river meanders. *Earth Surface Processes*, 1(4):337–347.

Ferreira da Silva, A. M. and Ebrahimi, M. (2017). Meandering Morphodynamics: Insights from Laboratory and Numerical Experiments and Beyond. *Journal of Hydraulic Engineering*, 143(9):03117005.

Fisk, H. N. (1947). Fine-grained alluvial deposits and their effects on Mississippi River activity. Technical report, War Departmen, Corps of Engineers, Mississipi River Commission, Vicksburg, Mississippi.

Frascati, A. and Lanzoni, S. (2009). Morphodynamic regime and long-term evolution of meandering rivers. *Journal of Geophysical Research*, 114(F2):1–12.

Frascati, A. and Lanzoni, S. (2010). Long-term river meandering as a part of chaotic dynamics? A contribution from mathematical modelling. *Earth Surface Processes and Landforms*, 35(7):791–802.

Frascati, A. and Lanzoni, S. (2013). A mathematical model for meandering rivers with varying width. *Journal of Geophysical Research: Earth Surface*, 118(3):1641–1657.

Fredlund, D., Rahardjo, H., and Fredlund, M. (2012). *Unsaturated Soil Mechanics in Engineering Practice*. John Wiley and Sons, Inc., New Jersey.

Fuller, I. C., Large, A. R. G., and Milan, D. J. (2003). Quantifying channel development and sediment transfer following chute cutoff in a wandering gravel-bed river. *Geomorphology*, 54(3-4):307–323.

Gao, B.-C. (1996). NDWI A Normalized Difference Water Index for Remote Sensing of Vegetation Liquid Water From Space. *Science Inc*, 58:257–266.

Gay, G. R., Gay, H. H., Gay, W. H., Martinson, H. A., Meade, R. H., and Moody, J. A. (1998). Evolution of cutoffs across meander neck in Powder River, Montana, USA. *Earth Surface Processes and Landforms1*, 23:651–662.

Ghinassi, M. (2011). Chute channels in the Holocene high-sinuosity river deposits of the Firenze plain, Tuscany, Italy. *Sedimentology*, 58(3):618–642.

Grass, A. J. (1971). Structural features of turbulent flow over smooth and rough boundaries. *Journal of Fluid Mechanics*, 50(02):233.

Grenfell, M., Aalto, R., and Nicholas, A. (2012). Chute channel dynamics in large, sand-bed meandering rivers. *Earth Surface Processes and Landforms*, 37(3):315–331.

Grenfell, M., Nicholas, A. P., and Aalto, R. (2014). Mediative adjustment of river dynamics: The role of chute channels in tropical sand-bed meandering rivers. *Sedimentary Geology*, 301:93–106.

Grubbs, F. E. (1969). Procedures for Detecting Outlying Observations in Samples. *Technometrics*, 11(1):1–21.

Guneralp, I. and Marston, R. A. (2012). Process-form linkages in meander morphodynamics: Bridging theoretical modeling and real world complexity. *Progress in Physical Geography*, 36(6):718–746.

Güneralp, n., Abad, J. D., Zolezzi, G., and Hooke, J. M. (2012). Advances and challenges in meandering channels research. *Geomorphology*, 163-164:1–9.

Hackney, C., Best, J., Leyland, J., Darby, S. E., Parson, D., Aalto, R., and Nicholas, A. (2015). Modulation of outer bank erosion by slump blocks: Disentangling the protective and destructive role of failed material on the three-dimensional flow structure. *Geophysical Research Letters*, 42.

Harrison, L. R., Dunne, T., and Fisher, G. B. (2015). Hydraulic and geomorphic processes in an overbank flood along a meandering, gravel-bed river: Implications for chute formation. *Earth Surface Processes and Landforms*, 40(9):1239–1253.

Hickin, E. and Nanson, G. (1975). The character of channel migration on the Beatton River, northeast British Colombia, Canada. *Geological Society of America Bulletin*, 86:487–494.

H&O - ECSA (2005). Estudio de la navegabilidad del río Ucayali en el tramo comprendido entre Pucallpa y la confluencia con el río Marañón. Technical report, Dirección general de transporte acuático, Ministerio de transportes y comunicaciones.

Hooke, J. M. (1995). River channel adjustment to meander cutoffs on the River Bollin and River Dane, northwest England. *Geomorphology*, 14(3):235–253.

Hooke, J. M. (2003). River Meander Behaviour and Instability: A Framework for Analysis. *Transactions of the Institute of British Geographers*, 28(2):238–253.

Hooke, J. M. (2007). Complexity, self-organisation and variation in behaviour in meandering rivers. *Geomorphology*, 91(3-4):236–258.

Hooke, J. M. (2013). River Meandering. In Shroder, J. F., editor, *Treatise on Geomorphology*, chapter River mean, pages 260–288. Elsevier, San Diego, CA.

Howard, A. (1996). Modeling channel evolution and floodplain morphology. In Anderson, M., Walling, D., and Bates, P., editors, *Floodplain processes*, pages 15–65. John Wiley and Sons Ltd., Chichester.

Howard, A. and Knutson, T. (1984). Sufficient conditions for river meandering: A simulation approach. *Water Resources Research*, 20(11):1659–1667.

Howard, A. D. (2009). How to make a meandering river. *Proceedings of the National Academy of Sciences of the United States of America*, 106(41):17245–17246.

Howard, A. D. and Hemberger, A. T. (1991). Multivariate characterization of meandering. *Geomorphology*, 4:161–186.

Ielpi, A. and Ghinassi, M. (2014). Planform architecture, stratigraphic signature and morphodynamics of an exhumed Jurassic meander plain (Scalby Formation, Yorkshire, UK). *Sedimentology*, 61(7):1923–1960.

Iglewicz, B. and Hoaglin, D. C. (1993). *How to detect and handle outliers*. ASQC Quality Press, Milwaukee, Wis.

Ikeda, S., Parker, G., and Sawai, K. (1981). Bend theory of river meanders. Part 1. Linear development. *Journal of Fluid Mechanics*, 112:363–377.

Iwagaki, Y. (1956). HYDRODYNAMICAL STUDY ON CRITICAL TRACTIVE FORCE. *Transactions of the Japan Society of Civil Engineers*, 1956(41):1–21.

Iwasaki, T., Shimizu, Y., and Kimura, I. (2016). Numerical simulation of bar and bank erosion in a vegetated floodplain: A case study in the Otofuke River. *Advances in Water Resources*, 93(Part A):118–134.

Jager, H. (2003). *Modelling planform changes of braided rivers.* PhD thesis.

Jiang, H., Feng, M., Zhu, Y., Lu, N., Huang, J., and Xiao, T. (2014). An automated method for extracting rivers and lakes from Landsat imagery. *Remote Sensing*, 6(6):5067–5089.

Johannesson, H. and Parker, G. (1989). Linear theory of river meanders. In Ikeda, S. and Parker, G., editors, *Meandering Rivers*, chapter Linear The, pages 181–213. American Geophysical Union.

Kasvi, E., Vaaja, M., Alho, P., Hyyppä, H., Hyyppä, J., Kaartinen, H., and Kukko, A. (2013). Morphological changes on meander point bars associated with flow structure at different discharges. *Earth Surface Processes and Landforms*, 38(6):577–590.

Kean, J. W. and Smith, J. D. (2006a). Form drag in rivers due to small-scale natural topographic features: 1. Regular sequences. *Journal of Geophysical Research*, 111(F4):F04009.

Kean, J. W. and Smith, J. D. (2006b). Form drag in rivers due to small-scale natural topographic features: 2. Irregular sequences. *Journal of Geophysical Research*, 111(F4):F04009.

Keller, E. and Swanson, F. (1979). Effects of large organic material on channel form and fl uvial processes: , v. 4. *Earth Surface Processes*, 4:361–380.

Khatua, K. K. and Patra, K. C. (2009). Flow distribution in meandering compound channel. *ISH Journal of Hydraulic Engineering*, 15(3):11–25.

Kimber, A. C. (1982). Tests for Many Outliers in an Exponential Sample. *Source Journal of the Royal Statistical Society. Series C (Applied Statistics) Appl. Statist*, 31(3):263–271.

Kiss, T. and Blanka, V. (2012). River channel response to climate- and human-induced hydrological changes: Case study on the meandering Hernád River, Hungary. *Geomorphology*, 175-176:115–125.

Kleinhans, M. G., Jagers, B., Mosselman, E., and Sloff, K. (2006). Effect of upstream meanders on bifurcation stability and sediment division in 1D, 2D and 3D models. In Ferreira, R., Alves, E., Leal, J., and Cardoso, A., editors, *River flow 2006 : proceedings of the International Conference on Fluvial Hydraulics, Lisbon, Portugal, 6-8 September 2006*, chapter Effect of, pages 1355–1362. Taylor and Francis, Lisbon, Portugal, first edit edition.

Kleinhans, M. G., Jagers, H. R. A., Mosselman, E., and Sloff, C. J. (2008). Bifurcation dynamics and avulsion duration in meandering rivers by one-dimensional and three-dimensional models. *Water Resources Research*, 44(8):1–31.

Kleinhans, M. G. and van den Berg, J. H. (2011). River channel and bar patterns explained and predicted by an empirical and a physics-based method. *Earth Surface Processes and Landforms*, 36(6):721–738.

Ko, B. C., Kim, H. H., Nam, J. Y., and Lamberti, F. (2015). Classification of Potential Water Bodies Using Landsat 8 OLI and a Combination of Two Boosted Random Forest Classifiers. *Sensors*, 15:13763–13777.

Kramer, H. (1935). Sand Mixtures and Sand Movement in Fluvial Model. *Transactions of the American Society of Civil Engineers*, 100(1):798–838.

Krey, H. (1925). Grenzen der übertragbarkeit der versuchsergebnisse und modellähnlichkeit bei praktischen flussbauversuchen. *Zeitschrift für Angewandte Mathematik und Mechanik*, 5:484–486.

Krone, R. B. (1962). *Flume studies of the transport of sediment in estuarial shoaling processes*. Hydraulic Engineering Laboratory and Sanitary Engineering Research Laboratory, University of California Berkeley, Berkeley, California.

Kruskal, W. H. and Wallis, W. A. (1952). Use of Ranks in One-Criterion Variance Analysis. *Source Journal of the American Statistical Association*, 47(260):583–621.

Lagasse, P., Spitz, W., Zevengergen, L., and Zachmann, D. (2004). *Handbook for Predicting Stream Meander Migration*, volume 53. NCHRP REPORT 533.

Langendoen, E. J., Simon, A., and Rousselot, P. (2009). Closure to "Modeling the Evolution of Incised Streams. II: Streambank Erosion" by Eddy J. Langendoen and Andrew Simon. *Journal of Hydraulic Engineering*, 135(12):1107–1108.

Levene, H. (1960). Robust testes for equality of variances. In Olkin, I., editor, *Contributions to Probability and Statistics: Essays in Honor of Harold Hotelling*, pages 278–292. Stanford University Press, Palo Alto, CA.

Lewis, G. W. and Lewin, J. (1983). Alluvial Cutoffs in Wales and the Borderlands. In Collinson, J. and Lewin, J., editors, *Modern and Ancient Fluvial Systems*. Blackwell Publishing Ltd., Oxford, UK.

Li, W., Du, Z., Ling, F., Zhou, D., Wang, H., Gui, Y., Sun, B., and Zhang, X. (2013). A comparison of land surface water mapping using the normalized difference water index from TM, ETM+ and ALI. *Remote Sensing*, 5(11):5530–5549.

Liu, C., Luo, X., Liu, X., and Yang, K. (2013). Modeling depth-averaged velocity and bed shear stress in compound channels with emergent and submerged vegetation. *Advances in Water Resources*, 60:148–159.

Liu, C., Wright, N., Liu, X., and Yang, K. (2014). An analytical model for lateral depth-averaged velocity distributions along a meander in curved compound channels. *Advances in Water Resources*, 74:26–43.

Liu, H.-K. (1957). Mechanics of sediment ripple formation. *Journal of Hydraulic Division*, 83(2):1–23.

Luchi, R., Hooke, J. M., Zolezzi, G., and Bertoldi, W. (2010). Width variations and mid-channel bar inception in meanders: River Bollin (UK). *Geomorphology*, 119(1-2):1–8.

Luppi, L., Rinaldi, M., Teruggi, L. B., Darby, S. E., and Nardi, L. (2009). Monitoring and numerical modelling of riverbank erosion processes: a case study along the Cecina River (central Italy). *Earth Surface Processes and Landforms*, 34(4):530–546.

McFeeters, S. K. (1996). The use of the Normalized Difference Water Index (NDWI) in the delineation of open water features. *International Journal of Remote Sensing*, 17(7):1425–1432.

McFeeters, S. K. (2013). Using the normalized difference water index (ndwi) within a geographic information system to detect swimming pools for mosquito abatement: A practical approach. *Remote Sensing*, 5(7):3544–3561.

McGowen, J. H. and Garner, L. E. (1970). Physiographic features and stratification types of coarse-grained pointbars: modern and ancient examples. *Sedimentology*, 14(1-2):77–111.

Mehta, A. J. and Partheniades, E. (1975). An Investigation Of The Depositional Properties Of Flocculated Fine Sediments. *Journal of Hydraulic ResearchOnline) Journal Journal of Hydraulic Research*, 134:22–1686.

Meyer-Peter, E. and Müller, R. (1948). Formulas for Bed-Load transport. Technical report, Intentational Association for Hydraulic Structures Research, Stockholm.

Micheli, E. R. and Larsen, E. W. (2011). River channel cutoff dynamics, Sacramento River, California, USA. *River Research and Applications*, 27(3):328–344.

Miori, S., Repetto, R., and Tubino, M. (2006). A one-dimensional model of bifurcations in gravel bed channels with erodible banks. *Water Resources Research*, 42(11).

Montgomery, K. (1996). Sinuosity and Fractal Dimension of Meandering Rivers. *Area*, 28(Montgomery1996):491–500.

Mood, A. M. (1954). On the Asymptotic Efficiency of Certain Nonparametric Two-Sample Tests. *The Annals of Mathematical Statistics*, 25(3):514–522.

Motta, D., Abad, J. D., Langendoen, E. J., and Garcia, M. H. (2012). A simplified 2D model for meander migration with physically-based bank evolution. *Geomorphology*, 163-164:10–25.

Motta, D., Langendoen, E. J., Abad, J. D., and Garcia, M. H. (2014). Modification of meander migration by bank failures. *Journal of Geophysical Research: Earth Surface*, 119(5):1026–1042.

Nagata, N., Hosoda, T., and Muramoto, Y. (2000). NUMERICAL ANALYSIS OF RIVER CHANNEL PROCESSES WITH BANK EROSION. *Journal of Hydraulic Engineering*, 126(4):243–252.

Nanson, G. and Croke, J. (1992). A genetic classification of floodplains. *Geomorphology*, 4(6):459–486.

Nardi, L., Campo, L., and Rinaldi, M. (2013). Quantification of riverbank erosion and application in risk analysis. *Natural Hazards*, 69(1):869–887.

Nardi, L. and Rinaldi, M. (2010). Modelling riverbank retreat by combining reach-scale hydraulic models with bank-scale erosion and stability analyses. *River Flow 2010*, (May 2014):1286–1291.

Nicholas, A. (2013). Morphodynamic diversity of the world's largest rivers. *Geology*, 41(4):475–478.

Nicholas, A. P., Sambrook Smith, G. H., Amsler, M. L., Ashworth, P. J., Best, J. L., Hardy, R. J., Lane, S. N., Orfeo, O., Parsons, D. R., Reesink, A. J., Sandbach, S. D., Simpson, C. J., and Szupiany, R. N. (2016). The role of discharge variability in determining alluvial stratigraphy. *Geology*, 44(1):3–6.

Nino, Y., Lopez, F., and Garcia, M. (2003). Threshold for particle entrainment into suspension. *Sedimentology*, 50(2):247–263.

Odgaard, A. J. (1990). River-Meander Model. I: Development. *Journal of Hydraulic Engineering*, 115(11):1433–1450.

Paphitis, D. (2001). Sediment movement under unidirectional flows: An assessment of empirical threshold curves. *Coastal Engineering*, 43(3-4):227–245.

Parker, G. and Andres, D. (1976). Detrimental effects of river channelization. In *Proc. Conf. Rivers*, pages 1248–1266.

Parker, G., Seminara, G., and Solari, L. (2003). Bed load at low Shields stress on arbitrarily sloping beds: Alternative entrainment formulation. *Water Resources Research*, 39(7):1–11.

Parker, G., Shimizu, Y., Wilkerson, G. V., Eke, E. C., Abad, J. D., Lauer, J. W., Paola, C., Dietrich, W. E., and Voller, V. R. (2011). A new framework for modeling the migration of meandering rivers. *Earth Surface Processes and Landforms*, 36(1):70–86.

Patra, K. C. and Kar, S. K. (2000). FLOW INTERACTION OF MEANDERING RIVER WITH FLOODPLAINS. *Journal of Hydraulic Engineering*, 126(August):593–604.

Patra, K. C., Kar, S. K., and Bhattacharya, A. K. (2004). Flow and Velocity Distribution in Meandering Compound Channels. *Journal of Hydraulic Engineering*, 130(5):398–411.

Peakall, J., Ashworth, P., and Best, J. (2007). Meander-Bend Evolution, Alluvial Architecture, and the Role of Cohesion in Sinuous River Channels: A Flume Study. *Journal of Sedimentary Research*, 77(3):197–212.

Perucca, E., Camporeale, C., and Ridolfi, L. (2005). Nonlinear analysis of the geometry of meandering rivers. *Geophysical Research Letters*, 32(3):1–4.

Piegay, H., Hupp, C. R., Citterio, A., Dufour, S., Moulin, B., and Walling, D. E. (2008). Spatial and temporal variability in sedimentation rates associated with cutoff channel infill deposits: Ain River, France. *Water Resources Research*, 44(5).

Rameshwaran, P. and Shiono, K. (2003). Computer modelling of two-stage meandering channel flows. *Proceedings of the Institution of Civil Engineers: Water and Maritime Engineering*, 156(4):325–339.

Redolfi, M., Zolezzi, G., and Tubino, M. (2016). Free instability of channel bifurcations and morphodynamic influence. *Journal of Fluid Mechanics*, 799(2016):476–504.

Riesterer, J., Wenka, T., and Brudy-zippelius, T. (2016). Bed load transport modeling of a secondary flow influenced curved channel with 2D and 3D numerical models. *Journal of Applied Water Engineering and Research*, 4:54–66.

Rinaldi, M., Mengoni, B., Luppi, L., Darby, S. E., and Mosselman, E. (2008). Numerical simulation of hydrodynamics and bank erosion in a river bend. *Water Resources Research*, 44(9):1–17.

Rinaldi, M. and Nardi, L. (2013). Modeling Interactions between Riverbank Hydrology and Mass Failures. *Journal of Hydraulic Engineering*, 18(10):1231–1240.

Rosner, B. (1983). Percentage Points for a Generalized ESD Many-Outlier Procedure. *Technometrics*, 25(2):165.

Santini, W., Martinez, J. M., Espinoza-Villar, R., Cochonneau, G., Vauchel, P., Moquet, J. S., Baby, P., Espinoza, J. C., Lavado, W., Carranza, J., and Guyot, J. L. (2014). Sediment budget in the Ucayali River basin, an Andean tributary of the Amazon River. *IAHS-AISH Proceedings and Reports*, 367(December 2014):320–325.

Savitzky, A. and Golay, M. J. E. (1964). Smoothing and Differentiation of Data by Simplified Least Squares Procedures. *Analytical Chemistry*, 36(8):1627–1639.

Scheffe, H. (1999). *The analysis of variance*. Wiley-Interscience Publication.

Schuurman, F., Shimizu, Y., Iwasaki, T., and Kleinhans, M. G. (2016). Dynamic meandering in response to upstream perturbations and floodplain formation. *Geomorphology*, 253(November):94–109.

Schwarz, G. (1978). Estimating the Dimension of a Model. *The Annals of Statistics*, 6(2):461–464.

Schwenk, J. and Foufoula-Georgiou, E. (2016). Meander cutoffs nonlocally accelerate upstream and downstream migration and channel widening. *Geophysical Research Letters*, 43(24):12,437–12,445.

Schwenk, J., Khandelwal, A., Fratkin, M., Kumar, V., and Foufoula-Georgiou, E. (2017). High spatiotemporal resolution of river planform dynamics from Landsat: The RivMAP toolbox and results from the Ucayali River. *Earth and Space Science*, 4:46–75.

Schwenk, J., Lanzoni, S., and Foufoula-Georgiou, E. (2015). The life of a meander bend: Connecting shape and dynamics via analysis of a numerical model. *Journal of Geophysical Research F: Earth Surface*, 120(4):690–710.

Seminara, G. (2006). Meanders. *Journal of Fluid Mechanics*, 554:271–297.

Seminara, G., Zolezzi, G., Tubino, M., and Zardi, D. (2001). Downstream and upstream influence in river meandering. Part 2. Planimetric development. *Journal of Fluid Mechanics*, 438:213–230.

SENAMHI (2016). Contenido :Comportamiento hidrológico de la cuenca amazónica durante el año hidrológico 2015-2016. Technical report, Servicio Nacional de Meteorología e Hidrología del Perú - SENAMHI, Lima.

Shan, Y., Liu, C., and Luo, M. (2015). Simple analytical model for depth-averaged velocity in meandering compound channels. *Applied Mathematics and Mechanics*, 36(6):707–718.

Shields, A. (1936). Application of similarity principles and turbulence research to bed-load movement. *Mitteilungen der Preussischen Versuchsanstalt fur Wasserbau und Schiffbau.*, 26:5 – 24.

Shiono, K., Chan, T. L., Spooner, J., Rameshwaran, P., and Chandler, J. H. (2009a). The effect of floodplain roughness on flow structures, bedforms and sediment transport rates in meandering channels with overbank flows: Part I. *Journal of Hydraulic Research*, 47(1):5–19.

Shiono, K., Chan, T. L., Spooner, J., Rameshwaran, P., and Chandler, J. H. (2009b). The effect of floodplain roughness on flow structures, bedforms and sediment transport rates in meandering channels with overbank flows: Part II. *Journal of Hydraulic Research*, 47(1):20–28.

Shiono, K. and Muto, Y. (1998). Complex flow mechanisms in compound meandering channels with overbank flow. *Journal of Fluid Mechanics*, 376:221–261.

Shiono, K., Muto, Y., Knight, D. W., and Hyde, A. F. L. (1999). Energy losses due to secondary flow and turbulence in meandering channels with overbank flows. *Journal of Hydraulic Research*, 37(May 2012):641–664.

Shiono, K. and Shukla, D. R. (2008). CFD modelling of meandering channel during floods. *Proceedings of the ICE - Water Management*, 161(1):1–12.

Shiono, K., Spooner, J., Chan, T., Rameshwaran, P., and Chandler, J. H. (2008). Flow characteristics in meandering channels with non-mobile and mobile beds for overbank flows. *Journal of Hydraulic Research*, 46(1):113–132.

Simoes, F. J. M. (2014). Shear velocity criterion for incipient motion of sediment. *Water Science and Engineering*, 7(2):183–193.

Simon, A., Curini, A., Darby, S. E., and Langendoen, E. J. (2000). Bank and near-bank processes in an incised channel. *Geomorphology*, 35(3-4):193–217.

Simon, A. and Robbins, C. H. (1987). Man-induced gradient adjustment of the South Fork Forked Deer River, west Tennessee. *Environ. Geol. Water Sci.*, 9(2):109–118.

Singer, M. B. (2008). Downstream patterns of bed material grain size in a large, lowland alluvial river subject to low sediment supply. *Water Resources Research*, 44(12):1–7.

Singh, A., Lanzoni, S., and Foufoula-Georgiou, E. (2009). Nonlinearity and complexity in gravel bed dynamics. *Stochastic Environmental Research and Risk Assessment*, 23(7):967–975.

Slowik, M. (2016). The influence of meander bend evolution on the formation of multiple cutoffs: Findings inferred from floodplain architecture and bend geometry. *Earth Surface Processes and Landforms*, 41(5):626–641.

Soulsby, R. and Whitehouse, R. (1997). Threshold of Sediment Motion in Coastal Environments. In Christchurch, N., editor, *Pacific Coasts and Ports '97: Proceedings of the 13th Australasian Coastal and Ocean Engineering Conference and the 6th Australasian Port and Harbour Conference; Volume 1*, chapter Threshold, pages 149–154. Centre for Advanced Engineering, University of Canterbury.

Stansby, P. K. (2003). A mixing-length model for shallow turbulent wakes. *Journal of Fluid Mechanics*, 495:369–384.

Stølum, H. H. (1998). Planform geometry and dynamics of meandering rivers. *Bulletin of the Geological Society of America*, 110(11):1485–1498.

Sumer, B. (1986). Recent Developments on the Mechanics of sediment suspension. In and Vollmers, B., editor, *Euromech 192: Transport of suspended solids in open channels*, chapter Recent Dev, pages 3–13. Balkema Publishers, Rotterdam.

Sun, T., Meakin, P., Jøssang, T., and Schwarz, K. (1996). A Simulation Model for Meandering Rivers. *Water Resources Research*, 32(9):2937–2954.

Surkan, A. J. and Van Kan, J. (1969). Constrained Random Walk Meander Generation. *Water Resources Research*, 5(6):1343–1352.

Tal, M. and Paola, C. (2010). Effects of vegetation on channel morphodynamics: Results and insights from laboratory experiments. *Earth Surface Processes and Landforms*, 35(9):1014–1028.

Thakur, T. R. and Scheidegger, A. E. (1968). A test of the statistical theory of meander formation. *Water Resources Research*, 4(2):317–329.

Thompson, D. M. (2003). A geomorphic explanation for a meander cutoff following channel relocation of a coarse-bedded river. *Environmental Management*, 31(3):385–400.

Toonen, W. H. J., Kleinhans, M. G., and Cohen, K. M. (2012). Sedimentary architecture of abandoned channel fills. *Earth Surface Processes and Landforms*, 37(4):459–472.

Troyan, V. and Kiselev, Y. (2010). *Statistical Methods of Geophysical Data Processing*. World Scientific Publishing Co. Pte. Ltd.

Tukey, J. W. (1949). Comparing Individual Means in the Analysis of Variance. *Source: Biometrics*, 5(2):99–114.

Uittenbogaard, R. and van Vossen, B. (2004). Subgrid-scale model for quasi-2D turbulence in shallow water. In *Shallow Flows*, pages 575–582. Taylor & Francis.

U.S. Geological Survey (2015). Landsat—Earth observation satellites. Technical report, U.S. Geological Survey, Reston, VA.

van de Lageweg, W. I., Schuurman, F., Cohen, K. M., van Dijk, W. M., Shimizu, Y., and Kleinhans, M. G. (2016a). Preservation of meandering river channels in uniformly aggrading channel belts. *Sedimentology*, 63(3):586–608.

van de Lageweg, W. I., van Dijk, W. M., Box, D., and Kleinhans, M. G. (2016b). Archimetrics: a quantitative tool to predict three-dimensional meander belt sandbody heterogeneity. *The Depositional Record*, 2(1):22–46.

van de Lageweg, W. I., van Dijk, W. M., and Kleinhans, M. G. (2013). Channel belt architecture formed by a meandering river. *Sedimentology*, 60(3):840–859.

Van Dijk, W. M., Schuurman, F., Van De Lageweg, W. I., and Kleinhans, M. G. (2014). Bifurcation instability and chute cutoff development in meandering gravel-bed rivers. *Geomorphology*, 213:277–291.

Van Dijk, W. M., Van De Lageweg, W. I., and Kleinhans, M. G. (2012). Experimental meandering river with chute cutoffs. *Journal of Geophysical Research: Earth Surface*, 117(3):1–18.

van Oorschot, M., Kleinhans, M., Geerling, G., and Middelkoop, H. (2016). Distinct patterns of interaction between vegetation and morphodynamics. *Earth Surface Processes and Landforms*, 41(6):791–808.

Van Rijn, L. C. (1984). Sediment transport Part I Bed load transport.

Viero, D. P., D'Alpaos, A., Carniello, L., and Defina, A. (2013). Mathematical modeling of flooding due to river bank failure. *Advances in Water Resources*, 59:82–94.

Visconti, F., Stefanon, L., Camporeale, C., Susin, F., Ridolfi, L., and Lanzoni, S. (2012). Bed evolution measurement with flowing water in morphodynamics experiments. *Earth Surface Processes and Landforms*, 37(8):818–827.

Walsh, J. E. (1950). Some Nonparametric Tests of Whether the Largest Observations of a Set are too Large or too Small. *The Annals of Mathematical Statistics*, 21(4):583–592.

Wickert, A. D., Martin, J. M., Tal, M., Kim, W., Sheets, B., and Paola, C. (2013). River channel lateral mobility: Metrics, time scales, and controls. *Journal of Geophysical Research: Earth Surface*, 118(2):396–412.

Wormleaton, P., Sellin, R. H. J., and Bryant, T. (2004). Conveyance in a two-stage meandering channel with a mobile bed Conveyance in a two-stage meandering channel with a mobile bed Transport. *Journal of Hydraulic Research*, 42(April 2013):493–506.

Wu, W. and Wang, S. S. Y. (1999). Movable Bed Roughness in Alluvial Rivers. *Journal of Hydraulic Engineering*, 125(12):1309–1312.

Xie, J. H. (1981). River sediment engineering. *Water Resources Press, Beijing (in Chinese)*, 1.

Xu, H. (2006). Modification of normalised difference water index (NDWI) to enhance open water features in remotely sensed imagery. *International Journal of Remote Sensing*, 27(14):3025–3033.

Yalin, M. (1963). An expression for bed-load transportation. *Journal of Hydraulic Division*, 89(3):221–250.

Zen, S., Zolezzi, G., Toffolon, M., and Gurnell, A. M. (2016). Biomorphodynamic modelling of inner bank advance in migrating meander bends. *Advances in Water Resources*, 93:166–181.

Zinger, J. A., Rhoads, B. L., and Best, J. L. (2011). Extreme sediment pulses generated by bend cutoffs along a large meandering river. *Nature Geoscience*, 4(10):675–678.

Zinger, J. A., Rhoads, B. L., Best, J. L., and Johnson, K. K. (2013). Flow structure and channel morphodynamics of meander bend chute cutoffs: A case study of the Wabash River, USA. *Journal of Geophysical Research: Earth Surface*, 118(4):2468–2487.

Zolezzi, G., Luchi, R., and Tubino, M. (2012). Modeling morphodynamic processes in meandering rivers with spatial width variations. *Reviews of Geophysics*, 50(4):1–24.